การพัฒนาแบบจำลองคณิตศาสตร์แสดงพลวัตของพลาสมาที่กำเนิดจากเครื่องพลาสมาโฟกัส

นายปรัชญา ตั้งจิตสมบูรณ์

วิทยานิพนธ์นี้เป็นส่วนหนึ่งของการศึกษาตามหลักสูตรปริญญาวิทยาศาสตรดุษฎีบัณฑิต
สาขาวิชาฟิสิกส์ ภาควิชาฟิสิกส์
คณะวิทยาศาสตร์ จุฬาลงกรณ์มหาวิทยาลัย
ปีการศึกษา 2558

DEVELOPMENT OF MATHEMATICAL MODEL REPRESENTING DYNAMICS OF PLASMA GENERATED FROM A PLASMA FOCUS DEVICE

Mr. Prajya Tangjitsomboon

A Dissertation Submitted in Partial Fulfillment of the Requirements
for the Degree of Doctor of Philosophy Program in Physics
Department of Physics
Faculty of Science
Chulalongkorn University
Academic Year 2015

Thesis Title	DEVELOPMENT OF MATHEMATICAL MODEL REPRESENTING DYNAMICS OF PLASMA GENERATED FROM A PLASMA FOCUS DEVICE
By	Mr. Prajya Tangjitsomboon
Field of Study	Physics
Thesis Advisor	Assistant Professor Rattachat Mongkolnavin, Ph.D.
Thesis Co-Advisor	Professor Chiow San Wong, Ph.D.

Accepted by the Faculty of Science, Chulalongkorn University in Partial Fulfillment of the Requirements for the Doctoral Degree

.....Dean of the Faculty of Science
(Associate Professor Polkit Sangvanich, Ph.D.)

THESIS COMMITTEE

.....Chairman
(Associate Professor Mayuree Natenapit, Ph.D.)

.....Thesis Advisor
(Assistant Professor Rattachat Mongkolnavin, Ph.D.)

.....Thesis Co-Advisor
(Professor Chiow San Wong, Ph.D.)

.....Examiner
(Associate Professor Satreerat Hodak, Ph.D.)

.....Examiner
(Assistant Professor Tonphong Kaewkongka, Ph.D.)

.....External Examiner
(Assistant Professor Dusit Ngamrungroj, Ph.D.)

ปรัชญา ตั้งจิตสมบูรณ์ : การพัฒนาแบบจำลองคณิตศาสตร์แสดงพลวัตของพลาสมาที่กำเนิดจากเครื่องพลาสมาโฟกัส (DEVELOPMENT OF MATHEMATICAL MODEL REPRESENTING DYNAMICS OF PLASMA GENERATED FROM A PLASMA FOCUS DEVICE) อ.ที่ปรึกษาวิทยานิพนธ์หลัก: ผศ. ดร. รัฐชาติ มงคลนาวิน, อ.ที่ปรึกษาวิทยานิพนธ์ร่วม: ศ. ดร. เชาว์ ชาน หว่อง, 101 หน้า.

เครื่องพลาสมาโฟกัสได้นำมาใช้เป็นแหล่งกำเนิดรังสีและอนุภาคต่างๆโดยเครื่องพลาสมาสามารถประยุกต์กับการปรับปรุงพื้นผิววัสดุได้เช่นกัน ในงานวิจัยนี้ศึกษาการเคลื่อนที่หรือการพลวัตของพลาสมาที่มาจากเครื่องพลาสมาโฟกัสชนิด UNU/ICTP โดยทำการศึกษาลึกลงไปในระดับจุลภาคซึ่งต่างจากแบบจำลองที่มีการใช้อยู่ในปัจจุบันซึ่งเป็นแบบจำลองที่ได้ถูกพัฒนาตามแบบจำลองของลี โดยแบบจำลองนี้สนใจการเคลื่อนที่ของพลาสมาในระดับมหภาคโดยพิจารณาให้พลาสมาประพฤติตัวเป็นแผ่นทรงกระบอกบางที่ถูกเร่งให้เคลื่อนที่ด้วยแรงโลเรนซ์โดยแรงดังกล่าวมาจากกระแสของพลาสมาและสนามแม่เหล็กที่ถูกเหนี่ยวนำซึ่งกระแสไฟฟ้านี้คำนวณจากสมการของวงจร ในงานวิจัยนี้ได้ใช้โปรแกรมการจำลองทางฟิสิกส์เพื่อจำลองการเคลื่อนที่ของพลาสมาในระดับจุลภาคโดยใช้วิธีการคำนวณด้วยระเบียบวิธีไฟไนต์เอเลเมนต์ ซึ่งการจำลองนี้ได้พิจารณารูปทรงของเครื่องพลาสมา สมบัติทางวัสดุที่ใช้ในเครื่องพลาสมา ทฤษฎีแม่เหล็กไฟฟ้าที่ใช้ในเครื่องชนิดนี้และทฤษฎีของพลาสมา โดยการกำเนิดพลาสมาจากการใส่กระแสไฟฟ้าเข้าไปในขั้วอิเล็กโทรดซึ่งนำไปสู่การคำนวณด้วยวิธีการไฟไนต์เอเลเมนต์ ในการคำนวณด้วยวิธีนี้นำมาเปรียบเทียบผลกับแบบจำลองของลีภายใต้การเปลี่ยนค่าความดันของแก๊สอาร์กอนที่ความดัน 1.0, 1.5 และ 2.0 มิลลิบาร์ ผลการจำลองโดยใช้แบบจำลองของลีคำนวณค่าแฟกเตอร์ของกระแสมีค่าอยู่ในช่วง 0.36-0.67 และแฟกเตอร์ของการกวาดมวลมีค่าในช่วง 0.024-0.0365 สำหรับผลการคำนวนโดยใช้โปรแกรมการจำลองฟิสิกส์แฟกเตอร์กระแสเฉลี่ยมีค่าอยู่ระหว่าง 0.48-0.55 ซึ่งค่าแฟกเตอร์ของกระดังกล่าวเป็นฟังก์ชันกับเวลา และโปรแกรมการจำลองทางฟิสิกส์ได้แสดงค่าของอุณหภูมิและความหนาแน่นของแก๊สที่เปลี่ยนแปลงเนื่องจากการเคลื่อนที่ของพลาสมา ซึ่งแสดงให้เห็นว่าแก๊สอาร์กอนทั้งหมดไม่ได้เคลื่อนที่ไปพร้อมกับพลาสมาซึ่งสอดคล้องกับแฟกเตอร์ของการกวาดมวลตามแบบจำลองของลี ในการจำลอง ได้อธิบายกระบวนการของพลาสมาในระดับจุลภาค โดยจำลองการพลวัติตั้งแต่ช่วงเฟสแตกตัวจนกระทั่งสิ้นเฟสตามแนวแกน โดยแบบจำลองลีไม่สามารถคำนวณในช่วงการเคลื่อนที่ของพลาสมาในช่วงเฟสแตกตัว การจำลองด้วยโปรแกรมการจำลองทางฟิสิกส์แสดงให้เห็นว่าการจำลองในระดับจุลภาคสามารถแสดงถึงสมบัติของพลาสมาที่สอดคล้องกับแบบจำลองของลี

ภาควิชา ฟิสิกส์ ลายมือชื่อนิสิต .....

สาขาวิชา ฟิสิกส์ ลายมือชื่อ อ.ที่ปรึกษาหลัก .....

ปีการศึกษา 2558 ลายมือชื่อ อ.ที่ปรึกษาร่วม .....

5373812023 : MAJOR PHYSICS
KEYWORDS: SIMULATION / PLASMA FOCUS DEVICE / PLASMA DYNAMICS / AXIAL PHASE / BREAKDOWN PHASE

PRAJYA TANGJITSOMBOON: DEVELOPMENT OF MATHEMATICAL MODEL REPRESENTING DYNAMICS OF PLASMA GENERATED FROM A PLASMA FOCUS DEVICE. ADVISOR: ASST. PROF. RATTACHAT MONGKOLNAVIN, Ph.D., CO-ADVISOR: PROF. CHIOW SAN WONG, Ph.D., 101 pp.

Plasma Focus (PF) device is known to be used as source of radiations and particles. It also has been used for materials surface modification. This research aims to investigate the dynamics of plasma generated by a standard UNU/ICTP PF device. More detailed microscopic modeling of the dynamics is attempted, which is different and can be complimentary to the widely used Lee model code. Lee model is considered to be a macroscopic model as it assumed that plasma behave as a thin solid cylinder that moves by Lorentz force. The Lorentz force is generated by the plasma current and the induced magnetic field from the discharge current where the circuit equation is used to represent the discharge characteristic. In this research, a software package is used to simulate the dynamics of plasma microscopically using finite element method. It considers geometry of PF, material properties, electromagnetic theory, plasma theory and input current characteristic for the finite element calculation. Both simulation results are compared with experimental results, where UNU/ICTP PF is operated with variable pressure of argon gas at 1.0, 1.5 and 2.0 mbar. Current factor and mass swept factor used by Lee model are found to be between 0.36-0.67 and 0.024-0.0365 respectively. The finite element simulation gives average current factor of 0.48-0.55. It is found to be varying with time. The finite element simulation also has shown that the density and the temperature of argon gas changes as plasma is moving along the electrodes. However, it has shown that not all argon gas is swept by the plasma which correspond to the assumption of mass swept factor applied in Lee model. In addition, the finite element simulation uses plasma processes to represent the behavior of the plasma generated by PF device microscopically, which allows graphical generation of plasma starting from breakdown phase to axial phase where Lee model cannot show. It has been demonstrated that a microscopic model can generate results and characteristics of plasma that are close to actual experiment. They also agree with the results from the macroscopic model based on Lee model code.

Department:	Physics	Student's Signature	.....
Field of Study:	Physics	Advisor's Signature	.....
Academic Year:	2015	Co-Advisor's Signature	.....

ACKNOWLEDGEMENTS

I would like to dedicate this section to give my special gratitude to the people who help and support me through my Ph.D. thesis work. Without anyone of them, it would be impossible for this thesis to be completed.

First of all I would like to express my great appreciation to my advisor, Assistant Professor Rattachat Mongkolnavin, Ph.D. and my co-advisor Professor Chiow San Wong, Ph.D. for their support, great understanding and excellent guidance, which make this thesis possible. This thesis work has gone through a lot of problems and difficult time, but they always have great patient and give suggestions which help me to solve all these problems. I am also grateful to the following people;

Associate Professor Mayuree Natenapit, Ph.D., Associate Professor Satreerat Hodak, Ph.D., Assistant Professor Tonphong Keawkongka, Ph.D., and Assistant Professor Dusit Ngamrungroj, Ph.D. members of the thesis committee for their useful suggestions and discussions.

Mr. Eakaluck Chandrema for his great understanding and excellent guidance on my simulation.

Assistance Professor Dusit Ngamrungroj, Ph.D for his understanding and excellent guidance on my experimental work.

Department of Physics, Faculty of Science, Chulalongkorn University and Plasma Technology and Nuclear Fusion Research Unit for their financial support.

Ondemand co-operation for their financial support and work experience.

I would like to thank my family who always understand and not putting any pressure on me during my study.

Finally, I would like to express my great thanks to Chulalongkorn University for giving six years of experience that is beyond the knowledge and the degree.

CONTENTS

Page

Page

Page

LIST OF FIGURES

LIST OF TABLES

LIST OF SYMBOLS

Symbol	Definitions	Unit
m	Mass of plasma slug	kg
$\vec{F}_B$	Magnetic force	N
$\vec{B}$	Magnetic field	T
ρ_o	Density of gas under operating pressure condition	$\mathrm{kg/m^3}$
M	Molecular mass	kg
T_0	Room temperature	K
P_o	Operating pressure of a gas	Pa
R	Gas constant	$\mathrm{J/mol.K}$
a	Radius of anode (0.0095 m)	m
b	Distance from center of the anode to the cathode (0.032 m)	m
z_o	length of anode (0.16 m)	m
I	Current of the circuit	A
z	Position of shock front along the axis of anode	m
v	Velocity of plasma	$\mathrm{m/s}$
r	Position along radial axis	m
f_m	Mass swept factor	-
f_c	Current factor	-
μ_o	Permeability of vacuum	$\mathrm{T.m/A}$
q	Charge of the circuit	C
L_P	Inductance of plasma	H
R_P	Plasma resistivity	Ω

Symbol	Definitions	Unit
R_o	Resistivity of circuit	Ω
L_o	Inductance of circuit	H
C_o	Capacitance of capacitor bank (30 μF)	F
V_o	Charging voltage	V
N_i	Density of ion at state i	m^{-3}
N_{i+1}	Density of ion at state $i+1$	m^{-3}
χ_i	Ionization energy of ion in a state *i*	eV
T_{eV}	Plasma temperature in electron volt	eV
N	Total number of ion density	m^{-3}
Z_{eff}	Effective charge	-
Z	Atomic number	-
$\vec{E}$	Electric field in a medium	N/C
ρ_v	Charge density in a medium	C/m^3
ε	Permittivity of medium	$C^2/N.m^2$
e	Unit charge of electron.	C
n_e	Electron's density	m^{-3}
n_i	Ion's density	m^{-3}
I_o	Maximum current of the circuit	A
$\vec{A}$	Vector potential	T.m
$\vec{J}_e$	External current density	A/m^2
σ	Conductivity in medium	$\Omega^{-1}.m^{-1}$
μ	Permeability in a medium	T.m/A
m_e	Mass of electron	kg
m	Molecular mass of ion in this research used mass of argon	kg
n_ε	Energy number density of electron	J/m^3

Symbol	Definitions	Unit
R_e	Electron creation rate	$m^{-3}.s^{-1}$
S_{en}	Energy loss/gain from inelastic collisions	$J/m^3.s$
$\vec{u}$	Vector field ions velocity	m/s
Q	Total heat source	W/m^3
$\overrightarrow{\Gamma_e}$	Electron flux	$m^{-2}s^{-1}$
$\overrightarrow{\Gamma_{en}}$	Electron energy flux	W/m^2
T_e	Electron temperature	K
ν_m	Collision frequency of electron	s^{-1}
k_B	Boltzmann's constant.	J/K
μ_e	Electron mobility	$m^2/V.s$
μ_{en}	Electron energy mobility.	$m/V.s$
D_e	Diffusion coefficient of electron	$J.s/kg$
D_{en}	Electron energy diffusion	$J.m^2/s$
$\overrightarrow{J_k}$	Diffusive flux vector	$kg/m^2.s$
R_k	The rate expression for species k	$kg/m^3.s$
ρ	Density of gas	kg/m^3
$\vec{u}$	Mass averaged fluid velocity	m/s
w_k	Mass faction of the k th species	-
$\overrightarrow{V_k}$	Diffusion velocity	m/s
k	Number species of ion	-
D_k	Mixture average diffusion coefficient	m^2/s
M_n	Mean molar mass of the mixture	kg
T_i	Ion's temperature	K
${D_k}^T$	Thermal diffusion coefficient for species k	$m^2.kg/s$
Z_k	Charge number for species k	-

Symbol	Definitions	Unit
μ_k	Mixture average mobility of species k	$\mathrm{m^2/V.s}$
M_k	Ion mass of species k	kg
$\emptyset$	Magnetic flux	Wb
$V(t)$	Induce voltage from magnetic field	V
A	Outer radius of Rogowski coil	m
A	Cross section area of Rogowski coil	$\mathrm{m^2}$
μ_o	Permeability of vacuum.	$\mathrm{T.m/A}$
R	Resistance of the device.	Ω
T'	Period of the current signal	s
v_{av}	Average speed between coils of the magnetic probe	$\mathrm{m/s}$
Δz	Displacement between coils of the magnetic probe	m
Δt	Time different between coils of the magnetic probe	s
I'	Current between the electrodes	A
P'	Electrical power	W
E	Electrical energy	J
V	Voltage of electrode.	$\mathrm{m^3}$
ρ	Density of plasma slug	$\mathrm{kg/m^3}$
V	Volume of plasma slug	$\mathrm{m^3}$
P_o	Operating pressure	Pa
P_n	Pressure act on the plasma slug	Pa
V_o	Volume of vacuum chamber	$\mathrm{m^3}$
V_n	Volume of plasma slug.	$\mathrm{m^3}$
γ	Specific ratio of argon gas; γ= 5/3	-

CHAPTER 1
INTRODUCTION

1.1 Background

Plasma Focus (PF) device is known to be used as source of radiations and particles [1-3]. It has also been used for materials surface modification [4-6]. However, the original intent of PF application was to be used as a compact device that is capable of producing fusion reaction [7]. The detail of PF operation and the dynamics of plasma inside PF will be explained more in later sections.

This research aims to investigate the movement or the dynamics of plasma in a standard United Nation University/ International Centre for Theoretical Physics (UNU/ICTP) PF device. Many researchers have tried to model the movement of plasma in PF in order to understand the processes that cause fusion as well as generation of radiation, ions and particles. Mathematical models have been developed by researchers to simulate the dynamics of the plasma that is comparable to real experimental results.

PF can be classified into two types; Mather type and Filipov type. The Mather type was built by J.W. Mather [8] and the Filippov type was designed by N.V Filipov et al. [9], these devices are shown in Figure 1.1.

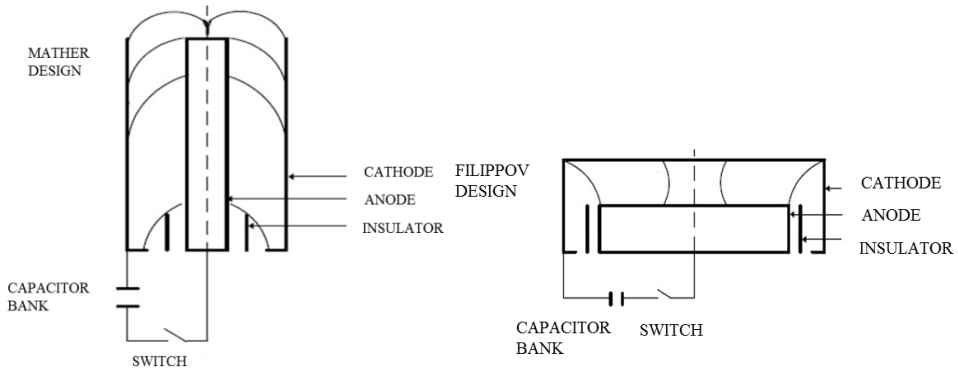

(a) (b)

Figure 1.1: Diagram showing of plasma focus device (a) Mather type (b) Filipov type.

The Mather type makes use of long electrodes configuration. The plasma is accelerated along the z axis of the anode and then it pinches at the top of the anode. In contrast, the Filippov type drives the plasma along the radial direction of the anode, and it pinches at the center of the electrode.

This research aims to study the dynamics of plasma based on 3.3 kJ UNU/ICTP Mather type PF device. This configuration is well established and easier to build than the Filippov type. This type of PF device is being used and being studied worldwide by many researchers.

The 3.3 kJ UNU/ICTP PF [2] configuration is based on a cylindrical tube design which composes of six cathodes placed around the central anode. The device is shown in Figure 1.2.

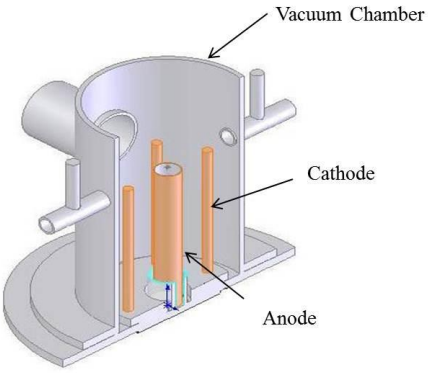

Figure 1.2: Diagram showing configuration of a typical UNU/ICTP PF device [2].

The dynamics of the plasma in the PF device can be classified into four different phases; breakdown, axial, radial and pinching phases [10]. These phases are shown in Figure 1.3.

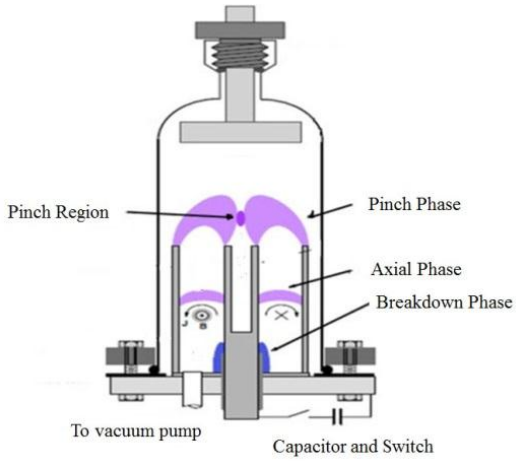

Figure 1.3: Diagram showing dynamics phases of plasma in a PF device [11].

Breakdown phase happens after the current discharge from a capacitor bank to the central anode. The high voltage potential between the electrodes causes gas in the chamber to breakdown at the surface of insulator as shown in Figure 1.4.

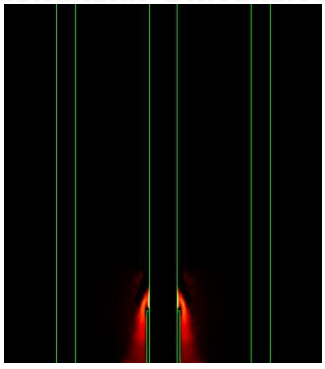

Figure 1.4: Picture showing gas breakdown at the surface of insulator generated by the finite element simulation.

The gas between the cathode and the anode is ionized, and electrons and ions are generated [12, 13]. These ions and electrons become plasma. The plasma is then pushed outward by the magnetic force and entering into the acceleration phase or the axial phase.

Axial Phase is the phase where plasma sheath is formed and the discharge current is flowing along the radial axis between the electrodes. The magnetic force $\vec{J} \times \vec{B}$ drives the plasma to move forward along the z axis. The detail of this phase will be explained in the Lee model in Chapter 2. Once the plasma sheath reaches the end of the anode, it enters into the radial compression phase or the radial phase.

Radial Phase starts when the plasma sheath moves radially towards center of the anode. Figure 1.5 shows shadowgraphs of the radial phase in a PF device.

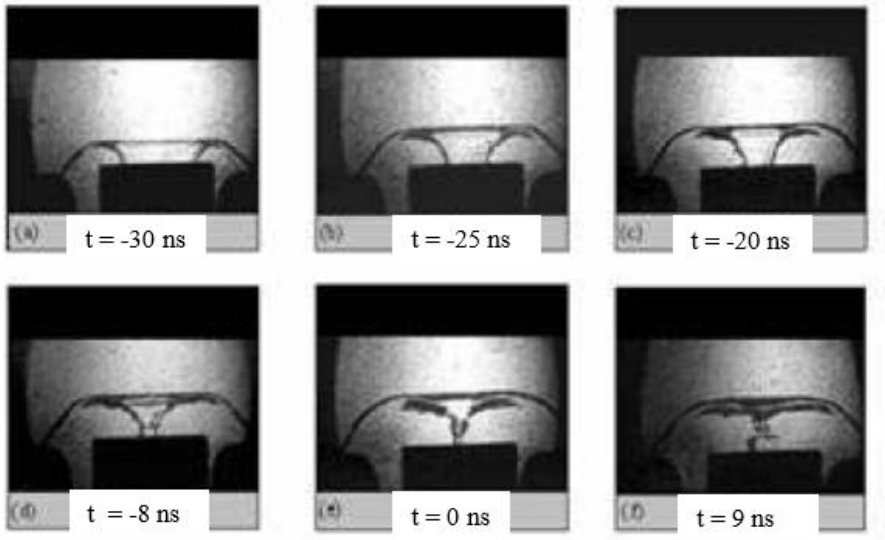

Figure 1.5: Shadowgraphs showing the dynamics of deuterium's plasma from the radial phase to the pinch phase of UNU/ICTP plasma focus under operating pressure at 4 mbar [14].

Pinch Phase happens after the radial phase has ended and the plasma is compressing or pinching. This causes the charge particles to collide and loose energy. If the energy of the plasma is high enough, then nuclear fusion reaction is also possible. This phase produces radiation as well as emission of high energetically charge particles and neutral particles as shown in Figure 1.3 and 1.4.

In 1965, J. W. Mather [15] considered a pinch of deuterium plasma from a PF device, where neutrons were generated from the pinching process of plasma. The neutron yield was calculated by using snowplow model. This plasma focus had a particle density ~ 2–3 × 10^{19}/cm^3, where the temperature of plasma could be raised to about 1–3 keV, time duration t ~ 0.2–0.3 μs, and a volume ~15 mm^3. The experimental results shown that neutron yields >10^{10}/burst and soft x-rays were observed.

Later in 1971, D. E. Potter [16] developed two-dimensional numerical fluid model to study dynamics of plasma and structure of the PF under approximation of the adiabatic compression and viscous heating. It was found that the kinetic energy densities from the experiment corresponded with numerical results.

In 1987, K. Behler and H. Bruhns [17] used three fluid codes that were developed from D. E. Potter code. This code took into account gas in addition to the plasma components such that ionization and recombination phenomena were modeled. Before that, S. Lee and T.Y Tou [18] simulated dynamics of plasma in pinch phase, both generalize slug model and energy balance were used to determine pinch radius. The experiment had shown that the pinch radius measured agreed with the calculation results.

In 1984, S. Lee [19] investigated and studied dynamics of plasma in PF device. He considered the movement of plasma in 1-D. Snowplow model was used to simulate the motion of plasma during the axial phase. In the radial phase, movement of plasma was also detailed by using slug model which considered the plasma that didn't transfer heat to the surrounding. The plasma was quasi-equilibrium.

In 1988, S. Mulyodrono and colleague [20] designed a small plasma focus device to be operated as a neutron source. Deuterium gas was used. Deuterium plasma was generated. It has been shown that the PF device operated with deuterium gas with at pressure of 3 Torr could emit neutron between 0.5-1.0× 10^8 particles per shot.

In 2005, S. Lee [10] modified the snowplow model and the slug model where he included mass swept factor and current factor in these models. These factors were estimated by fitting the actual current signal from experiment. This model has been accepted and has been studied by many researchers ever since. The model and the computational code published have been called "Lee model code".

Recently, S. Lee and S. H. Saw [21] published further work which derived the flux equation of the ion beam of any gas which was linked to the Lee Model code, and this research computed the ion beam properties of the PF device.

From these results, they have shown that the fluence, flux, ion number and ion current decrease from the lightest to the heaviest gas except for trend-breaking higher values for Ar fluence and flux. Also, the energy fluence, energy flux, power flow, and damage factors were relatively constant from H_2 to N_2 but increase for Ne, Ar, Kr and Xe due to radiative cooling and collapse effects.

Other researcher like M. Akel et al. [22] also operated the numerical experiments using the modified Lee model code on various PF devices based on nitrogen gas operation. They reported the ion beam properties produced from various PF devices. The results show that the average ion energies decrease with increasing operating gas pressure, while the ion beam number increases with higher pressure. The fluence, flux, ion current, power flow density and damage factor have maximum values at some optimum pressure. The results also show that, the maximum power flow densities range from 10^{12} to 10^{14} W m^{-2} and the damage factor values reach almost $10^9 – 10^{11}$ W m^{-2}.

Alternative model has also been published by M. Scholz and I.M. Ivanava-Sanik [23]. They reported a two-dimensional computer simulation of the breakdown phase performed by a PF device. The spatial and temporal development of the electron density and the potential of the electric field are calculated by numerically solving the continuity equations for electrons and ions together with the Poisson equation.

From the simulation, it was found that a PF device operated with hydrogen gas had duration of 19.97 ns for the breakdown phase. W. Stepniewski [24] also simulated the motion of plasma sheet inside a specific type of PF device that is called Plasma Focus-1000 device. His research also considered the dynamics in two-dimension.

The physical model which is used in the research was a full dissipative set of MHD equations with Braginski transport. This simulation started from partially ionized plasma and the kinetics of ionization was taken into account. The numerical results were less differs from experimental results.

More attempts have been made by R. Amrollahi and M. Habibi [25] to investigate the shock front dynamics of plasma after hitting at the central electrode. Lagrangian equations were used to solve for a parabolic shock trajectory yielding first and second approximation for the moving path of plasma's current sheath. S. Garanin and V. Mamyshev [26] formulated the dynamics of plasma, and developed a numerical model for calculating MHD flows in PF devices. They were able to describe plasma flows with drastically different densities and, therefore, to take into account the presence of a vacuum region behind the PF current sheath.

This allowed them to numerically simulate the focusing process and adequately describe the acceleration mechanism for the generation of fast ions and fusion neutrons. Again, the results from the calculations were compared with the experimental data on the plasma dynamics in two different types of PF device. A model of accelerated ions had been proposed which were able to estimate the contribution of the acceleration mechanism to the total neutron yield.

Similarly, J.H. Gonzalez et al. [27] investigated plasma phenomena during the pinching phase, the calculation model based on Von Karman approximations where the radial density and velocity profiles were used to calculate under apply input energy between 1 to 250 kJ. This research also compared the results with experimental results.

M. Zambra et al. [28] modified the snowplow model and calculated the thickness of plasma sheath which is formed in the device. The researchers were able to show the dynamics of plasma from the beginning.

In all these reviews, the dynamics of plasma in a PF device were considered based on the macroscopic assumption that a thick plasma sheath is moved by Lorentz force, however in reality, plasma composes of ions, electrons, and neutral particles, and these particles do interact among each other. It would be more realistic to consider plasma dynamics basing on its interaction within a microscopic system. However, microscopic scale is more complicated, therefore, the use of simulation tool is necessary.

The simulation tool aimed for simulating the dynamics of plasma is COMSOL Multiphysics Software because this simulation software can compute the dynamics of plasma in microscopic system which takes into account collisions between particles, and it can also interface with the electromagnetics theory which is the cause of the plasma movement.

C.H. Hollenstein and A.A. Howling [29] had successfully used the simulation software to simulate the edge plasma in a large area capacitively-coupled RF reactor. The properties of plasma in each position were computed by using finite element method. They have shown that plasma physics and plasma-wall interaction are strongly influenced by plasma elementary structures. The simple model and simple geometry had been shown to be an important tool giving new insights and understanding into the physics of RF edge plasmas. The simulation can help designing reactor walls to optimize the RF plasma in industrial reactors.

I. Rafatov et al. [30] also developed and tested 2D “extended fluid model” of a DC glow discharge using the simulation software and implemented two different approaches. First, by assembling the model from the simulation software’s general form partial differential equation. Secondly, using the simulation software’s built-in Plasma Module.

The discharge models were based on the fluid description of ions and excited neutral species and use drift diffusion approximation for the particle fluxes. The electron transport as well as the rates of electron-induced plasma-chemical reactions were calculated by using the Boltzmann equation for the Electron Energy Distribution Function (EEDF) and corresponding collision cross-sections. The self-consistent electric field was calculated by using the Poisson equation. Basic discharge plasma properties such as current-voltage characteristics and electron and ion spatial density distributions as well as electron temperature and electric field profiles were studied. This research also studied spatial distributions of particle fluxes in discharge plasma and identified the existence of vortex component of the discharge current.

S. Rebiai et al. [31] also studied plasma of helium gas which was generated by radio frequency plasma device. The dynamics in two-dimensional (2D) was investigated. The model solved the continuity equations for charged species and the electron energy balance equation, coupled with Poisson's equation by finite element method, using the simulation software. The simulations able to show the two-dimensional profiles of plasma components as well as the charge densities, electric field, electron temperature and ionization rate between symmetric parallel plate electrodes. The effects of low and high frequency sources parameters such as frequency values and applied voltage amplitude on the discharge characteristics were investigated.

Cheng Jia et al. [32] used the simulation software to study two-dimensional axisymmetric inductively coupled plasma (ICP) model, where argon plasma generated by radio frequency plasma device was investigated. These results were compared with the experimental results. It was found that the general trends of the number density and

temperature of electrons with radial scanning area were approximately correct.

M. Valentinuzzi1 et al. [33] used the simulation software to help designing an extraction pipe for electron beam generated from a PF device. However, the simulation software has never been used to modeling the dynamics of plasma in a PF device.

In this research, the simulation software is used to simulate the movement of the plasma starting from the breakdown phase and the axial phase in a microscopic system. The result obtained from this simulation will be compared with both experimental results and the results obtained from the macroscopic system of Lee Model. It is hoped that the results generated by the finite element simulation will give more insight into the starting process of the plasma in any PF systems which will definitely help the modification and designing process for PF applications mention earlier.

1.2 Motivation

Lee model code has been accepted and widely used in many research for calculating parameters of plasma that is generated by a PF device [19-23]. However, the model is based on a macroscopic system that does not include interactions between particles; therefore it cannot show details or real characteristics of the plasma. The model requires adjustment of factors which are mass swept factor and current factor to fit with the current signal from the experiment to start the calculation.

However, the simulation software has been shown to be able to work with different plasma systems as mentioned earlier, where concept of finite element is used and dynamics of plasma is constructed. This allows inclusion of particle interactions as well as electromagnetic interaction of plasma which means in depth investigation of plasma sheath dynamics can be carried out. This will also be the first time that such simulation software is used to simulate the dynamics of plasma in a PF device.

Therefore, by using the simulation software to simulate and construct the dynamics of plasma during the breakdown to axial phase should give us insight into the meaning of mass swept factor and current factor used by Lee model from microscopic system perspective as well.

1.3 Objective

This research aims to;

1. Develop a mathematical model that represents dynamics of plasma generated by a PF device.
2. Understand the meaning of mass swept factor and current factor from finite element simulation results.

1.4 Beneficial Outcome

It hopes that;

1. The mathematical model can explain behavior of plasma generated by different PF device configurations.
2. The mathematical model can be used to predict plasma characteristics from different types of PF device. It can also be used to optimize PF parameters for different applications such as ions source, EUV radiation source, fusion experiment and material's modification.

1.5 Thesis Structure

The thesis is arranged into 5 chapters. The next chapter, Chapter 2 will explain in detail theory of Lee model, related plasma physics and electromagnetic theories used by the simulation software. Chapter 3 will describe experimental methodology and set up, as well as plasma diagnostics technique used in experimental measurement, simulation of Lee model, and application of the simulation software in simulating the plasma process in a PF device. The discussion of the results obtained will be presented in Chapter 4. Final concluding remarks and suggestion of further work will be presented in Chapter 5.

CHAPTER 2
PLASMA DYNAMICS MODEL

This chapter will present the model of plasma dynamics that can be used to describe the movement of the plasma sheath in a PF device. One model that bases on a macroscopic assumption is the Lee Model. This model has been introduced in previous chapter and it has been widely used by many researchers. Another model that is the main focusing point of this thesis is a microscopic model that uses finite element method to calculate plasma characteristics. Each model will consider plasma characteristics such as average speed of plasma, plasma density variation with time and plasma temperature variation with time. In order to verify the result from simulations, experiments on UNU/ICTP PF were carried out. The next chapter will describe the diagnostic tools that have been used in the experiment. Electrical energy and average speed of plasma sheath were calculated from the signal obtained by electric probes and magnetic probes.

Plasma temperature and Plasma density will be computed by Lee model and the finite element simulation, these results will be shown in Chapter 4.

2.1 Lee Model

Plasma dynamics in PF device can be classified into 4 phases as mentioned in Chapter 1. Lee model also follows this classification namely; the breakdown phase, axial phase, radial phase and emission phases [10]. This is shown in Figure 2.1. However, in this work only axial phase of Lee model is considered as it is widely accepted.

In the axial phase, the plasma current sheath is assumed to be a thin sheath of plasma and the friction with wall is neglected. The model is based on a snowplow model, also known as slug model. This thin sheath of plasma will be driven by Lorentz force $\vec{J} \times \vec{B}$, where $\vec{J}$ is the plasma current and $\vec{B}$ is the induced magnetic field from the input current discharge [10, 34].

The plasma slug is created by the movement of plasma sheath as its speed is more than the speed of the ambient gas. A shock front is also assumed to be created when the plasma sheath sweeps mass of the ambient gas at a very fast speed. The diagram of the model is shown in Figure 2.2.

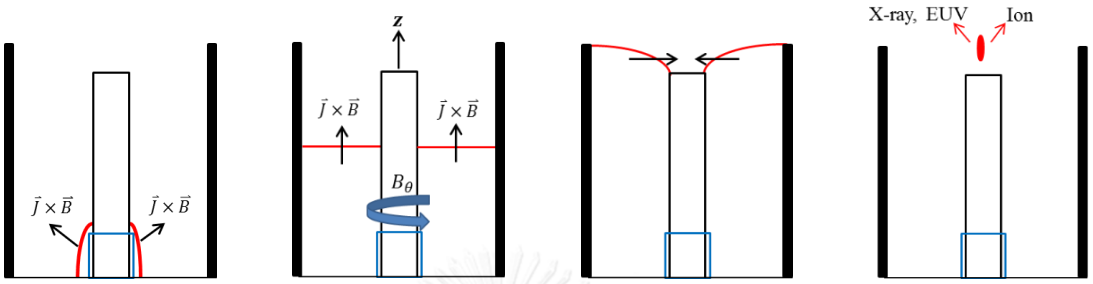

(a) (b) (c) (d)

Figure 2.1: Diagram showing phases of plasma dynamics: (a) Breakdown phase, (b) Axial phase, (c) Radial phase, and (d) Pinch phase.

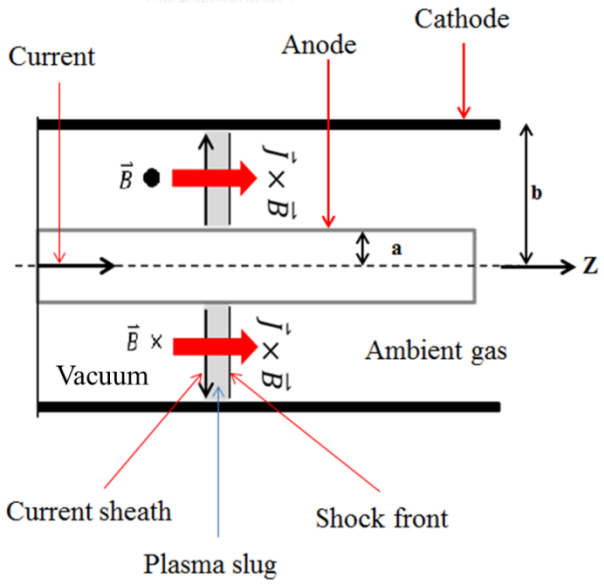

Figure 2.2: Diagram showing Lorentz force acting on the plasma sheath moving along the anode in a PF device [34].

The dynamics of the plasma sheath that sweeps mass of ambient gas in front of the sheath can be represented by a set of mathematic equations. Components of plasma sheath are assumed to composing of plasma slug, shock front surface, and current sheath as mentioned.

The plasma slug and shock front is generated by the high speed of the plasma sheath which increases by the magnetic pressure.

The equation of motion of this model based on the second law of Newton [10] is presented in Equation 2.1 as follow;

$$\frac{d(m\vec{v})}{dt} = \vec{F}_B, \tag{2.1}$$

where

$m = f_m \rho_o \pi (b^2 - a^2) z,$

$F_B = \int_a^b \frac{B^2}{2\mu_o} 2\pi r dr,$

$B = \frac{\mu_o f_c I}{2\pi r},$

$\rho_o = \frac{P_o M}{R T_0},$

The plasma slug is created by the fast motion of the plasma sheath that its speed exceeds the speed of the ambient gas [34]. The mass swept factor is assumed to be the ratio of the mass of plasma slug and the total mass of plasma. The current factor is the ratio of the current between electrode and the input current, and these variables are investigated and presented in Chapter 4.

By substituting the magnetics force F_B, mass of the plasma slug m and the magnetic field B into Equation 2.1, thus the equation can be rewritten as;

$$\frac{d}{dt}\left(f_m \rho_o \pi (b^2 - a^2) z \frac{dz}{dt}\right) = \int_a^b \frac{1}{2\mu_o} \left(\frac{\mu_o f_c I}{2\pi r}\right)^2 2\pi r dr. \tag{2.2}$$

By rearranging and integrating the right hand side of Equation 2.2, then the equation can be modified to be in a form of second derivative of the position. This is shown as;

$$\frac{d^2z}{dt^2} = \frac{\frac{{f_c}^2}{f_m}\frac{\mu \ln\frac{b}{a}}{4\pi^2\rho_o\left(\frac{b^2}{a^2}-1\right)}\left(\frac{I}{a}\right)^2-\left(\frac{dz}{dt}\right)^2}{z}. \qquad (2.3)$$

Since the plasma sheath is driven by a current discharged from a capacitor bank, LCR circuit equation can be used.

The circuit diagram is shown in Figure 2.3. In the beginning, the charging voltage V_o is stored in a capacitor bank with capacitance C_o as shown in the circuit. After the charging voltage is raised to an operating voltage, and the spark gap switch is closed, then the charges stored in the capacitor bank will flow to the plasma focus device and the plasma itself will become part of the circuit.

From this diagram, the current is estimated by using the circuit equation based on Kirchhoff's law. This can be represented by Equation 2.4.

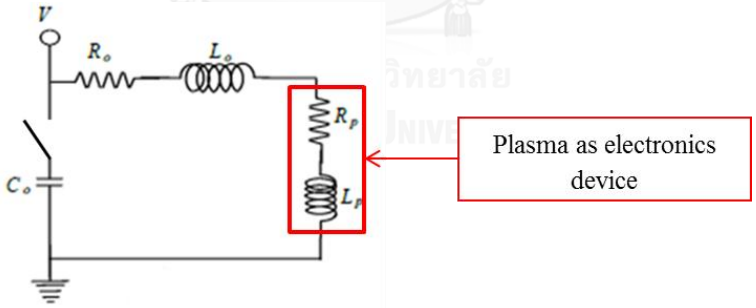

Figure 2.3: Circuit diagram of a PF device [34].

$$V_o = \frac{d(L_P+L_O)f_cI}{dt} + f_cI(R_P+R_o) + \frac{q}{C_o}. \qquad (2.4)$$

The plasma in the PF device is assumed to have both resistance R_P and inductance L_P as shown in the circuit diagram. However, the plasma resistance R_P and the resistance of the circuit R_o can be neglected as the voltage across the inductance would be larger, therefore the circuit equation can be rewritten as;

$$V_o = \frac{d(L_P+L_o)f_c I}{dt} + \frac{q}{C_o}, \tag{2.5}$$

where

$L_P = \frac{\mu_o f_c z}{2\pi} \ln \frac{b}{a}$.

Equation 2.5 can be rewritten as the rate of change of the current by substituting the inductance of plasma as shown by Equation 2.6. The voltage of the PF device can be represented by the voltage different across the plasma resistance R_P and the plasma inductance L_P. This is shown by Equation 2.7.

$$\frac{dI}{dt} = \frac{V_o - \frac{q}{C_o} - \frac{I f_c \mu}{2\pi}(\ln(\frac{b}{a}))\frac{dz}{dt}}{L_0 + \frac{f_c \mu z}{2\pi}(\ln(\frac{b}{a}))} \tag{2.6}$$

$$V = \frac{d(L_P+L_o)f_c I}{dt} \tag{2.7}$$

During the axial phase, the energy of the plasma generated by the magnetics pressure is expected to be increased. The plasma temperature depends directly with this energy thus different species of ions are created. Species of ions generated by this energy can be estimated by using Corona Equilibrium (CE) model [35]. CE model is the model that commonly used to calculate plasma characteristics such as electron densities and density of ion species of plasma in the sun.

The detail of the CE model can be found in my previous work [36]. The density of ion species can be shown as a function of plasma temperature as;

$$\frac{N_{i+1}}{N_i} = 1.27 \times 10^8 \frac{1}{{\chi_i}^2} \left(\frac{T_{eV}}{\chi_i}\right)^{\frac{3}{4}} \exp\left(-\frac{\chi_i}{T_{eV}}\right). \quad (2.8)$$

and, the fraction of ions α_i is written as;

$$\alpha_i = \frac{N_i}{N}. \quad (2.9)$$

From Equation 2.9, the fraction of ions of different species at different plasma temperatures can be shown as in Figure 2.4.

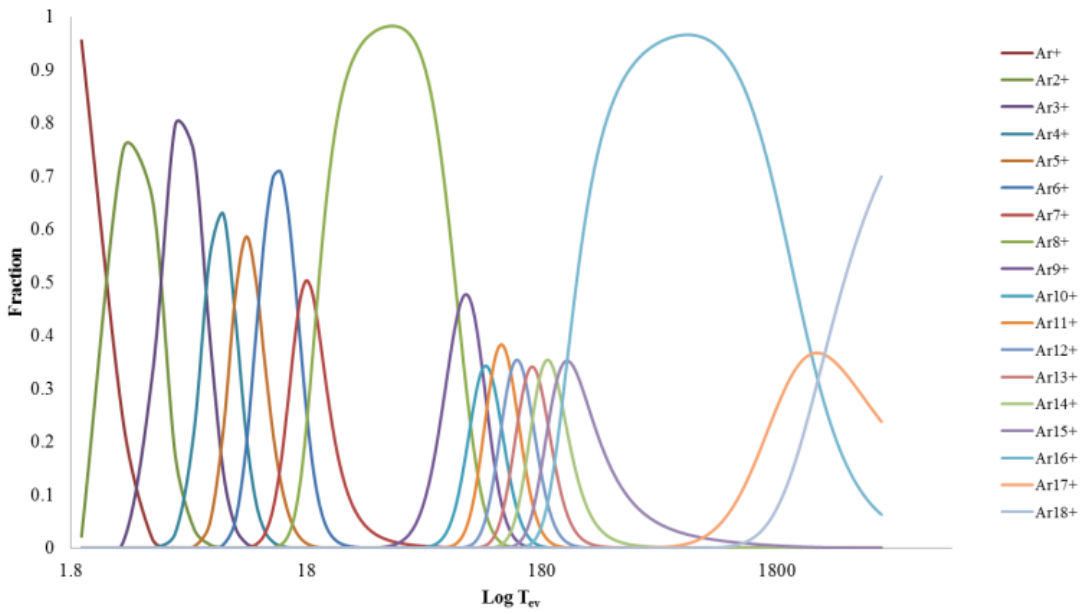

Figure 2.4: Plot showing fractions of argon species from Ar^+ to Ar^{18+} at different plasma temperature.

From the fractions of ions α_i in the state i, the effective charge shown in Equation 2.10 is also evaluated by the averaging charge of ions, and it can be shown by;

$$Z_{eff} = \sum_{i=1}^{Z} i(\alpha_i). \quad (2.10)$$

The effective charge is also used to calculate the plasma temperature according to Equation 2.11. The plasma temperature is shown to be dependent directly on the plasma speed.

$$T = \frac{M(\gamma-1)}{R(\gamma+1)^2(1+Zeff)}\left(\frac{dz}{dt}\right)^2. \quad (2.11)$$

2.2 Finite Element Model

In this section, simulation of the dynamics of plasma is described by electromagnetic theory and transport theory [37-39]. The simulation results will be compared with both experimental results and results obtained from Lee model. The mass swept factor and current factor which are used in Lee model will be investigated from this microscopic simulation process. In Chapter 3, the detail steps of the finite element simulation will be explained.

COMSOL Multiphysics is the simulation program which is used to simulate the dynamics of plasma by interfacing between plasma theory and electromagnetics theory. Simulation method of this program uses both the plasma theory and electromagnetics theory to determine physical properties of plasma, and finite element method is used to compute variables of the dynamics as a function of density of ion and density of electron in space.

The first theory considered is electromagnetic theory, and this theory was conducted to calculate Lorentz's force and electrical energy which cause the plasma dynamics moving of the plasma, and transport theory is used to compute properties of plasma such as conductivity of plasma, dynamics variables as plasma speed, position of plasma motion etc.

2.2.1 Electromagnetics Theory

The PF device is a device which generates both electric field and magnetic field. These fields interact to produce electromotive force that accelerates the plasma. Plasma is known to be quasi-neutral and consists of both positive and negative charges. Therefore the electric field in the medium can be evaluated by using Poisson's equation. This is written as;

$$\vec{\nabla}.\vec{E} = \frac{\rho_v}{\varepsilon}. \qquad (2.12)$$

Charge density in the plasma medium is generated by the breakdown process of the gas. The charge density shown in Equation 2.12 can be written as;

$$\rho_v = e * (n_e - n_i). \qquad (2.13)$$

In the PF device, the plasma is represented by an inductance L_P and a resistanceR_P. The plasma focus device is shown schematically in Figure 2.5.

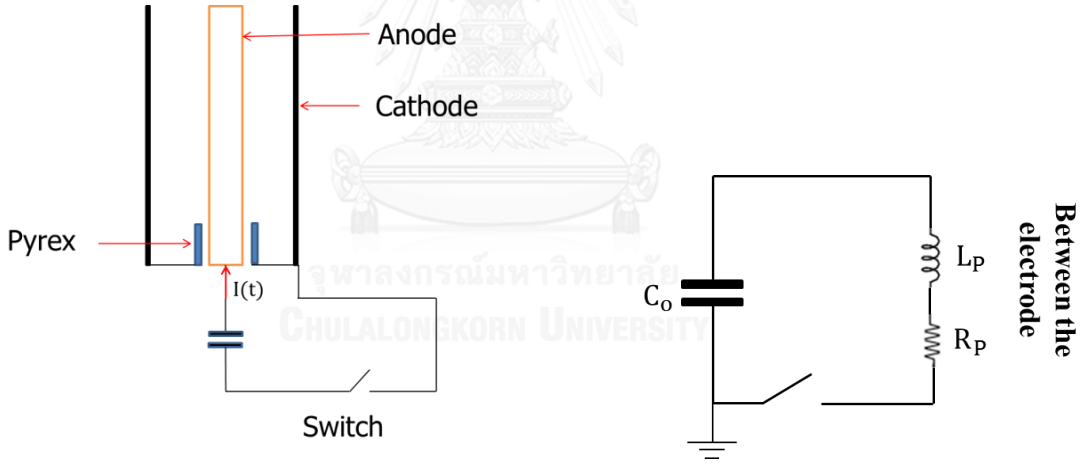

(a) (b)

Figure 2.5: (a) Diagram showing the component of a PF device and the input current I(t). (b) Equivalent electrical circuit of the PF device used in the finite element simulation.

The current of the circuit is described by Equation 2.14, and the general solution of current is given by Equation 2.15.

$$V_o = \frac{d(L_P I)}{dt} + I(R_P) + \frac{q}{C_o}. \quad (2.14)$$

$$I(t) = I_o \sin(\sqrt{\frac{1}{L_P C_o}}\, t). \quad (2.15)$$

From Equation 2.15, the methods of evaluating the inductance of plasma L_P and the maximum current I_o will be shown Chapter 3. These variables are calculated by fitting with the previous data [2].

The current density between the electrodes $\vec{J}$ can be calculated using the expression of current given by Equation 2.15. The value of current density is then be used to estimate the Lorentz force and the energy lost due to joule heating effect by using Equation 2.16.

$$\vec{J} = (\sigma + \varepsilon \frac{\partial}{\partial t})\vec{E} + \vec{J}_e. \quad (2.16)$$

The magnetic field induced by the current can be calculated by using Maxwell-Ampère's Law [40]which can be written as;

$$\nabla \times \frac{\vec{B}}{\mu} = \sigma\left(\vec{E} + \vec{v} \times \vec{B}\right) + \vec{J}_e. \quad (2.17)$$

From the simulation, the magnitude and the direction of the electric field can be illustrated as shown in Figure 2.6.

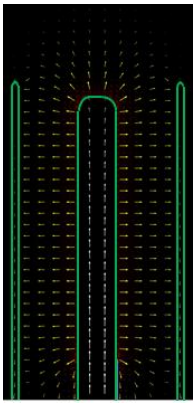

Figure 2.6: Diagram showing the electric field (yellow arrow) and the current (white line) inside the PF device.

The conductivity of plasma σ is a one of the important variable which determines the creation of electrons and ions from plasma by Joule heating. Calculation of the plasma conductivity based on the property of plasma will be explained in the following section.

2.2.2 Plasma Theory

In the finite element simulation, the plasma interaction is incorporated into the calculation. For argon plasma is investigated in this research, possible interaction channels of argon atom and electron used by the simulation software are shown in Table 2.1

Table 2.1 Types of particle reaction in the process of plasma generation.

Reaction	Formula	Type
1	$e + Ar \rightarrow e + Ar$	Elastic collision
2	$e + Ar \rightarrow e + Ar^*$	Excitation
3	$e + Ar^* \rightarrow e + Ar$	Super elastic collision
4	$e + Ar \rightarrow 2e + Ar^+$	Ionization
5	$e + Ar^* \rightarrow 2e + Ar^+$	Ionization
6	$Ar^* + Ar^* \rightarrow e + Ar + Ar^+$	Penning ionization
7	$Ar^* + Ar \rightarrow Ar + Ar$	Metastable quenching

Ar^* is referred an excitation state of Argon atom.

From Table 2.1, the probability of different types of plasma reaction is calculated by using the cross section data [41]. These particle interaction processes are considered to be the foundation of the microscopic system. In reality, plasma composes of electrons, ions and neutral particles, and in a PF device these particles are subjected to the effect from both electric field and magnetic field. They are moved by Lorentz force, thus it is necessary to consider further the transport theory of electrons and ions. These are explained in the following sections.

2.2.2.1 Electrons Transport Theory

Electron transport theory, the dynamics of plasma is estimated by using diffusion theory of ions, electron and neutral particles.

The electrons diffusion can be explained by number density and energy number density of electron. These can be written as;

$$\frac{\partial n_e}{\partial t} + \nabla.\overrightarrow{\Gamma_e} = R_e - \vec{u}.\nabla n_e, \tag{2.18}$$

$$\frac{\partial n_\varepsilon}{\partial t} + \nabla.\overrightarrow{\Gamma_{en}} + \vec{E}.\overrightarrow{\Gamma_{en}} = S_{en} - \vec{u}.\nabla n_\varepsilon + (Q), \tag{2.19}$$

where

$\overrightarrow{\Gamma_e} = -\left[n_e\left(\mu_e\left(\vec{E}\right)\right) + \nabla(D_e n_e)\right]$,

$\overrightarrow{\Gamma_{en}} = -\left[n_\varepsilon\left(\mu_{en}\left(\vec{E}\right)\right) + \nabla(D_{en} n_\varepsilon)\right]$,

$\nu_m = \frac{m_e}{m}\frac{Z^2 e^4 n_e}{(2\pi)^{\frac{1}{2}} 3\pi\epsilon_0^2 m_e^{\frac{1}{2}} (K_B T_e)^{\frac{3}{2}}}$,

$\mu_e = \frac{e}{m_e \nu_m}$,

$D_e = \frac{k_B T_e}{m_e \nu_m}$,

Considering the electron creation rate R_e and the energy loss/gain from inelastic collisions S_{en}, which are taken from reactions in Table 2.1. This is used to calculate the number density of electrons.

Dynamics of electrons can be represented by the diffusion process which is used to calculate the conductivity σ, of the plasma. This is also used for calculation of the current density of plasma between the electrodes as shown Equation 2.16. The conductivity can be written as;

$$\sigma = e n_e \mu_e. \tag{2.20}$$

This conductivity is also linked to the electromagnetic theory. It is used for the calculation of current density by substituting into Equation

2.16. Similarly, it is used for magnetic field calculation in Equation 2.17.

The average kinetic energy of electrons can be understood in term of electron temperature calculated from Equation 2.21 as;

$$\frac{n_\varepsilon}{n_e} = K_B T_e. \quad (2.21)$$

The total heat related to the energy density from Joule heating of plasma, can be written as;

$$Q = \vec{J}.\vec{E}. \quad (2.22)$$

From the wall boundary, the electrons are constrained by the following assumption;

- A net electron flux from the plasma bulk resulted in the lost of electrons to the wall.
- The electron at the wall is lost if it is within the distance of one mean free path of the wall.
- Secondary emission from the wall is the main factors for the gain of electrons.

However, the complete plasma dynamics must include the movement of ions species, since ions are generated by collisions processes mentioned in Table 2.2.

The movement of ions is represented by transport equation of ions as well as neutral gas molecules. In our case, they are argon atom and ions.

2.2.2.2 Ions and Neutral Gas Transport

In the plasma that is composed of many species of ions, and the number density of each species can be calculated by the continuity equation which has a source term for each species. The source term can be estimated by the particle reactions which are shown in Table 2.1. The equation of ionic reaction can be presented by;

$$\rho\left(\frac{\partial w_k}{\partial t} + \vec{u}.\nabla w_k\right) = \nabla.\overrightarrow{J_k} + R_k\ , \quad (2.23)$$

where
$\overrightarrow{J_k} = \rho w_k \overrightarrow{V_k}$.

The diffusion velocity $\overrightarrow{V_k}$ is computed by Equation 2.24, and it is related to Lorentz force that is the cause of plasma dynamics;

$$\overrightarrow{V_k} = D_k \frac{\nabla w_k}{w_k} + D_k \frac{\nabla M_n}{M_n} + \frac{{D_k}^T}{\rho w_k} \frac{\nabla T_i}{T_i} - Z_k \mu_k \left(\vec{E} + \vec{u} \times \vec{B}\right). \qquad (2.24)$$

The motion of plasma is now determined by diffusion velocity which will be shown in Chapter 3.

The ion temperature can also be found from its kinetic energy. This can be computed by using Equation 2.25 below;

$$T_i = T_0 + \left(\frac{M_k + M_n}{5M_k + 3M_n}\right) \frac{M_n}{k_B} \left(\mu_k (\vec{E} + \vec{u} \times \vec{B})\right)\left(\mu_k (\vec{E} + \vec{u} \times \vec{B})\right). \qquad (2.25)$$

The finite element simulation is aimed to imitate the dynamics of particles in the plasma. It is expected to explain the movement of the plasma in a microscopic manner. In contrast, Lee model does not imitate the movement of plasma microscopically as a solid plasma sheath is assumed. Moreover, Lee model only consider magnetic field, where in reality a PF device generate both electric field and magnetic field simultaneously. These fields cause movement of charge particles in the plasma.

The results of simulation software are shown in Chapter 4, and the implementation of this program is presented in Chapter 3.

CHAPTER 3
EXPERIMENT AND SIMULATION

In this chapter, the experiment performed on UNU/ICTP PF device is described. The first section explains both experimental setup and diagnostics used for necessary plasma characteristic measurement. The next section then, explains the calculation process of Lee model. The model is used to calculate average plasma speed, plasma energy, plasma temperature, and density of plasma. The results will be shown in Chapter 4. The last section describes the setup and processes employed in the finite element simulation using COMSOL Multiphysics where the plasma dynamics are simulated microscopically.

3.1 Experiment and Diagnostics

The experiment performed on UNU/ICTP PF device in this work is based on a standard operation of 3.3kJ UNU/ICTP PF with argon as the operating gas. Discharge current and the voltage across the electrodes provide the discharge characteristic of a particular device setup and operating conditions. In our case the only variable is the operating pressure. These characteristics are, then, used for comparative work with both Lee model and the finite element simulation.

The diagnostic tools used for detecting signals from the PF device are designed and built specifically such that it can response to fast, high current and high voltage discharge. The voltage signal is measured by a high voltage probe, and the current signal is detected by using Rogowski coil. The movement of plasma is measured by magnetic probes. The signals from magnetic probes can be used to estimate the average plasma speed, and this speed is also compared with the simulation results. The details operation of these diagnostics are explained in Section 3.1.2

3.1.1 Experimental Setup

In this section, 3.3kJ UNU/ICTP plasma focus device described in Chapter 1 is used in the research. The radius of anode is 0.95 cm, and the length of anode is 16.0 cm. The capacity of the capacitor bank is 30 μF and the charging voltage is 12.5 kV. The distance between anode and cathode is 3.2 cm. The device used is as shown in Figure 3.1.

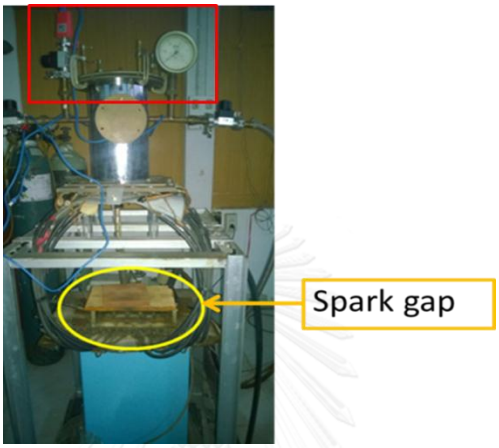

(a)

(b)

Figure 3.1: (a) Picture of the PF device sowing the spark gap. (b) Picture showing the configuration of electrodes where six cathodes are surrounding the central anode, and the base of the anode is covered by a glass insulator.

From Figure 3.1, the blue capacitor bank is connected to the spark gap switch. The spark gap switch is used to transfer the discharge current

from the capacitor bank to the electrode. The current flows from the capacitor bank to the electrode through multiple coaxial. Multiple coaxial cables are used to reduce the inductance of the system. The charger system used for charging the capacitor bank is built by using a variac, a step neon transformer and a half-wave rectifier diode network.

The transformer is able step the 220V mains voltage to 15kV. The charger system is shown in Figure 3.2

Figure 3.2: Picture of the charging unit used in the experiment.

Once the voltage of the capacitor bank is raised to the operating voltage at 12.5 kV then the current is discharged through the spark gap to flow into the electrodes. The spark gap is switched by using a fast triggering unit.

The gas control system comprises of a vacuum pump, pressure gauge and valves. The operating gas is argon. In this work, the operating pressure of 1.0 mbar, 1.5 mbar and 2.0 mbar are used. Argon gas is used as the operating gas because it is a single atomic gas. It is inert and its ionization process and energy are known.

The setup of this experiment is shown in Figure 3.3. The diagnostic tools are also shown in this picture. The signals that are detected in this experiment and calibration of the diagnostics is shown in the next section.

The dimension of electrodes are radius of anode a (0.95cm), distance from center of the anode to the cathode b(3.2 cm), length of anode z_o(16.0 cm). These are shown in Figure 3.4.

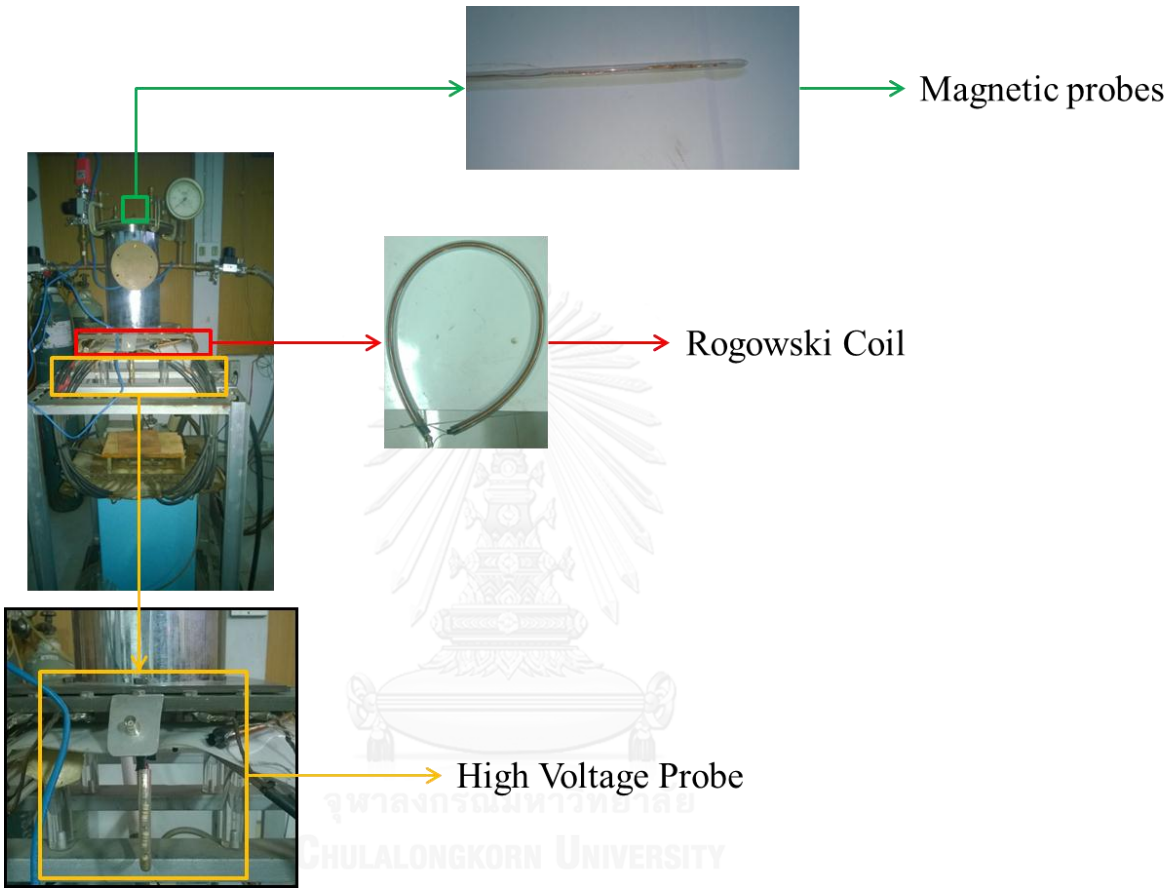

Figure 3.3: Picture of the PF device and the diagnostics used in the experiment.

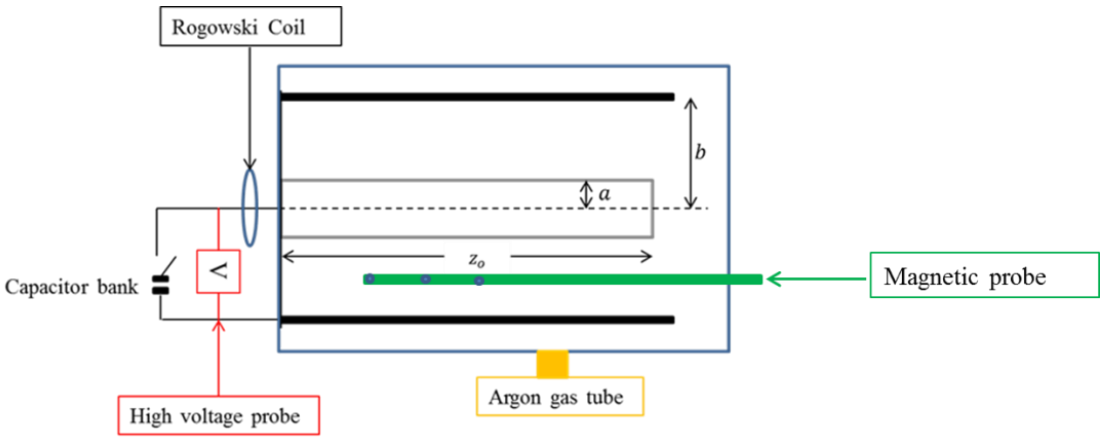

Figure 3.4: Diagram showing the experimental setup.

Figure 3.5 shows the schematic layout of experimental setup with operating conditions and related diagnostics. Samples of signal measured from the experiment can be seen in the Appendix I and Appendix II.

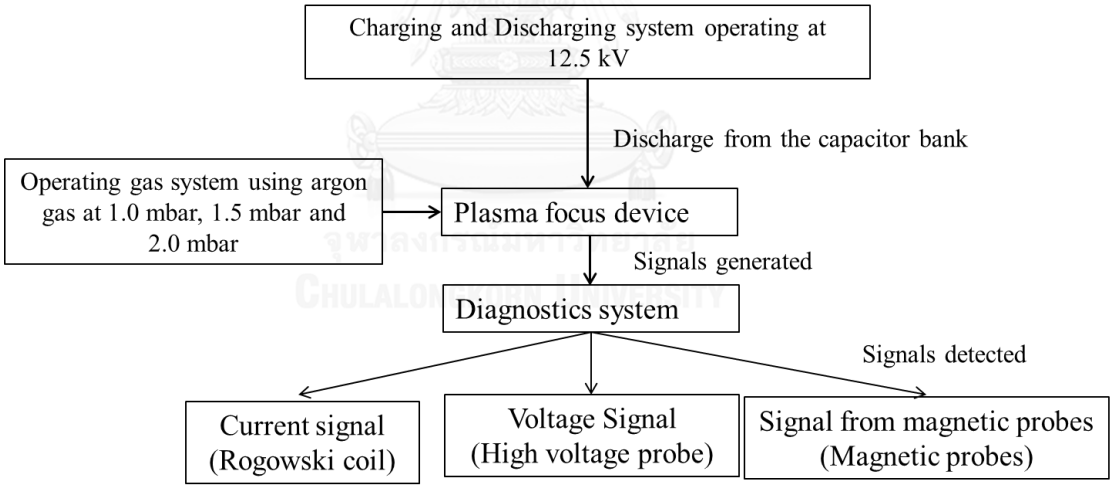

Figure 3.5: Schematic layout of operating conditions and measurements used in the experiment.

3.1.2 Diagnostics

The diagnostic tools for detecting signals from the PF device are designed and built specifically such that it can response to fast, high current and high voltage discharge. The voltage signal is measured by a high voltage probe, and the current signal is detected by using Rogowski coil. The movement of plasma is measured by magnetic probes. The details operation of these diagnostics are explained below.

3.1.2.1 Rogowski Coil

Rogowski coil is a toroidal solenoid coil consisting of many turns of copper wire. The end of the coil is shorted by a low resistance. This device is used to measure the discharge current flowing through the discharge circuit. The construction of the coil is shown schematically Figure 3.6.

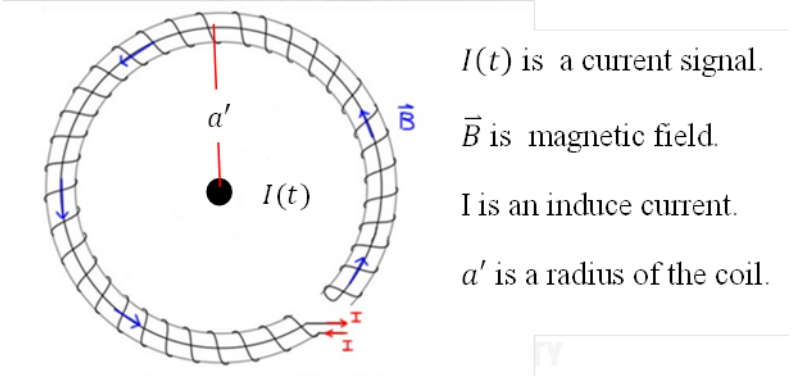

Figure 3.6: Diagram of Rogowski coil showing induced current generated from current through enclosed area of the coil [35].

Magnetic field and magnetic flux detected are calculated by using Ampere's law. The magnetic field induced by the discharge current can be expressed as;

$$B = \frac{\mu_o I(t)}{2\pi a'}. \qquad (3.1)$$

The magnetics flux is given by;

$$\emptyset = \left(\frac{\mu_o I(t)}{2\pi a'}(A)\right). \quad (3.2)$$

The induced voltage can be determined by differentiating Equation 3.2as shown in Equation 3.3.

$$V(t) = \frac{\mu_o A}{2\pi a'}\frac{dI(t)}{dt}. \quad (3.3)$$

By measuring this induced voltage, the temporal function of the rate of change of discharge current can be obtained. To get the time profile of the discharge current, the Rogowski coil can be operated either as current transformer by shorting the terminal of the coil with a small resistor, or by using RC integrator [35]

Rogowski coil needs to be calibrated before it can display value of current. The calibrating factor K is used to transform voltage unit into current unit. For calibration we make use of a sinusoidal current waveform which can be expressed in the form;

$$I = I_o e^{-\alpha t} \sin \omega t, \quad (3.4)$$

where

$I_o = V_o\sqrt{\frac{C_o}{L_o}}$,

$\alpha = \frac{R}{2L_o}$,

$\omega = \frac{2\pi}{T'} = \frac{1}{\sqrt{L_o C_o}}$,

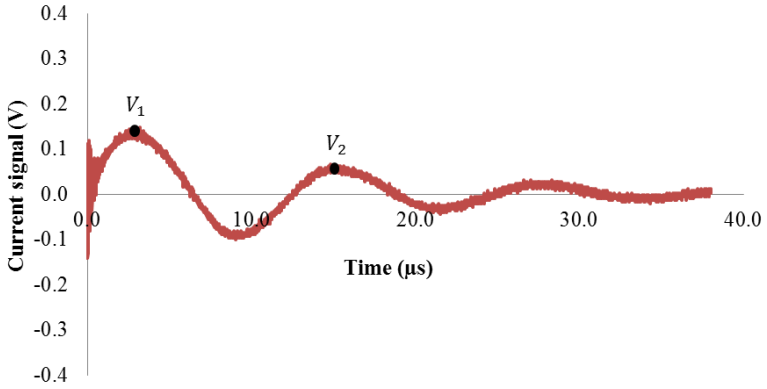

Figure 3.7: Graph showing current signal of argon gas under operating pressure 3 mbar.

Considering the current signal which is presented in the Figure 3.7, factor K can be determined by considering peaks from this graph as V_1 and V_2. By knowing the amplitude at V_1 and V_2, and the period of the signal, T factor K can be computed from; [35]

$$K = \frac{2\pi C_o V_o}{T V_1} \left(\frac{V_2}{V_1}\right)^{\frac{1}{4}} . \qquad (3.5)$$

In this work, current signals of operating pressure of 1.0 mbar, 1.5 mbar and 2.0 mbar are investigated. These signals is shown in Appendix I. These signals are also used to determining current factor and mass swept factor in Lee Model.

3.1.2.2 High Voltage Probe

The voltage signal is an important signal that shows characteristic of the dynamics of plasma especially from the breakdown phase to the pinching phase. The pinching phase happens when the voltage signal shoots up to a very large value as the circuit resistance increases. The circuit resistance increases due to the pinching process of the plasma therefore the conductivity between the electrodes reduces. Voltage signals measured between the anode and the cathodes.

The high voltage probe is connected to the digital oscilloscope for display and data recording.

The high voltage probe is a series of ten resisters. Each resister has a resistivity value of 500Ω. They are connected with one 50Ω resistor and the end of the probe where a BNC plug is connected. The diagram of the high voltage probe is shown by Figure 3.8.

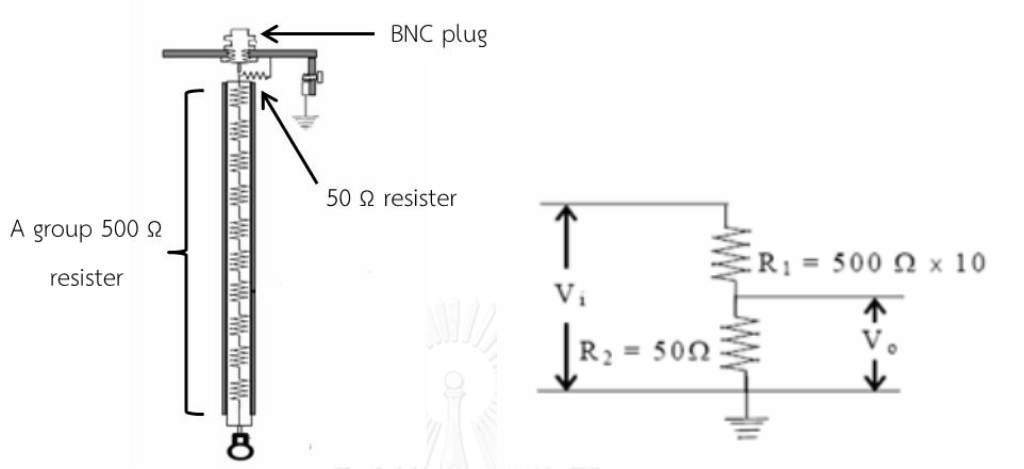

(a) (b)

Figure 3.8: (a) Diagram showing the configuration of a high voltage probe [35]. (b) Circuit diagram of the high voltage probe [35].

Since the high voltage probe is connected as mentioned, therefore the voltage is divided 100 time the original voltage signal. The relation of output voltage and the input voltage is $V_{out} = \frac{50}{500\times10+50} V_{in}$. Figure 3.9, shows the voltage signal measured when the PF device is operating with pressure of 1 mbar and 3 mbar. A large voltage spike that represents the pinching process can be observed for PF device operation with pressure of 1 mbar. No voltage spike is observed when operating at higher pressure. The signals of other operating pressures are presented in Appendix II.

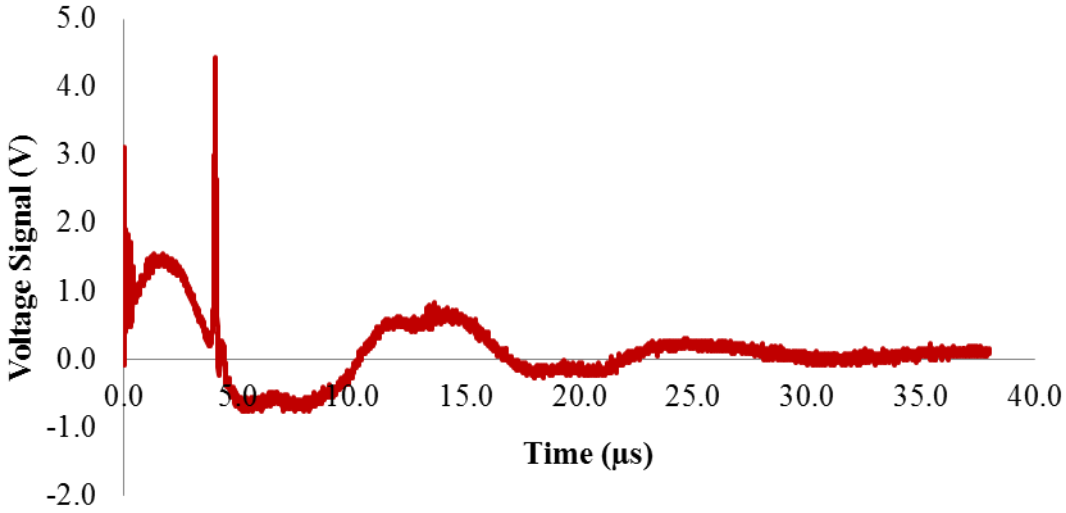

(a)

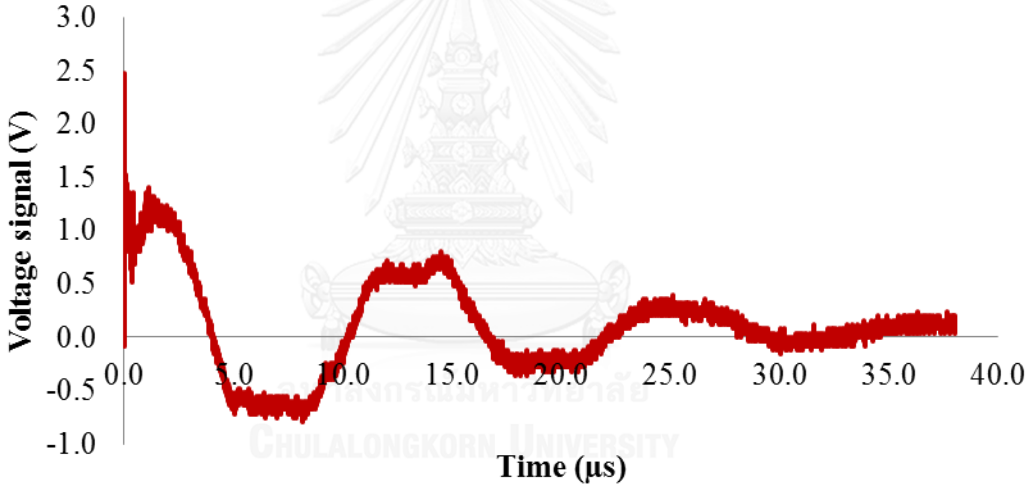

(b)

Figure 3.9: (a) Graph showing voltage signal under operating pressure of 1 mbar. (b) Graph showing voltage signal under operating pressure of 1 mbar.

3.1.2.3 Magnetic Probe

Since the plasma sheath moves at great speed, thus a possible measurement of the plasma speed at each position can be made by using magnetic probes. These probes are placed evenly apart, therefore it is

possible to measure the speed of the plasma sheath between each probed as the signal from the probe is produced at the same time that the plasma sheath is passing through.

Magnetics probe is a small solenoid multi-turn coil. In this research three coils are placed at 2 cm apart. The signal from the coil generated from the induce current when plasma sheath is moving pass the coil. This is the same operating principle as Rogowski's coil mentioned earlier. The signal from the magnetic coil is recorded and shown by a digital oscilloscope. A diagram of this probe is shown in Figure 3.10.

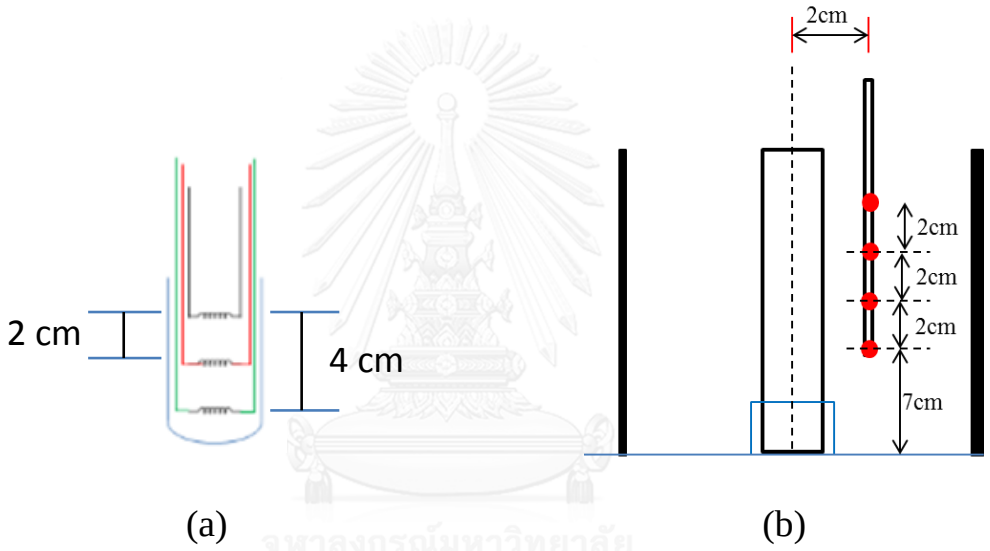

Figure 3.10: (a) Diagram showing of configuration of magnetic probes. (b) Diagram showing the setup of magnetic probes in a PF device.

The signal from the magnetic probes are shown in Figure 3.11. The average plasma speed can be estimated by considering where the signal rapidly increases or decreases. These are represented by the dash line in the figure.

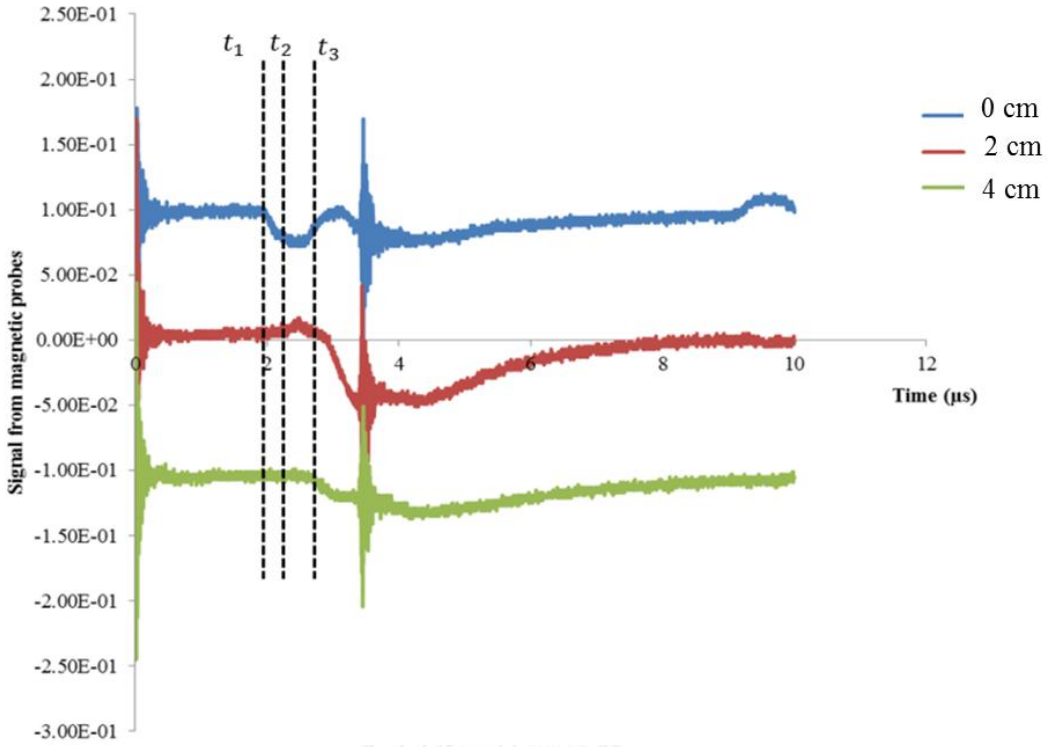

Figure 3.11: Graph showing signals from magnetics probes under operating pressure 1 mbar.

The average plasma speed can be calculated by;

$$v_{av} = \frac{\Delta z}{\Delta t}. \tag{3.6}$$

The experimental data which is detected by using these diagnostics tools will be used for comparison with simulation results from Lee model and the finite element simulation. These results obtained will be shown and discussed in Chapter 4.

3.2 Lee Model Simulation

From Lee model presented in Chapter 2, we are only interested in the axial phase. The average plasma speed, density of plasma, plasma temperature, and electric energy of electrode are plasma properties that can be calculate from Lee Model simulation. These results will be compared with the results obtained from the finite element simulation and experimental results mentioned earlier.

Table 3.1 shows initial condition that is applied for Lee model calculation.

Table 3.1 Initial condition for Lee model calculation**.**

Variables	**Initial value**
Time (t)	0 sec
Acceleration $(\frac{d^2z}{dt^2})$	$\sqrt{\frac{2{f_c}^2}{3f_m}\frac{\mu \ln\frac{b}{a}}{4\pi^2\rho_o a^2\left(\frac{b^2}{a^2}-1\right)}}$
Velocity of plasma $(\frac{dz}{dt})$	0 m/s
Position of plasma dynamics (z)	0 m
Derivative of current $(\frac{dI}{dt})$	$\frac{V_o}{L_o}$
Current (I)	0 A
Charge (q)	0 C

The calculation process of Lee model can be represented by a flow chart shown in Figure 3.12. The calculation ends when the position of plasma reaches z_0. In each step, the plasma speed, the position of plasma, plasma current, and plasma temperature are calculated.

This simulation is written in EXCEL program. The calculation is made once mass swept factor f_m and current factor f_c are adjusted. These are highlighted by the red square box shown in Figure 3.13.

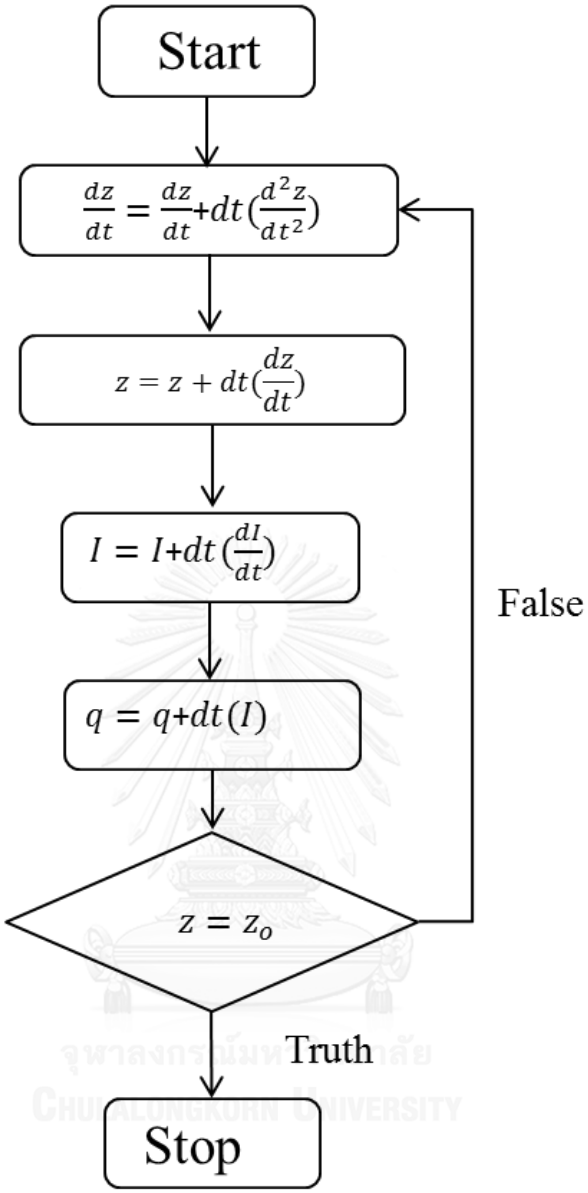

Figure 3.12 Flow diagram of Lee model calculation.

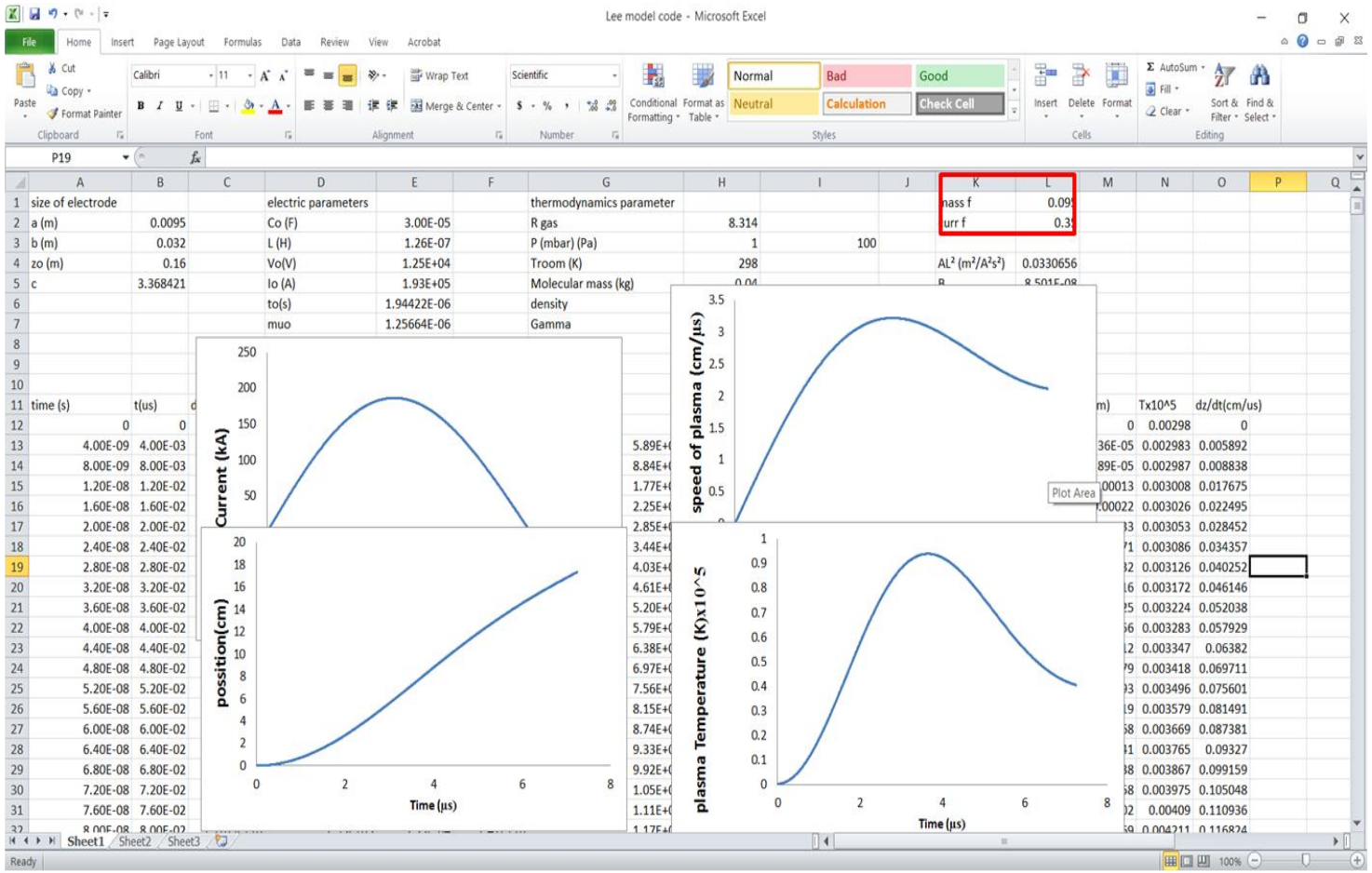

Figure 3.13: Picture of EXCEL worksheet showing computation of plasma position, circuit current, speed of plasma, and plasma temperature.plasma temperature.

Figure 3.14 shows fitting of the current signal from experiment to the current generated by Lee model calculation. The fitting only applies for the axial phase.

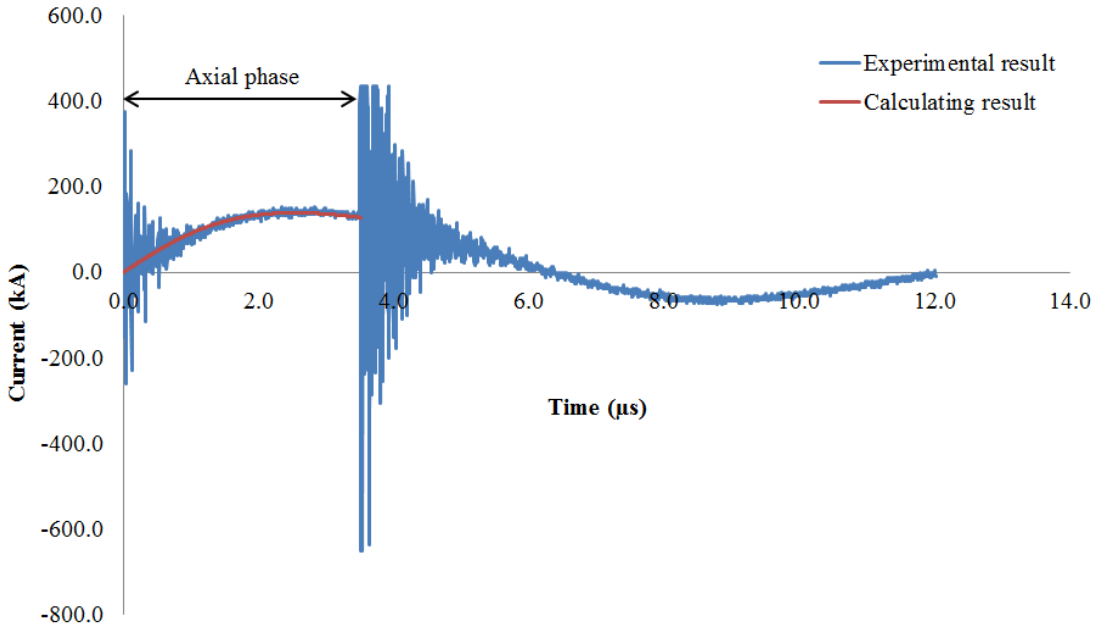

Figure 3.14 Graph showing current which are fitted with experimental data under the operating pressure of 1 mbar.

From the simulation results, the current factor f_c and mass swept factor f_m is estimated under operating pressure 1.0 mbar, 1.5 mbar and 2.0 mbar. These results are shown these values in Table 3.2.

Table 3.2 Values of mass swept factor and current factor estimated by fitting with experimental data.

Pressure (mbar)	**Mass swept factor f_m**	**Current factor f_c**	**Inductance of the circuit L_o (nH)**
1	0.0365 ± 0.0379	0.667 ± 0.288	124.0 ± 2.0
1.5	0.0293 ± 0.0208	0.412 ± 0.128	123.0 ± 1.0
2	0.0242 ± 0.004	0.362 ± 0.028	125.0 ± 3.0

The period from experimental data is also used to evaluate the inductance of the system. This can be written as;

$$T' = 2\pi\sqrt{L_o C_o}\ . \qquad (3.7)$$

3.3 Finite Element Simulation

COMSOL Multiphysics software is a software package that is uses finite element method to simulate physics phenomena. In this work, it is used to simulate the dynamics of plasma in a PF device. The fundamental theory of plasma that the software package uses has been highlighted in Chapter 2.

COMSOL Multiphysics software is a general-purpose software platform, based on advanced numerical methods, for modeling and simulating physics-based problems. This software has many physics module which is applied in research. In this work, plasma theory and electromagnetics theory are used to simulate the dynamics of plasma. These modules are part of many physics modules shown in Figure 3.15. Electromagnetics theory is found in AC/DC Module.

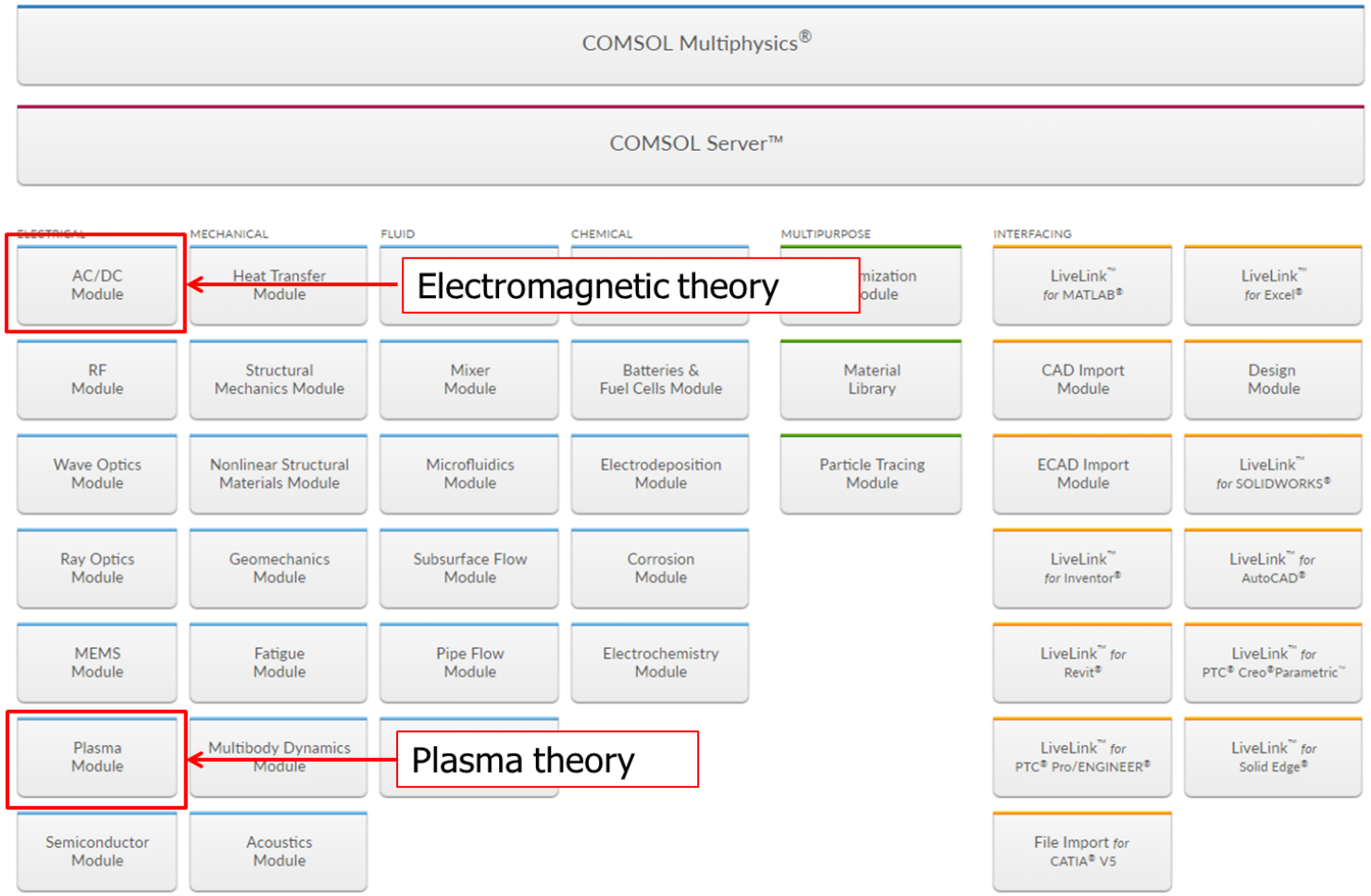

Figure 3.15: Diagram showing physics module available in the simulation

First step of the simulation is done by setting the geometry of the PF device as shown in Figure 3.1. Since the PF device is radially symmetrical, therefore it is possible to set the geometry function as “2D Axisymmetric”. This function is shown in Figure 3.16.

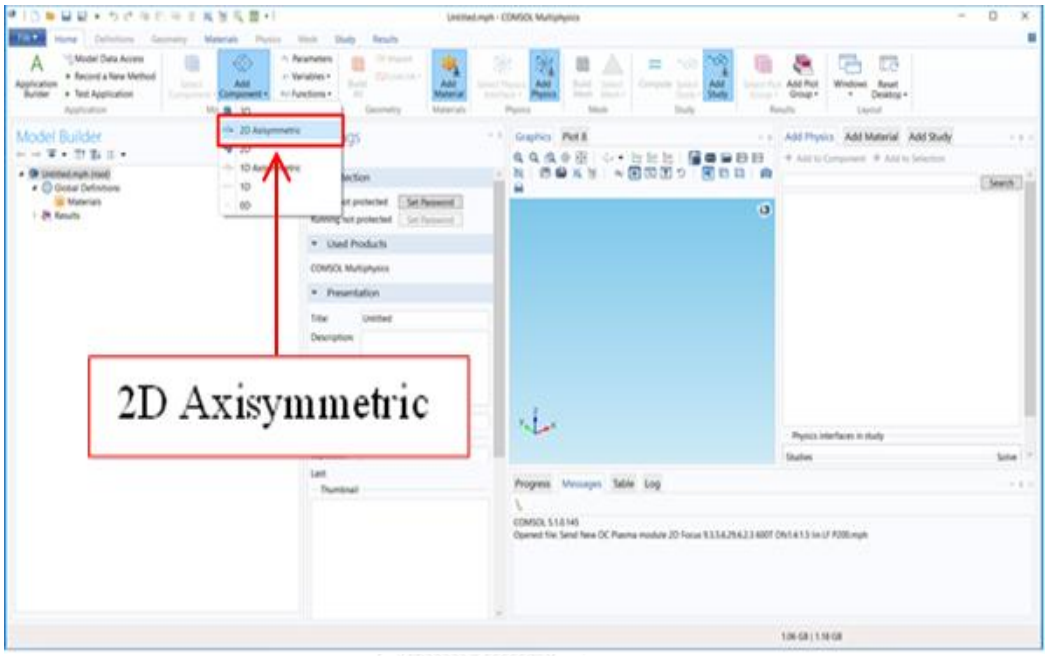

Figure 3.16: Picture showing function in the simulation software.

Second step is performed by configuring the PF device under “Geometry Function”. As the PF device is radially symmetrical therefore only one anode and one cathode in necessary for the simulation. The “Geometry function can” is shown in Figure 3.17. The PF device designed is shown as in the Figure 3.18.

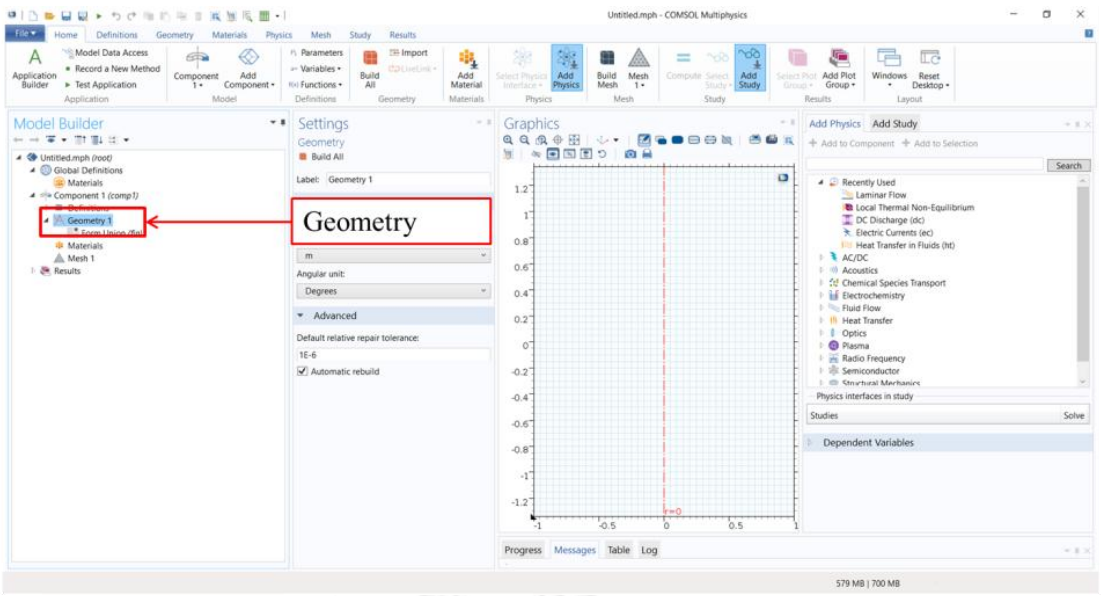

Figure 3.17: Picture showing geometry functions of the simulation software.

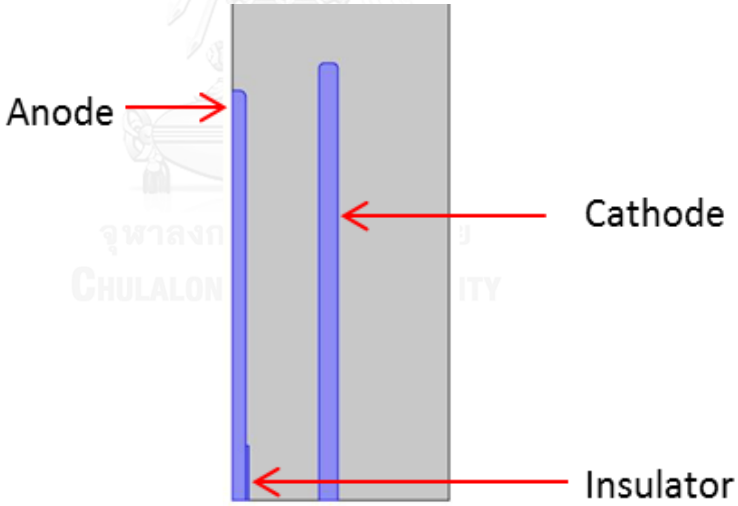

Figure 3.18: Diagram showing the geometry setup of PF device used for finite element simulation.

Table 3.3 shows the configuration of the PF device simulated where the actual size of the UNU/ICTP PF is used.

Table 3.3 Dimensions of the plasma focus device**.**

Machine composition	Size (cm)
Anode radius	0.95
Anode Length	16.0
Cathode radius	0.05
Cathode Length	17.0
Chamber radius	8.0
Chamber Length	30.0
Insulator thickness	0.1
Insulator Length	2.0

For the third step, material associated with the design is assigned to each component by using “Add Material” function which is presented in Figure 3.19.

Types of material assigned for the simulation is shown in Table 3.4. The material assign replicate the actual components of the UNU/ICTP PF device.

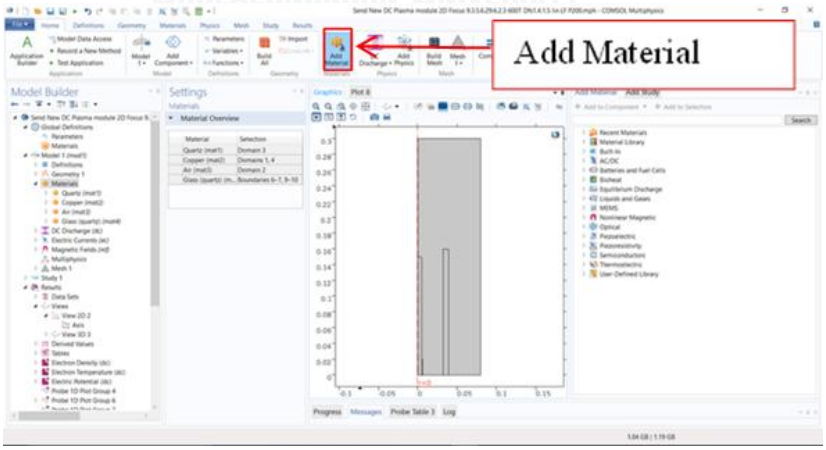

Figure 3.19: Picture showing “Add Material function” of the simulation software.

Table 3.4 Types of material used in the simulation of the plasma focus device**.**

Component	Material
Anode tube	Copper
Cathode tube	Copper
Insulator	Pyrex
Chamber tube	Blass coat
gas	Argon

Assigning types of material is important as each material has different electrical properties. The electric properties have effect on the dynamics of the plasma. For example, the plasma can only be generated when the voltage of the anode is higher than breaking down voltage of the gas.

Once all geometry and physical properties are set, then appropriate physics theories are chosen and used to calculate the dynamics of plasma. Operating process of the simulation is shown the diagram in Figure 3.20.

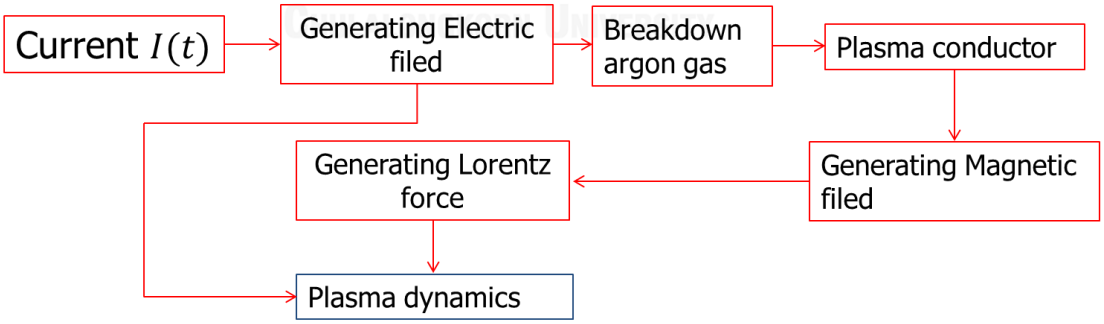

Figure 3.20 Flow diagram of the finite element simulation.

From Figure 3.20, plasma is generated by the ionization process between the electrodes. The input current $I(t)$ shown in Equation 2.15 is used to generate the electric field by charges that are stored on the surface of anode.

Once the voltage of anode is higher than the breakdown voltage of argon gas, the argon gas becomes ionized and plasma is formed. The plasma behaves like a conductor, and the current flow in the plasma. At the same time, the magnetics field is generated by the induced plasma current. The movement of plasma is caused by both the magnetic field and the electric field. The current and the magnetic field produce Lorentz force which causes plasma to move in the direction orthogonal to both current and the field.

Form the simulation software, the “Direct Current Discharge” (DC Discharge) module is used to simulate the initial plasma generation process. In this module, the dynamics of electrons and ions are simulated by using the transport theory. These particles collide with each other in the system.

“The Electric Current” module is also used for electric field calculation in the device. The electric filed is then used to calculate the Joule heating that causes further ionization of the argon gas. The “DC Discharge: module is linked to the module by the conductivity of plasma, and the current through the electrode.

The “Magnetic field” module is used to determine the Lorentz force that acts on plasma. This module is connected to the other modules also by the conductivity of plasma, and the current through the electrode. These physics modules are selected in the simulation software as shown in the Figure 3.21.

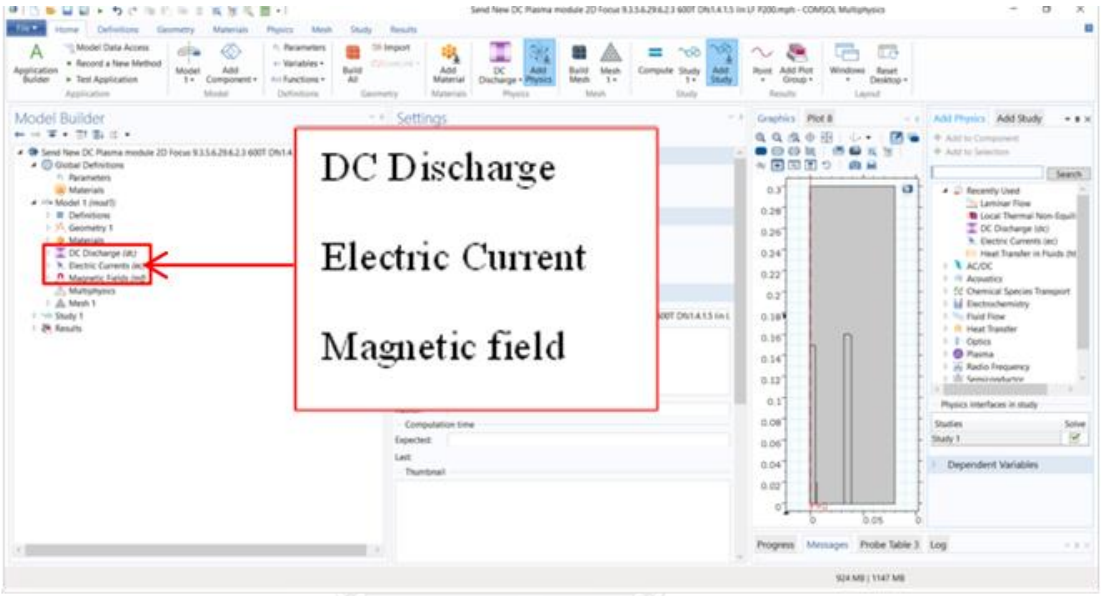

Figure 3.21: Picture showing relevant physics modules used in the simulation software.

From Equation 2.15, $I(t) = I_o \sin(\sqrt{\frac{1}{L_P C_o}}t)$ is used where the current amplitude I_o is 125 kA, L_P is 128 nH and C_o is 30 μF as obtained in actual experiment from previous research work [2].

Once initial setting up is completed, the simulation software uses finite element method to compute the parameters in each module. A spatial division or “mesh” must be specified.

The “mesh” is shown in Figure 3.22. Each mesh contains physics variables that have been previously mentioned.

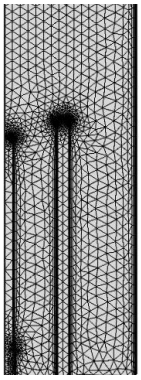

Figure 3.22: Diagram PF device geometry showing mesh used for finite element simulation.

The dynamics of the plasma can now be simulated. Pictures of the dynamics are shown in Chapter 4.

The current of plasma and voltage between electrodes simulated by using this software are shown in the Figure 3.22(a) and 3.22(b). The voltage and the current signals can be used to calculate the energy of plasma. The energy of plasma will be discussed in more detail in Chapter 4.

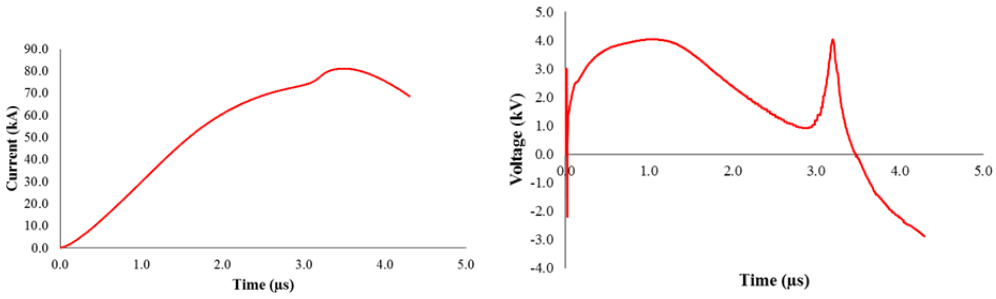

(a) (b)

Figure 3.23 (a) Graph showing voltage across electrodes varying in time. (b) Graph showing current between electrodes varying in time.

The change in the magnetic field at different positions can also be computed. These results imitate the measurement by the magnetic probe mentioned in Section 3.1.2.3. The result obtained is shown in Figure 3.23. The magnetic field profile can then be used to determine the average speed of the plasma that is moving along the z axis. The results will also be discussed more in Chapter 4.

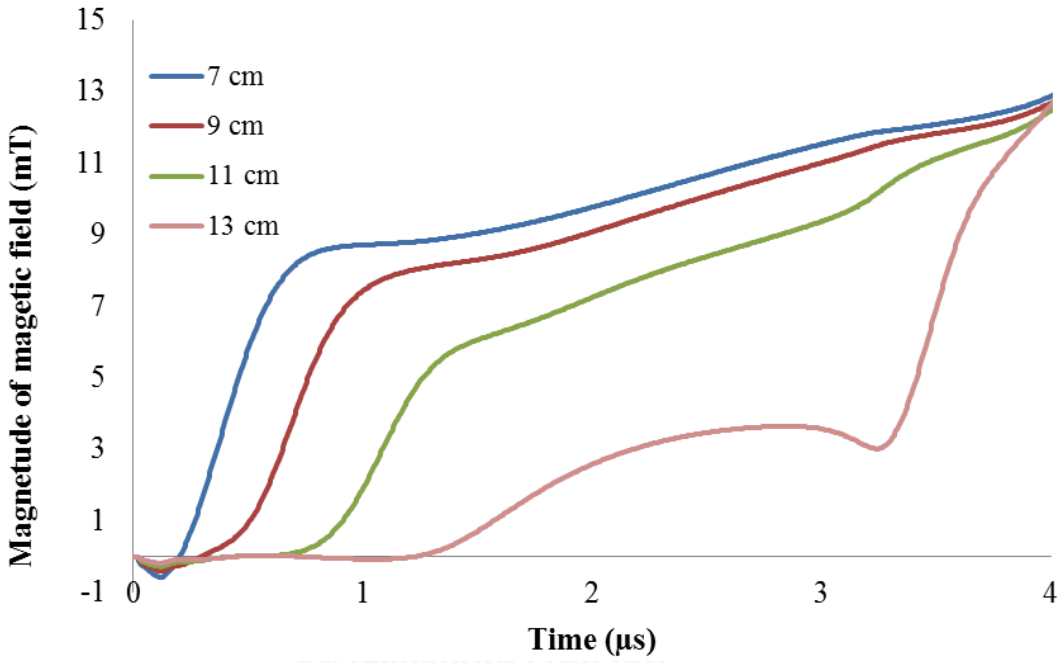

Figure 3.24: Graph showing magnitude of the magnetic field from plasma varying in time.

A diagram summarizes the scope of this research work is shown in Figure 3.24.

Both experiment and simulations are based on the operation of UNU/ICTP PF device. Charging voltage used to charge the capacitor bank is 12.5 kV. Argon gas at various operating pressures are investigated. These operating pressures are 1.0 mbar, 1.5 mbar, and 2.0 mbar.

The key measurements investigated in the research are current signal, voltage signal and magnetic signal generated by the movement of the plasma. Both current and voltage are used for calculation of electrical energy. The energy obtained experimentally is compared with the simulation results.

For Lee model, the current factor and mass swept factor are obtained by fitting of current signal obtained from experiment. Plasma temperature and the density of gas are compared with results obtained from the finite element simulation.

For the finite element simulation, the initial input current which is shown by Equation 2.15 is used. The magnitude of current I_0 and L_P is taken from previous research work [2].

The plasma theory and electromagnetics theory is used to calculate the plasma dynamics. The finite element method is used to construct the dynamics of plasma in the PF device.

In actual experiment, there are limitations in real measurement that can be made. Fast framing camera is required for capture image of plasma during all dynamic phases. Time resolved ions spectroscopy is needed to be able to determine species of argon ions and to observe changes when the plasma gains energy. These are sophisticated equipment and are not widely available. However, the results from our finite element simulation should be able to give some insight into the spatial distribution of plasma as well as the ions species at each different time.

However, there is a limitation to the current finite element simulation as the only argon interaction data consider is for Ar^+ therefore the result will not be accurate when the plasma has higher energy. In this research, the finite element simulation is only restricted to the breakdown phase and axial phase.

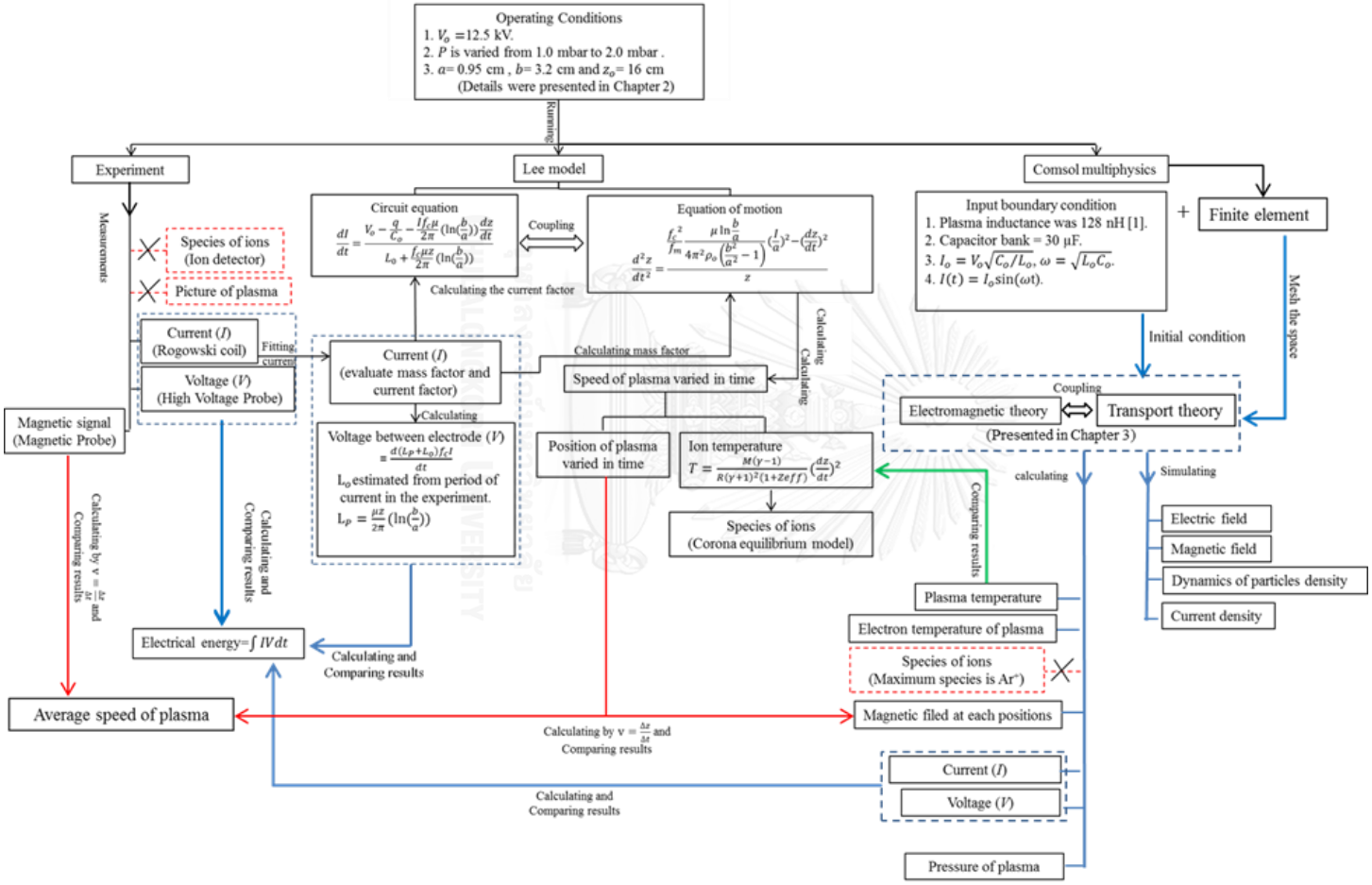

Figure 3.25: Diagram showing overview of experiment and simulations carried out in this research.

Different comparisons between experimental result, Lee model calculation and the finite element simulation will be discussed in the next chapter. Table 3.5 summarizes possible comparison that can be investigated.

Table 3.5 Summary of experimental and simulation results comparison**.**

Discussion results	**Experimental results**	**Calculation from Lee model**	**Simulation from COMSOL**
Comparing current and voltage results	✔	-	✔
Comparing average the plasma speed	✔	✔	✔
Comparing the energy of plasma	✔	✔	✔
Comparing temperature of plasma	-	✔	✔
Comparing pressure of plasma	-	✔	✔

In the next chapter, results and discussion are presented. Plasma energy, average plasma speed, and density of the plasma will be compared.

CHAPTER 4
RESULTS AND DISCUSSION

In this chapter, the results of experiments and simulations of the PF device will be presented. The dynamics of plasma under the operating pressure 1.0 mbar, 1.5 mbar, and 2.0 mbar are investigated. The results investigated are current signal, voltage signal, average speed of plasma, plasma density, plasma temperature, and the electric energy. These results are shown in each section below.

4.1 Current and Voltage Characteristics

As mentioned in Section 3.1.2, the current and voltage of the PF device are measured by Rogowski coil and the high voltage probe respectively. The results from the experiment and simulations are shown in Figure 4.1. It can be seen that the voltage signals measured from the experiments that operated with different operating pressure have peak voltage at different times. The lowest operating pressure at 1.0 mbar has the voltage peak the earliest which means the plasma reaches the pinching phase the quickest of all three. For 2.0 mbar, there is no voltage peak which means that the plasma does not pinch when the PF device is operated at this pressure.

However, the results from the finite element simulation show similar voltage signal profile. The peak voltage appears later as the operating pressure increases. Peak voltage can still be seen when simulating with operating pressure of 2.0 mbar.

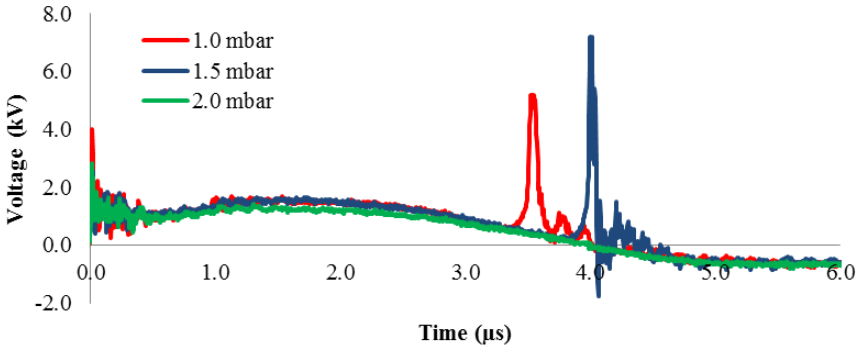

(a)

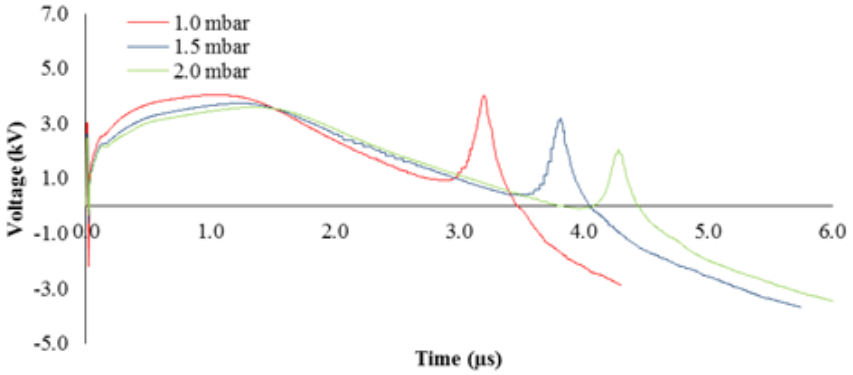

(b)

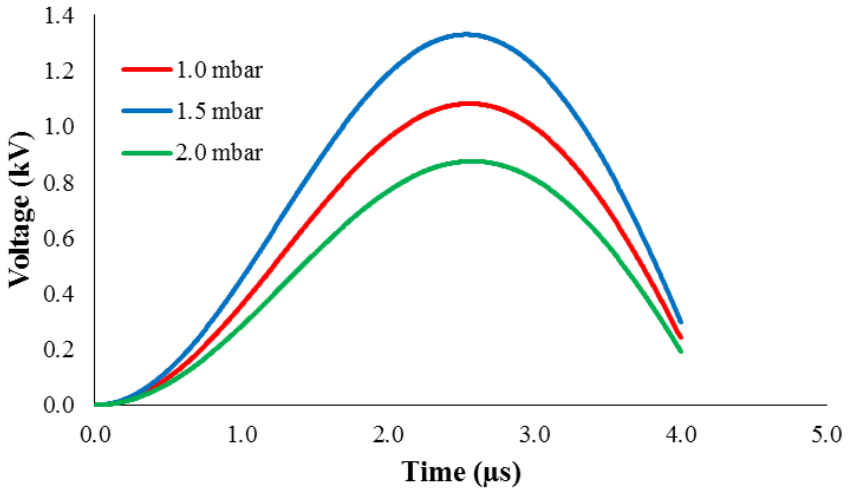

(c)

Figure 4.1: Graph showing voltage from (a) experiment (b) simulation (c) Lee model.

From Figure 4.1 (c), only the axial phase is investigated in the Lee model calculation. It is interesting to note that the voltage signal from the finite element simulation is not zero as shown in Figure 4.1 (b). As mention earlier, breaking down of the gas requires that he surface charge exceed certain potential. In our case, the voltage must be higher than the ionization energy of the argon atom. The ionization energy of the argon atom is 15.76 eV [40].

The voltage obtained by the finite element method is also higher than voltage measured from actual experiment. It is possible that in real experiment, we cannot get all charge transfer from the capacitor bank to the anode as the charge may be lost through the spark gap and electrical line. On the other hand, the voltage signal calculated from Lee model is lower than the result from the finite element simulation. Also the initial voltage starts from zero which is expected as this model does not consider the breakdown phase.

The time of the dynamics in our interest is from the breakdown phase to the end of axial phase. This represents the time before voltage spike occur. Figure 4.2 shows the voltage signal from experiment where a voltage spike is clearly identifiable. The voltage at breakdown moment is not zero. This corresponds to the voltage signal generated by the finite element simulation. Table 4 shows time taken to complete breakdown and axial phase for each different operating pressure.

This time from the breakdown phase to the end of axial phase can be shown in the Figure 4.2, and this time is shown the values in Table 4.1.

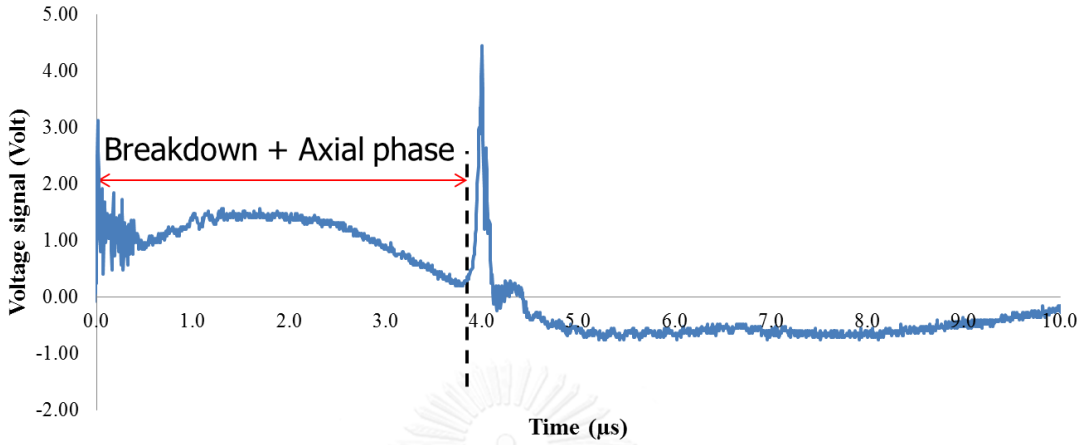

Figure 4.2: Graph of the voltage signal showing breakdown phase to the end of axial phase.

Table 4.1 Time taken from breakdown phase to pinch phase at various operating pressures.

Operating Pressure (mbar)	**The time at spike (µs)**	
	Experiment	**Finite Element Simulation**
1.0	3.51 ± 0.01	3.18
1.5	4.20 ± 0.10	3.78
2.0	-	4.26

We can see that the time taken to complete the two dynamics phases measured from the experiments are in agreement with the result from the finite element simulation that the time taken increases as the operating pressure is increased.

Increasing of operating pressure increases the collision probability of particles in the plasma; therefore the kinetic energy of plasma is transferred to the surrounding. This causes reduction in the speed of plasma, hence the longer the time to complete the phases.

Similarly by considering the current signal of the PF device, a comparison of the current measured from the experiment and the current generated from the finite element simulation is shown in Figure 4.3

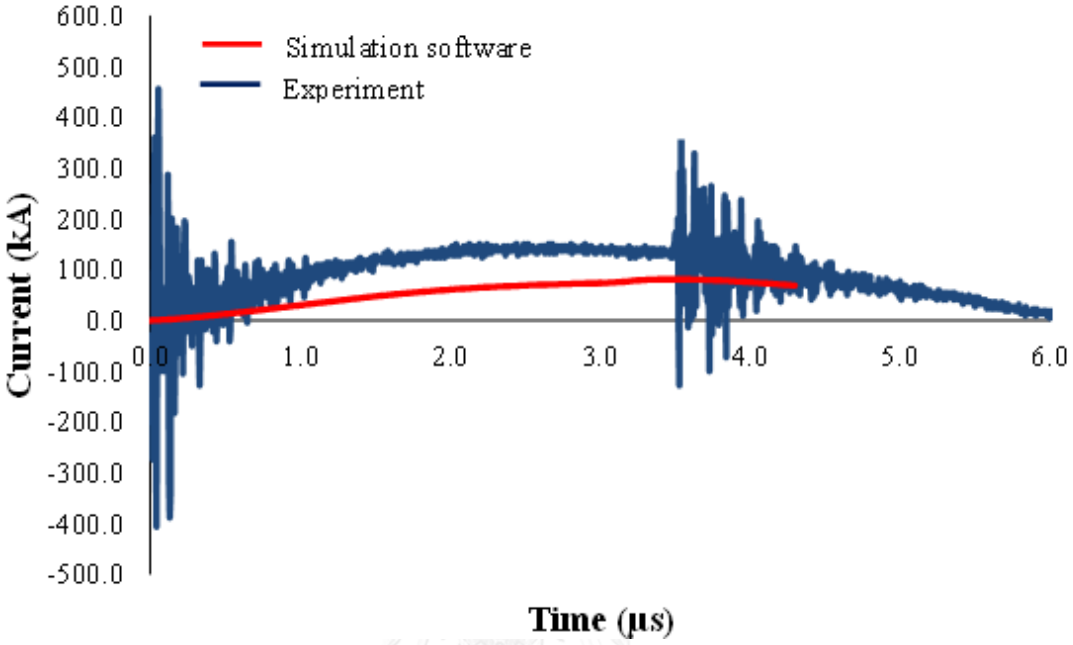

Figure 4.3: Graph showing current from experiment and simulation of PF device operating at pressure of 1 mbar.

The result from the finite element simulation differs from the experimental results. The difference can be explained by the way that the signals are observed differently. The current from the experiment is the input current which flow into the anode, which is measured by the Rogowski coil, while the result from the simulation is the current of plasma that is generated between the electrodes. It is obvious that the current of the plasma will be lower than the input current as a whole. We have investigated this difference in observation. The input current function mentioned in Chapter 3 is plotted and compare with the current generate by the dynamics of plasma.

This is shown by Figure 4.4. The ratio of the current generated by the simulation and the input current is shown in Figure 4.5

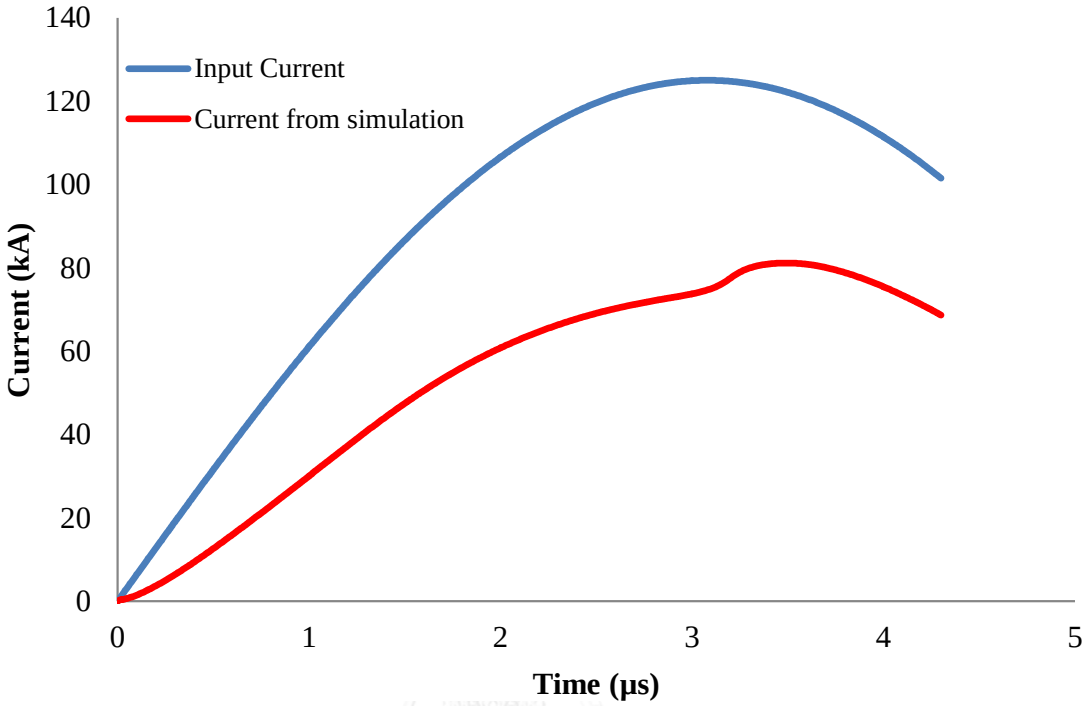

Figure 4.4: Graph showing comparison of current input and current generated by finite element simulation.

From Figure 4.5, we can see that the ratio of input and the current of plasma changes with time. The ratio changes rapidly at the beginning and becomes steadier as the time progress. The average value of the current ratio is shown in Table 4.2. It can be seen that as the operating pressure of the PF device increases then the current ratio slightly decreases.

The current of plasma between the electrodes is approximately a half of the current measured through the anode.

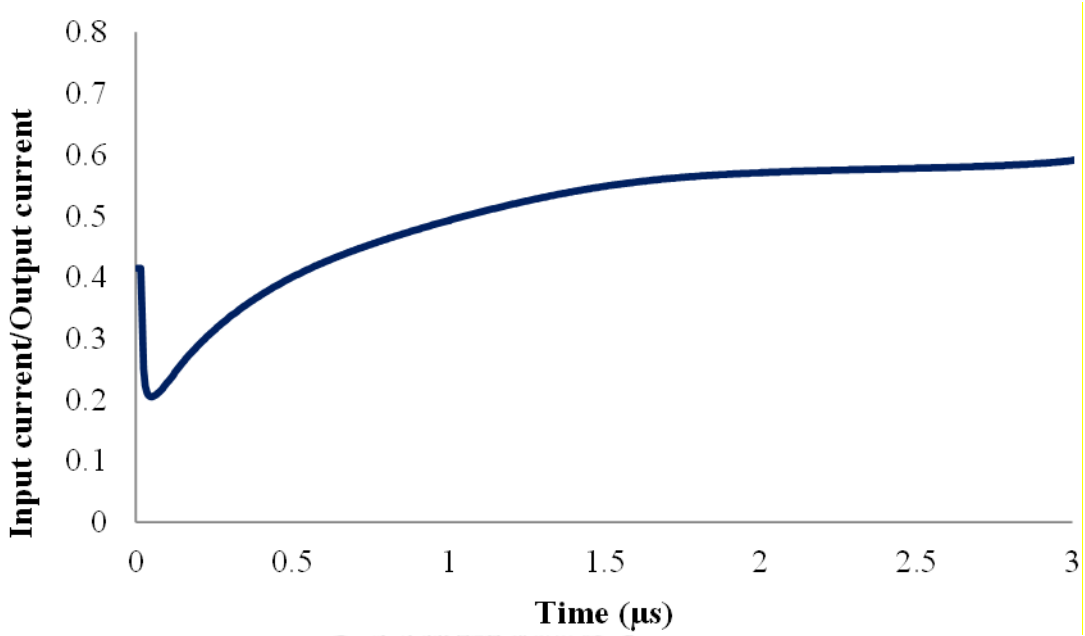

Figure 4.5: Graph showing the ratio of currents from simulation and input current under operating pressure of 1.0 mbar during the axial phase.

This ratio averaged value is shown values in Table 4.2.

Table 4.2 Current ratio between current from the simulation and input current at various operating pressures.

Operating pressure (mbar)	Current from simulation/Input current
1.0	0.55
1.5	0.48
2.0	0.49

Considering the current used in Lee model, the current of the circuit I shown in the circuit equation is adjusted to fit with the experimental data by the current factor f_c. The current from the circuit can relate to the current between the electrodes I' as;

$$I' = f_c I. \qquad (4.1)$$

Figure 4.6 shows a comparison of the current factor f_c and the average current ratio from the finite element simulation can for various operating pressure. It can be seen that the current factor applied in Lee model depends on the operating pressure and somewhat in agreement with the average current ratio from the finite element simulation.

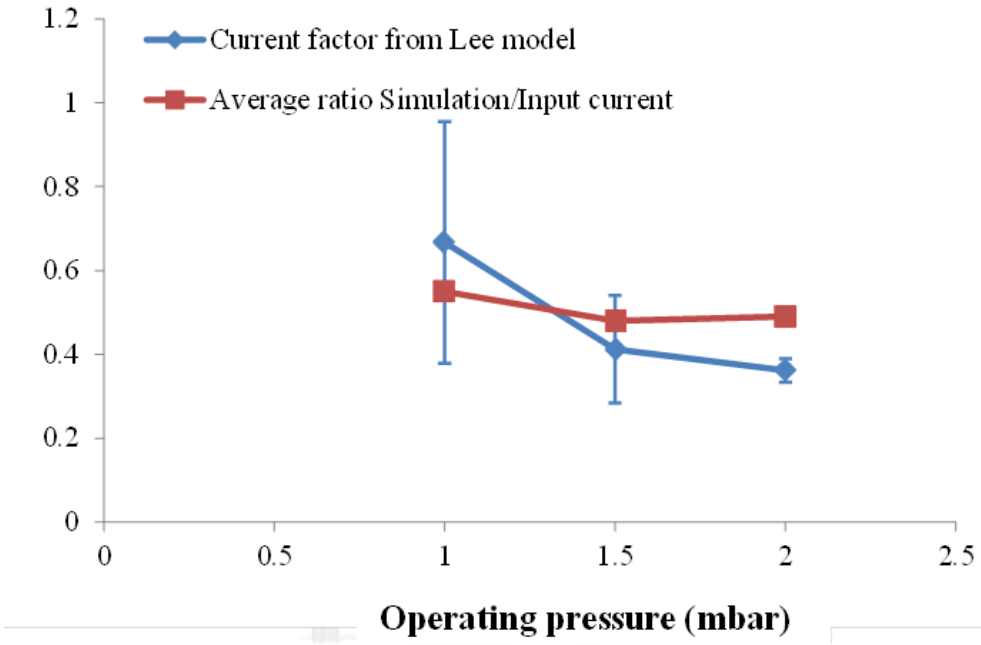

Figure 4.6: Plot showing current factor from Lee model and the average ratio obtained from simulation software.

In both cases, the discrepancy between the input current and the current of plasma between the electrodes can be explain by back Electro Motive Force (EMF) $V_L = \frac{d(L_P+L_o)f_cI}{dt}$ generated in the plasma. It is known that when there is a flow of electrical current then a magnetic flux is created. The induced magnetic flux also create current flow in opposite direction of the input current therefore the current flow from anode to cathode is reduced.

4.2 Average Plasma Speed

The speed of plasma is one of the important characteristics of the plasma sheath generated by a PF device. However it is not easy to measure the speed of the plasma sheath directly. In the experiment, the speed of plasma is calculated from the time taken by the plasma to move from one position to another position where the distance between both positions is known. In our experiment, the position of the plasma is identify by using the magnetic probe described in Section 3.1.2.3. Each coil is 2 cm apart. The average plasma speed is investigated for the operating pressure of 1.0 mbar, 1.5 mbar, and 2.0 mbar.

Table 4.3 shows average speed of plasma passing through three different positions for different operating pressures used.

Table 4.3 Average plasma speed calculated from experiment data at various operating pressures.

Pressure	**average plasma speed × 10^4 (m/s)**		
(mbar)	**7 cm – 9 cm**	**9 cm – 11 cm**	**11 cm – 13 cm**
1.0	3.48 ± 0.21	5.80 ± 0.22	4.30 ± 0.07
1.5	2.58 ± 0.07	6.11 ± 0.79	4.06 ± 1.07
2.0	2.10 ± 0.11	3.64 ± 0.09	2.88 ± 0.15

These results are plotted and shown in Figure 4.7. In this figure, the x-axis is the position of the magnetic probes.

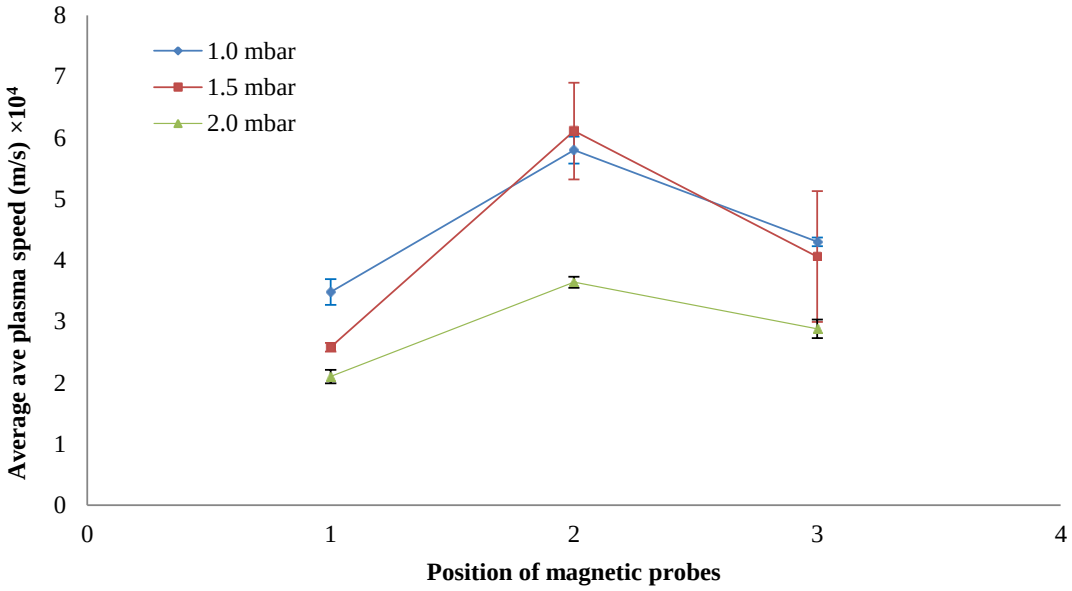

Figure 4.7: Plot showing average plasma speed measured experimentally.

The second position is the position where the magnetics probes is placed at 9 cm and 11 cm. The third position is where the magnetic probe is placed at 11 cm – 13 cm .The diagram of magnetic probes can be found in Figure 3.10.

From the plot in Figure 4.7, it can be seen that the average plasma speed increases when the plasma is moving from the first position to the second position. The average speed of plasma starts to decrease when the plasma is moving from the second position to the third position. This behavior can be explained by the Lorentz force. The Lorentz force increases at the beginning of the axial phase as the current in the circuit is raising. During the second and third position the plasma slows down as the plasma is approaching the end of the anode. At this point, the Lorentz force changes the direction to pointing inwards to the center of the anode, this causes the reduction in the plasma speed.

However, the speed of plasma in the radial direction will be increased by this force in the radial direction.

From the results, the average plasma speed decreases when the applied operating pressure is increased. At position 2 the plasma has maximum average speed when the PF device is operated with 1.5 mbar. With operating pressure of 1.5 mbar, the collision of particles causes the reduction of the plasma speed, but this pressure is also the optimum operating pressure of the PF device and the dynamics it produces.

In the Lee model code, the plasma is assumed to be the solid circular sheet. The sheet is moved by the Lorentz force. The equation of this motion is described in Chapter 2.

The position of plasma plotted according to Lee model is shown in Figure 4.8.

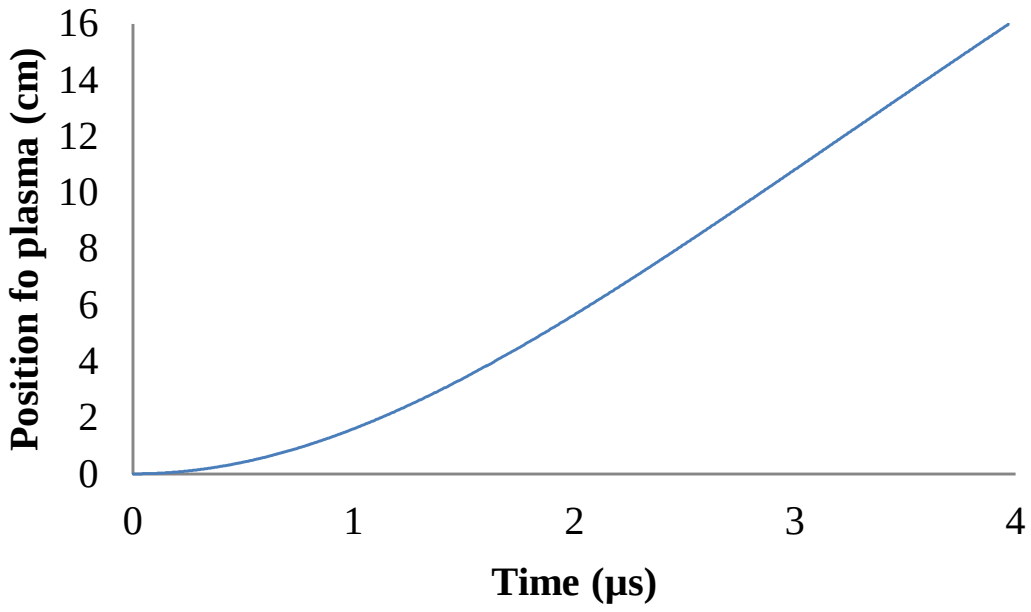

Figure 4.8: Plot showing change in position of plasma with time under the operating pressure of 1 mbar.

From Figure 4.8, the average plasma speed is calculated by using Equation 3.6. The average plasma speed between 7cm to 9cm , 9cm to 11cm , and 11cm to 13cm is the gradient of this plot. The results are shown in Table 4.4

Table 4.4 Average plasma speed calculated by Lee model at various operating pressures.

Pressure (mbar)	**average plasma speed × 10^4 (m/s)**		
	7 cm – 9 cm	**9 cm – 10 cm**	**11 cm – 13 cm**
1.0	6.04 ± 0.89	6.25 ± 0.01	7.42 ± 0.39
1.5	5.13 ± 0.19	5.86 ± 0.84	5.41 ± 0.21
2.0	4.31 ± 0.20	4.58 ± 0.59	3.84 ± 0.86

The average plasma speed calculated by Lee model is plotted and shown in the Figure 4.9.

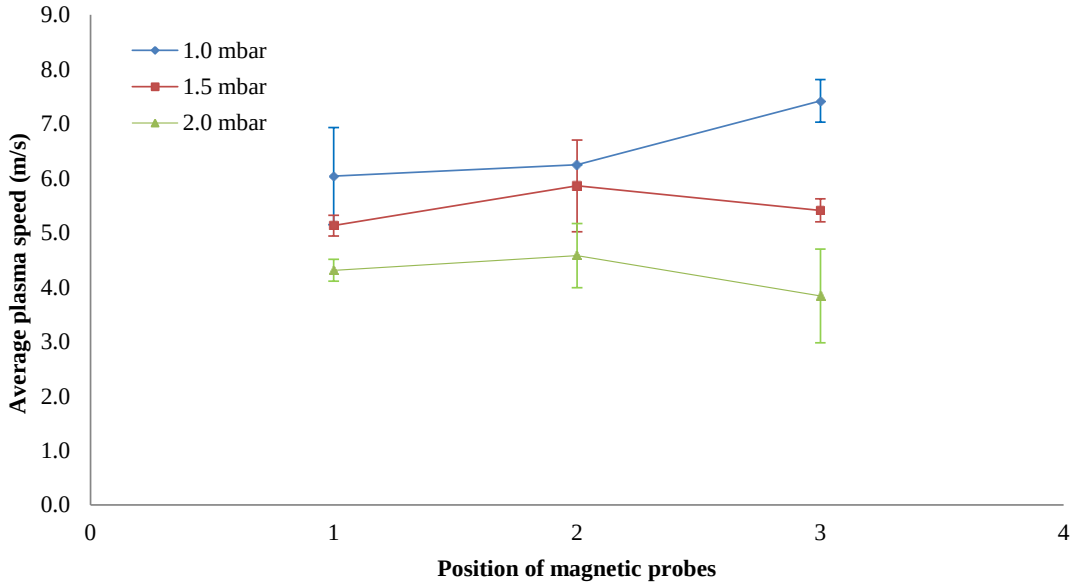

Figure 4.9: Plot of average plasma speed at each position calculated by Lee model.

The average plasma speed between the position 1 and 2 increasing due to the experiment result. However, only 1 mbar differ from the experimental results.

From Figure 4.9, it can be seen that the average plasma speed between the position 1 and 2 increases which is in agreement with the experimental result. However, with operating pressure of 1 mbar there is a discrepancy with the experimental results. The speed of plasma is still increasing from position 2 to position 3 of the magnetic probe. This discrepancy can be explained by the assumption of the model where the Lorentz force is assumed to act in the z direction in the axial phase, therefore the speed of plasma with correspond to the change in the current. However, it can be seen that the average speed of plasma reduces when the operating pressure increases. This is in agreement with the experiment as more mass of plasma being moved as the operating pressure increase.

For the finite element simulation, the average plasma speed is calculated by the magnetics field generated from the simulation at positions correspond to the magnetic probe measurement. This is shown in Figure 4.10.

The dash lines shown in Figure 4.10 mark the position where plasma reaches the positions of magnetic probe measurement. The simulation imitates the movement of plasma that moves near to the observation points where the magnetic field increases rapidly.

After the plasma move through this position, the magnetic field increase slowly because there is only the magnetic field from the current at anode is only recorded at those points.

Table 4.5 shows the average plasma speed calculated from the finite element simulation. The results are plotted and show in Figure 4.11.

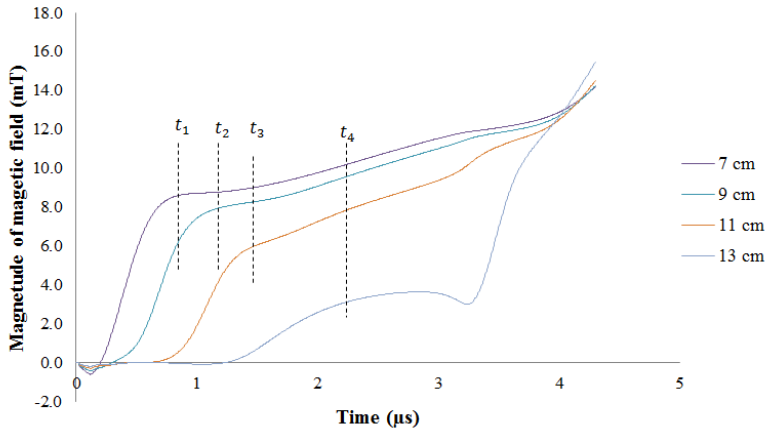

Figure 4.10: Graph showing magnetic field simulated by the simulation software under operating pressure of 1.0 mbar.

Table 4.5 Average plasma speed calculates from the result obtained by finite element simulation.

Pressure (mbar)	**average plasma speed × 10^4 (m/s)**		
	7 cm – 9 cm	**9 cm – 10 cm**	**11 cm – 13 cm**
1.0	6.45	7.14	2.54
1.5	5.56	8.88	2.07
2.0	6.35	6.45	2.00

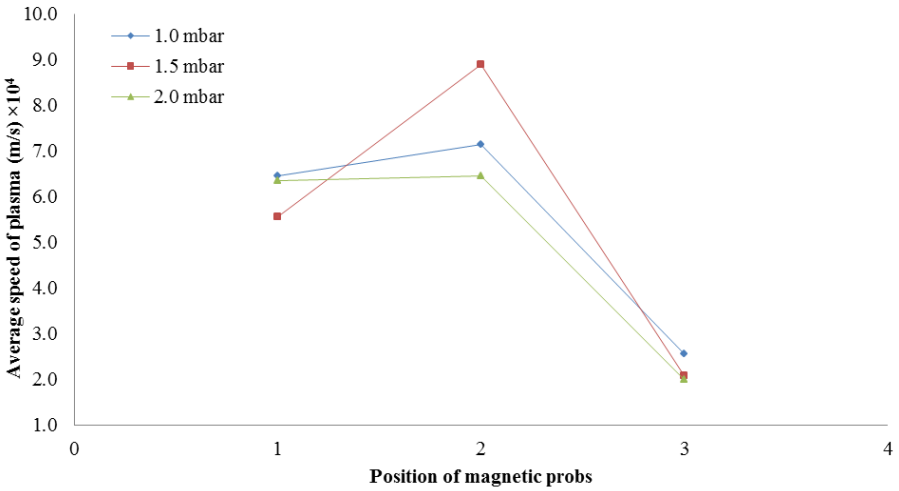

Figure 4.11: Plot showing average plasma speed computed by the simulation software.

From the results, the trend of plasma speed is like the experimental results. This speed is reducing when the operating pressure is increasing.

4.3 Electrical Energy of Electrode

The electrical energy of electrode is another important property of the PF device. The dynamics of plasma is driven by the electrical energy. This energy is stored in the capacitor bank and discharged through the spark gap into the anode of the PF device. The electrical power and the electrical energy can be calculated by Equation 4.2 and 4.3.

$$P' = IV. \tag{4.2}$$

$$E = \int P dt. \tag{4.3}$$

Considering Lee model, the current and voltage as explained Chapter 2 is calculates and shown in Figure 4.12.

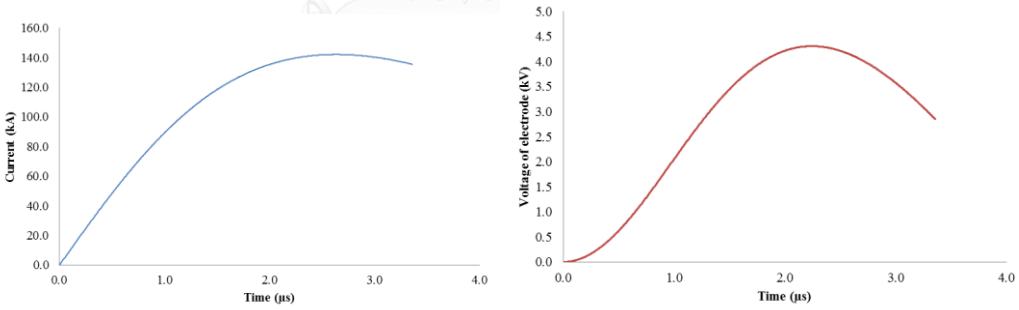

(a) (b)

Figure 4.12: (a) Graph showing the current calculated by Lee model under operating pressure of 1 mbar. (b) Graph showing the voltage calculated by using Lee model code under operating pressure of 1 mbar.

From the current and voltage signal, we can calculate the electrical power for experiment, Lee model and the finite element simulation. The comparison of the electrical power is shown in the Figure 4.13.

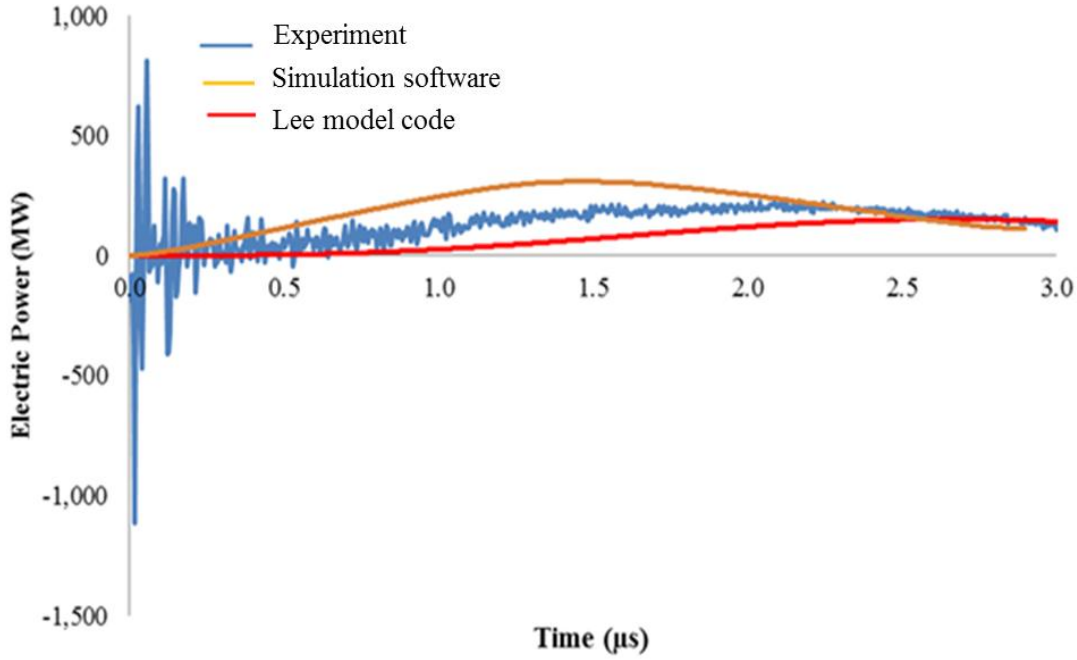

Figure 4.13: Graph showing electrical power absorbed by plasma when operating with pressure of 1 mbar.

The electrical energy can also be computed as explained earlier by Equation 4.4. The calculation results are shown in Figure 4.14. The value of electrical energy is presented in Table 4.6.

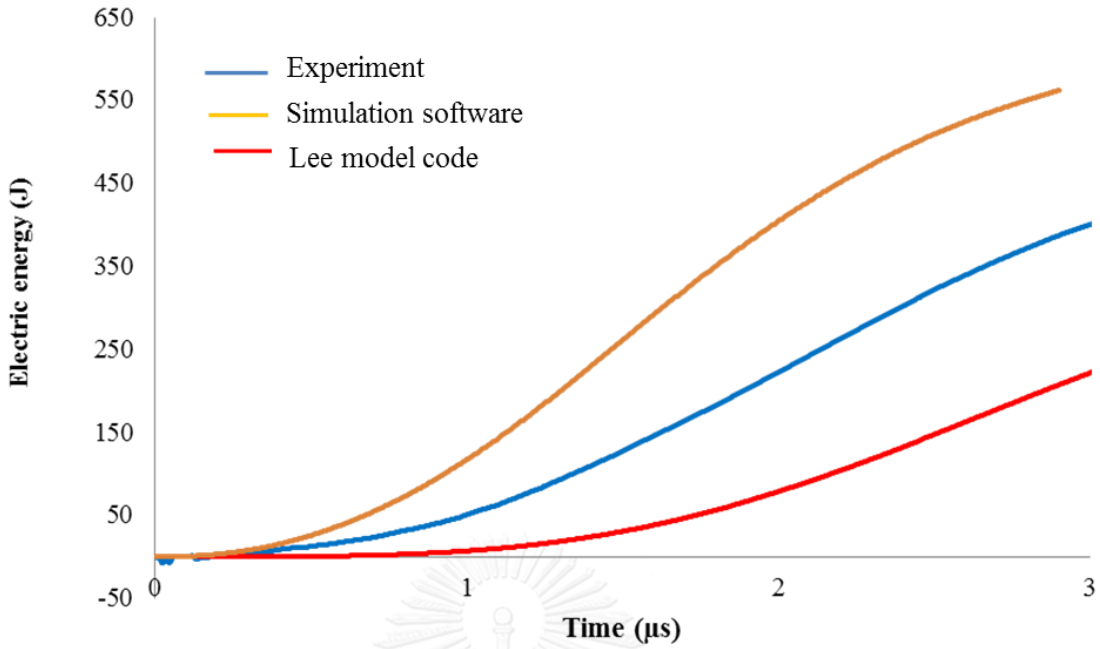

Figure 4.14: Graph showing electrical energy of plasma under the operating pressure of 1 mbar.

The electric energy is averaged and shown results in Table 4.6.

Table 4.6 Average electric energy at various operating pressures.

Pressure (mbar)	**Average electrical energy (J)**		
	Finite Element	**Experiment**	**Lee Model**
1.0	250.45	159.31 ± 13.70	104.40 ± 73.39
1.5	324.19	190.72 ± 44.23	118.72 ± 62.62
2.0	361.00	221.60 ± 47.24	159.58 ± 99.58

From Table 4.6, these results can be plot and shown Figure 4.15.

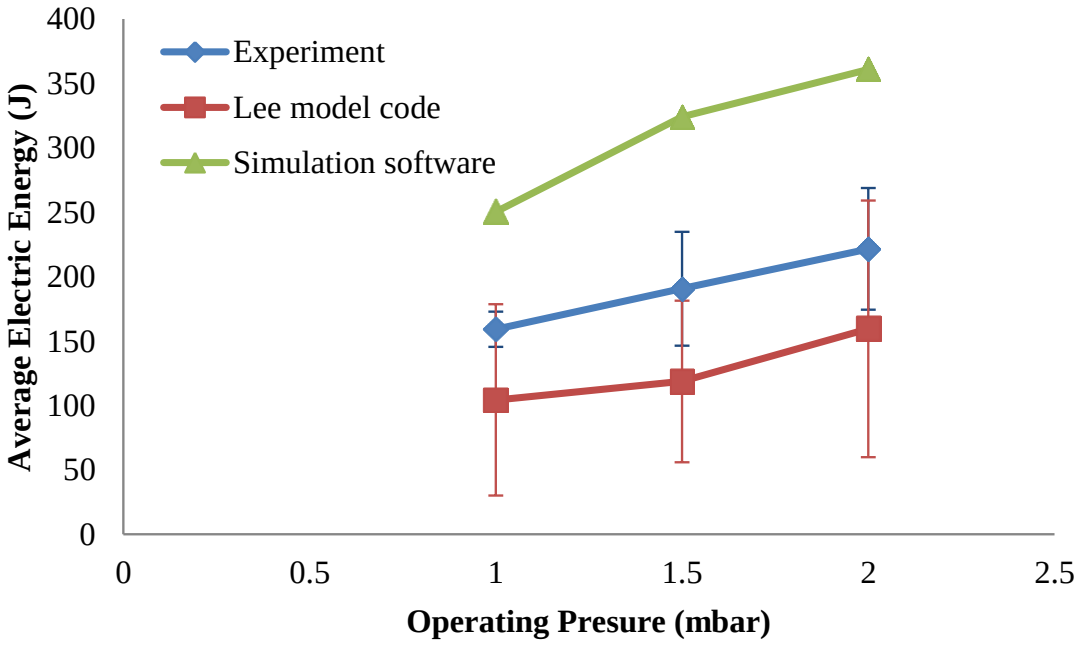

Figure 4.15: Plot showing comparison of average electrical energy obtained from experiment and simulations.

From Figure 4.15, it can be seen that the average electrical energy relates to the operating pressure. Higher electrical energy is required to drive the plasma when the PF device is operated with higher operating pressure. The kinetic energy of plasma is lost through the collision process therefore if the operating pressure is increased, then it is more likely that the energy lost will also increase. Therefore, the plasma's motion uses more energy when the pressure is raised.

The average energy computed by Lee model code is the lowest, and the average energy computed by the finite element simulation is the highest. This can be explained by the assumption used for the finite element simulation that the energy lost is neglected where in real situation the energy can be lost though the spark gap, electrical lines and other loads in the discharge circuit.

From Lee model, the initial voltage is zero at the start of the axial phase. This is different for both experiment and the finite simulation as plasma only occur after breakdown voltage is reached. Therefore, it can be seen that the electric energy calculated by Lee model is the lowest.

The average plasma speed shown in Figure 4.16 also highest for the value determined from the finite element simulation. In the finite element simulation, the plasma got full energy transfer to drive the plasma; therefore, the average plasma speed is expected to be the highest in comparison to the experiment and Lee model calculation.

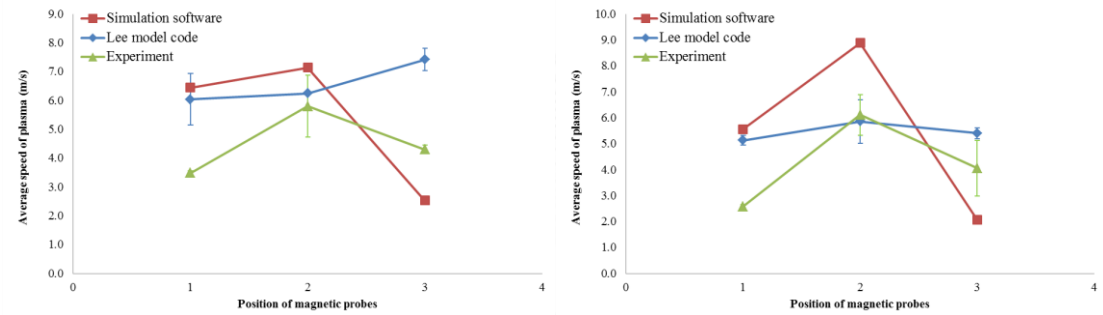

(a) (b)

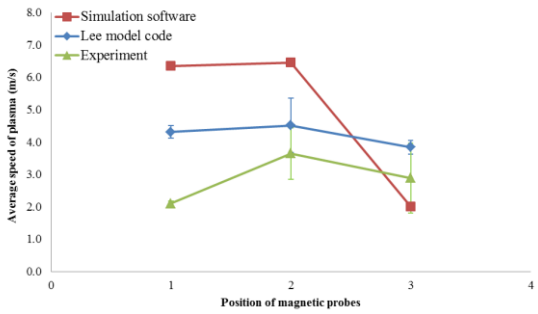

(c)

Figure 4.16: Plot showing comparison of average plasma speed under operating pressure (a) 1.0 mbar (b) 1.5 mbar (c) 2.0 mbar.

The average plasma speed determined from Lee model, however, is higher than the average plasma speed measured in the experiment as Lee model assume the plasma to be a thin circular sheath and no heat is transferred to the surrounding.

In comparison to the experiment, the electrical energy is lost through resistance in the circuit, and the kinetic through collision. Therefore, the average plasma speed is found to be the lowest.

Because of the different in the value of electrical energy for each different model, it is also interesting to see the profile of the voltage signal. The voltage signal measured in the experiment and the finite element simulation is compared. This voltage signal is shown in Figure 4.17.

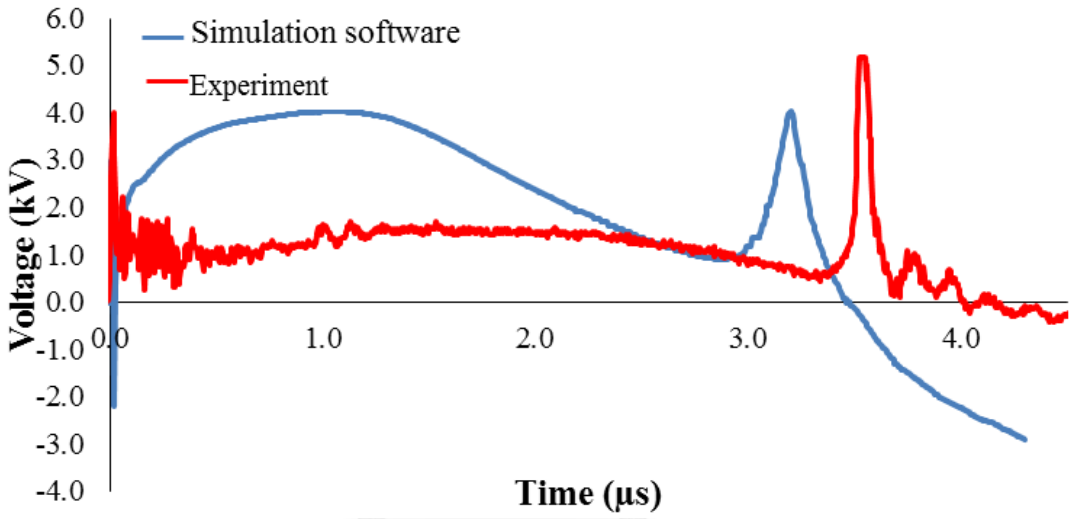

Figure 4.17: Graph showing voltage signal from the experiment and the finite element simulation under operating pressure of 1 mbar.

Since the electrical energy calculated from the finite element simulation is larger, it can be seen that the plasma reaches the end of the axial phase faster than the actual experiment as shown in Figure 4.17. The result is in agreement with issues discussed earlier in terms of the average plasma speed, voltage and current signal.

4.4 Argon Density and Temperature

In the Lee model, snowplow model is used to describe the increasing mass of the slug plasma. During the movement of plasma, the plasma sweeps the ambient gas which is in front of the plasma sheath. The ambient gas compressed by the magnetic pressure to generate plasma slug. The plasma slug has density and plasma temperature higher than the ambient gas. Figure 4.18 shows the diagram of the ambient gas being swept by the plasma sheath.

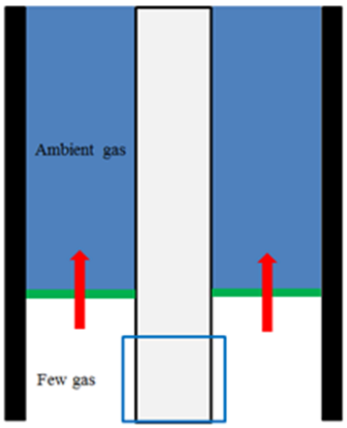

Figure 4.18: Diagram of plasma moving forward along the anode showing the difference in density of the ambient gas.

In order to try to understand the existence of mass swept factor, the density of plasma and plasma temperature is investigated. In this model, the interaction of plasma and the ambient gas is neglected. In the Lee model calculation, the density of plasma increases when the plasma temperature increases. The density of plasma slug is calculated by the mass of plasma slug per volume of plasma slug which can be shown as;

$$\rho = \frac{m}{V}. \qquad (4.4)$$

The volume of plasma slug is computed on the assumption that the plasma is in thermal equilibrium and adiabatic. It can be calculated by giving;

$$P_o V_o^{\gamma} = P_n V_n{}^{\gamma}. \qquad (4.5)$$

From Equation 4.5, the volume of plasma decreases when the magnetic pressure acts on the plasma. However, from Equation 4.4 and 4.5, the density of plasma increases when mass of plasma slug increases while the volume of plasma decreases.

The plasma temperature calculated by Lee model relates to the plasma speed and species of argon ions. The plasma temperature can be found in Equation 2.11 in Chapter 2. From Lee model, the plasma density and plasma temperature can be determined at each position as shown in Figure 4.19.

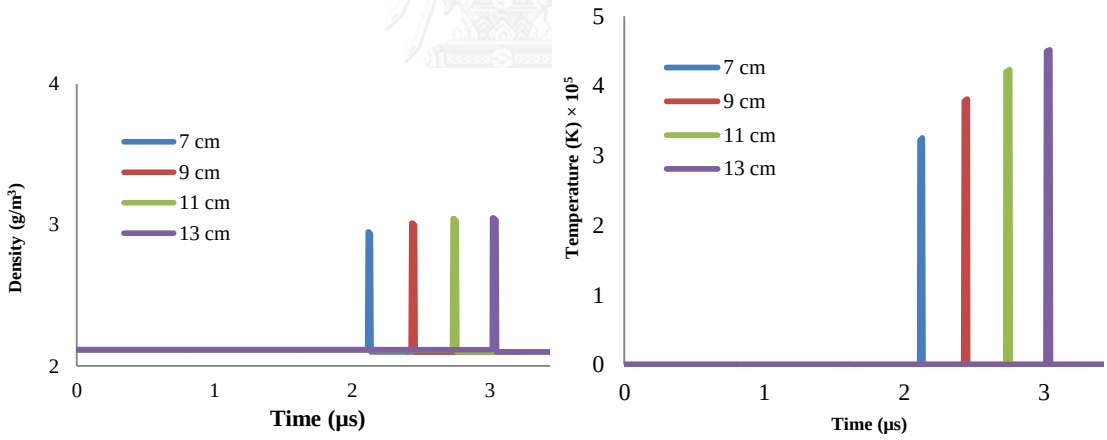

(a) (b)

Figure 4.19: Graph showing simulation results from Lee model a) density of plasma b) plasma temperature at various observing position and time.

It can be seen that at each positions, both the plasma density and the plasma temperature is higher at each increasing distance position. It is obvious that the density does not go to zero because there always the ambient gas.

The mass swept factor f_m found and shown in Table 3.2 is less than 1.0. This means that the plasma sheath only sweeps a fraction of the ambient gas when it is moving along the z axis during the axial phase.

From the finite element simulation, the dynamics of plasma is uses both electromagnetic theory and plasma theory. The plasma generated is shown in Figure 4.20. The simulation of the dynamics of the plasma from breakdown phase to axial phase is shown with changes of the electric filed. The magnetic field cannot be shown here as it is perpendicular to the diagram. These results differ from the Lee model calculation as breakdown phase is being incorporated.

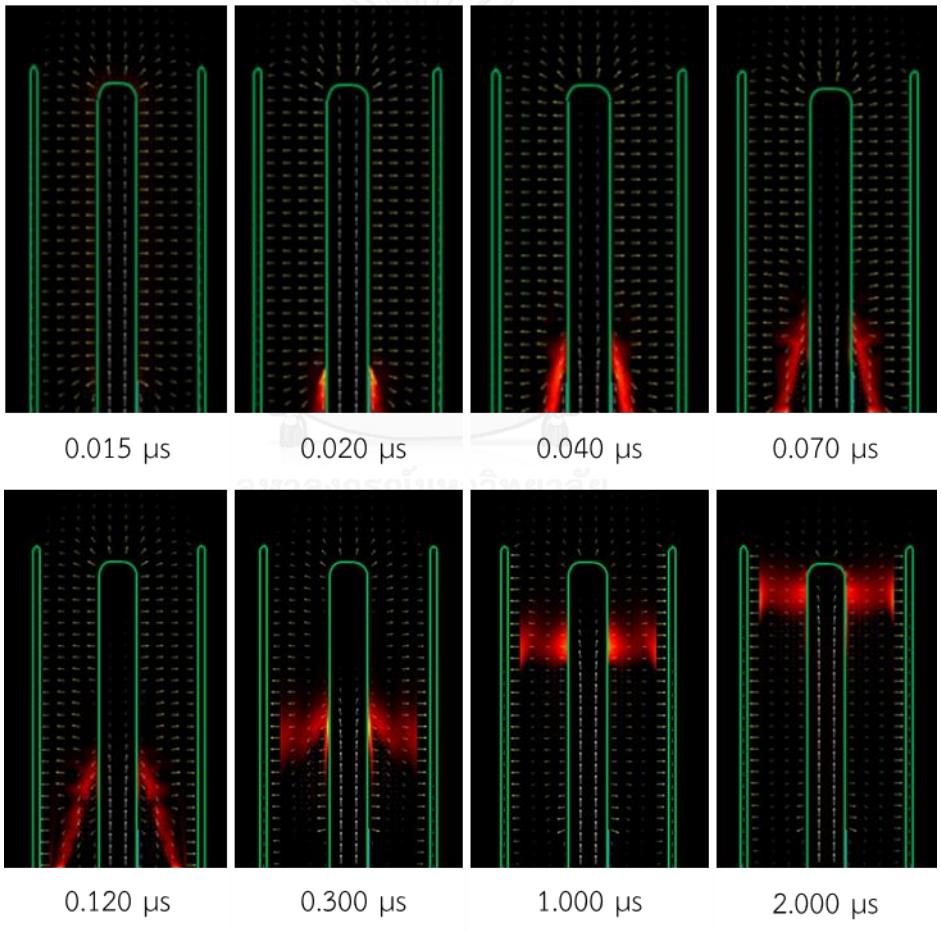

Figure 4.20: Picture showing dynamics of plasma generated by the finite element simulation from breakdown phase to the axial.

The density of argon gas and temperature of the plasma at different positions computed by the finite element simulation is shown in Figure 4.21.

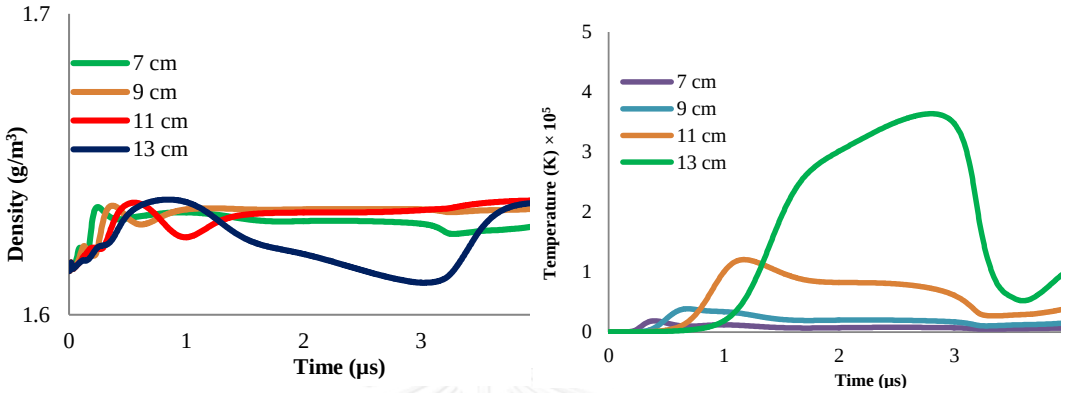

(a) (b)

Figure 4.21: Graph showing simulation results of a) density of argon gas b) temperature of argon gas.

In comparing the results between Lee model and the finite element simulation, it can be seen that the finite element simulation can show how the plasma density and temperature change more realistically where Lee model will only give a discrete value at each positions. The results from the finite element simulation give more realistic profile of the plasma as it is evolving microscopically where Lee model make used of the assumption of plasma being as plasma slug which is a macroscopic assumption.

It can be seen that as plasma go through each observation points, the temperature of the plasma and the plasma density decreases. The results from the finite element simulation show that not all the mass of the gas is being swept by the plasma. These results confirm the significant of mass swept factor used in Lee model. The value of mass swept factor also depends on interaction of particles.

4.5 Ions Species

As described in Section 2.1, the plasma temperature can be used to determine ion species generated during the movement of plasma in the axial phase.

Figure 4.22 shows the speed of plasma sheath calculated by Lee model and the voltage potential across the electrodes.

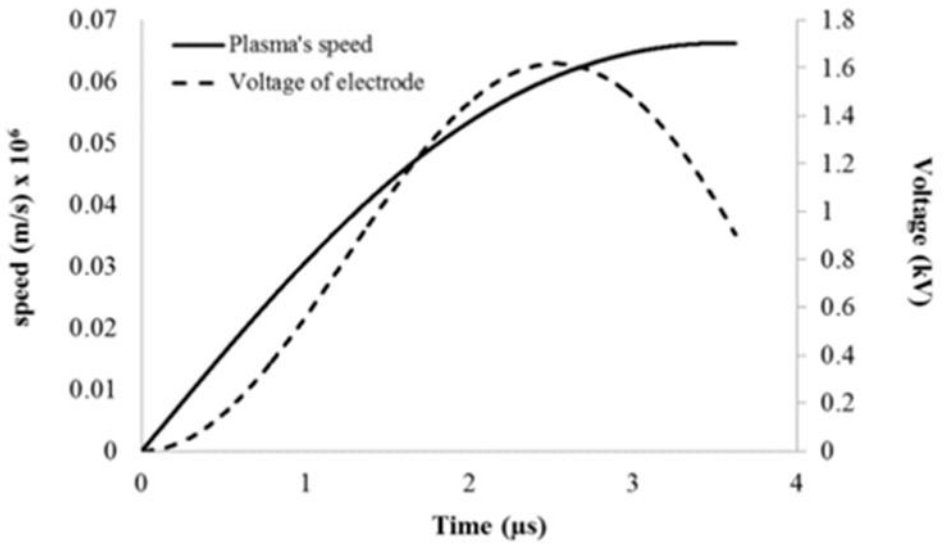

Figure 4.22: Graph showing both the speed of plasma and plasma temperature vary in time in the axial phase under the operating pressures 1.0 mbar.

The maximum plasma temperature calculated by Lee model is shown in Table 4.7. This temperature decreases with increasing the operating pressure as expected.

Table 4. 7 Maximum plasma temperature obtained for various operating pressures.

Operating Pressure (mbar)	Maximum Plasma Temperature(keV)
0.5	0.020
0.75	0.019
1	0.017
1.2	0.015

The plasma temperature reduced with increasing the pressure due to slowdown the plasma speed. Fractions of argon's ions species is calculated by using corona equilibrium model that is mentioned in Chapter 2. Figure 4.23 shows the plotted of argon's ions species evolving in time during the axial phase for each different operating pressures.

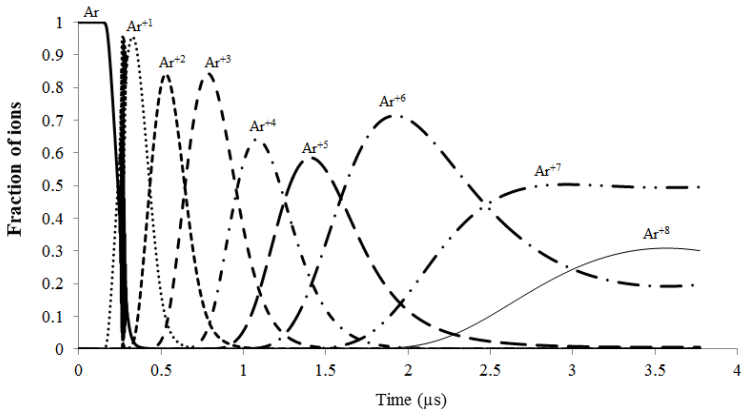

(a)

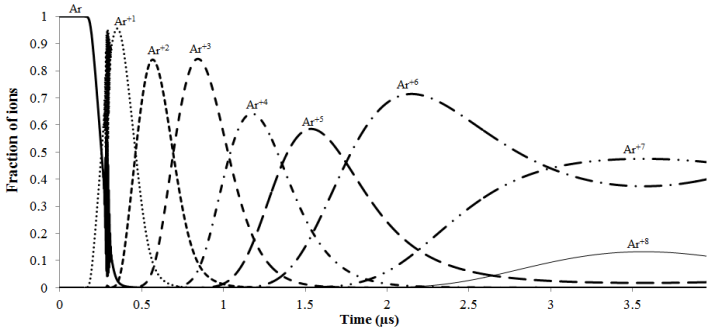

(b)

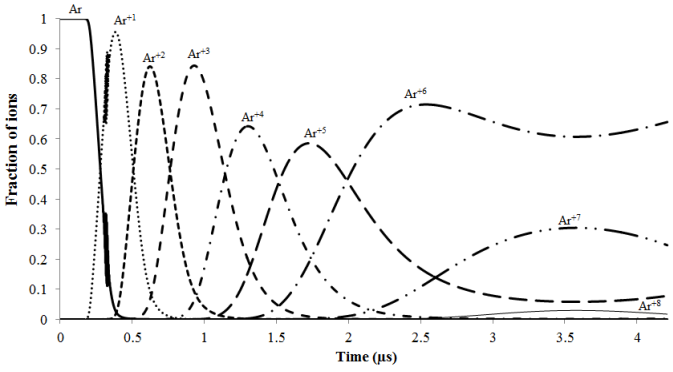

(c)

Figure 4.23:Plots showing fraction of argon's ions changes in plasma operated at (a) 0.75 mbar (b) 1.0 mbar and (c) 1.2 mbar.

The effective charge of the plasma is determined by averaging fraction of ions species for each time. From Figure 4.24 it can be seen that the effective charge increases with time. This can be explained by the increasing of plasma temperature.

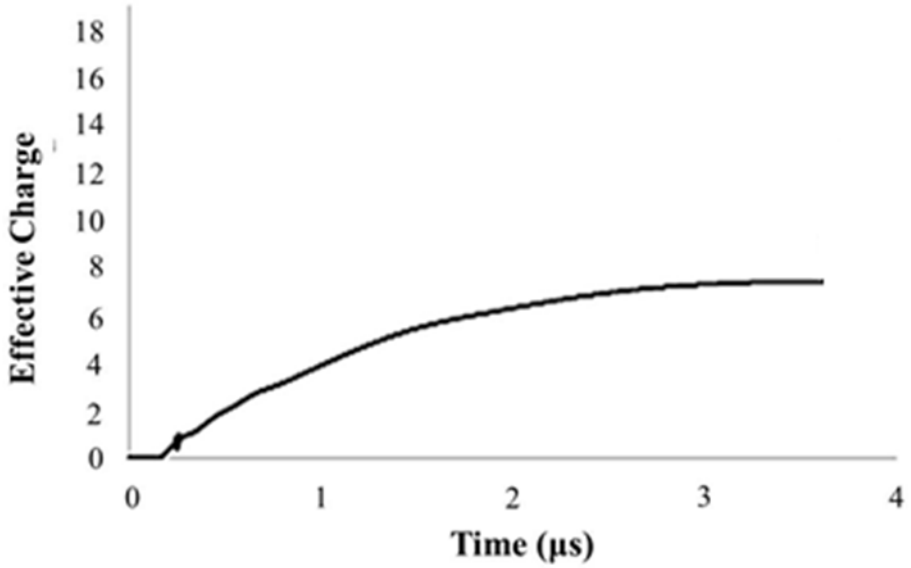

Figure 4.24: Plot showing the evolution of calculated effective charge over time.

In the axial phase, the temperature of plasma can rise to 0.02 eV where species of argon ion can be generated up to Ar^{+8}. However, temperature of plasma is not high enough to generate Ar^{+18}. In the radial phase and pinch phase, the plasma temperature increases rapidly and the ions species up to Ar^{+18} can be generated.

However, this is the limitation in the finite element simulation. For the plasma interaction done by COMSOL Multiphysics, the ions species of argon considered is only up to Ar^{+}. Thus the simulation is only consider the movement of Ar^{+} species. The ionization process calculated in the simulation software will only be based on the cross section data of Ar and Ar^{+}. The result of species of argon's ions cannot be compared the result from Lee model.

It has been demonstrated that the finite element simulation can be used to explain the plasma dynamics during the axial phase where the plasma temperature has not yet been raised to high value. However, this limitation does not applied to the breakdown phase as majority of the ion species will be Ar^+. The breakdown phase is not considered by the Lee model.

The next chapter will present the conclusion of this work, and suggest how the limitation issue can be improved in future work.

CHAPTER 5
CONCLUSION

5.1 Conclusion

In the research, the dynamics of plasma in the UNU/ICTP plasma focus device is investigated. This device is known to be used as source of radiations and particles. The device can be applied in many researches such as surface modification of materials, source of radiations and energetic particles, and source of fusion reaction.

It is important to understand the dynamics of plasma generated by the plasma focus device, especially, to understand the properties of plasma. The dynamics of plasma plays important part in radiations and particles generation, therefore in depth understanding of the dynamics can help optimizing the operating condition of the plasma focus for the intended applications.

In this research, we have attempted to simulate the dynamics of plasma by using finite element simulation using COMSOL Multiphysics simulation software. Both plasma theory and electromagnetics theory are taken into account to generate the dynamics of plasma inside the plasma focus device. The simulation results are compared with the experimental results and results from a well-known Lee model. The measurement and the properties investigated are current signal, voltage signal, average plasma speed, electric energy, plasma density, and plasma temperature.

Necessary diagnostics are presented in Section 3.1.2. The voltage signal is measured by a high voltage probe, and the current signal is detected by using Rogowski coil. The movement of plasma is measured by magnetic probes.

For the finite element simulation, the dynamics of plasma investigated is limited to the breakdown phase and the axial phase. This dynamics parameters is compared with Lee model which is limited to the axial phase. This is because Lee model calculation only starts from the axial phase.

In the experiment, 3.3kJ UNU/ICTP plasma focus device is investigated in thins research. The device is composed of vacuum chamber, electrodes, capacitor bank and vacuum system. The radius of the anode is 0.95 cm, and the length of the anode is 16.0 cm. The storage size of capacitor bank is 30 μF and the charging voltage applied is 12.5 kV. The distance between anode and cathode is 3.2 cm.

From Lee model, the calculation process can be represented by a flow chart shown in Figure 3.12. This simulation is written in EXCEL program. The calculation is made once mass swept factor f_m and current factor f_c are adjusted. The current factor f_c is 0.362-0.667 and mass swept factor f_m is found to be 0.0242-0.0365. These factors are obtained by fitting with actual experimental results of PF device operated with pressure of 1.0 mbar, 1.5 mbar and 2.0 mbar. These parameters are used to further simulate the dynamics of plasma, and they are used to calculate the plasma speed, the position of plasma, plasma current, and plasma temperature.

It is found that, the results from the finite element simulation show similar voltage signal profile to the experiment. The peak voltage appears later as the operating pressure increases. It is interesting to note that the voltage signal from the finite element simulation is not zero.

The voltage obtained by the finite element method is also found to be higher than voltage measured from actual experiment. It is possible that in real experiment, we cannot get all charge transfer from the capacitor bank to the anode as the charge may be lost through the spark gap and electrical line. On the other hand, the voltage signal calculated from Lee model is lower than the result from the finite element simulation. Also the initial voltage starts from zero which is expected as this model does not consider the breakdown phase.

We can see that the time taken to complete the two dynamics phases measured from the experiments are in agreement with the result from the finite element simulation that the time taken increases as the operating pressure is increased. The can be explained by the collision probability of particles in the plasma. In collision process the kinetic

energy of plasma is transferred to the surrounding. This causes reduction in the speed of plasma, hence the longer the time to complete the phases.

For the current signal, the result from the finite element simulation differs from the experimental results. The difference can be explained by the way that the signals are observed differently. The current from the experiment is the input current which flow into the anode, which is measured by the Rogowski coil, while the result from the simulation is the current of plasma that is generated between the electrodes. It is obvious that the current of the plasma will be lower than the input current as a whole. The current of plasma between the electrodes is approximately a half of the current measured through the anode. It can be seen that the current factor applied in Lee model depends on the operating pressure and somewhat in agreement with the average current ratio from the finite element simulation.

The discrepancy between the input current and the current of plasma between the electrodes can be explained by back Electro Motive Force (EMF) generated in the plasma. It is known that when there is a flow of electrical current then a magnetic flux is created.

It has been shown that higher electrical energy is required to drive the plasma when the PF device is operated with higher operating pressure. The kinetic energy of plasma is lost through the collision process therefore if the operating pressure is increased, then it is more likely that the energy lost will also increase. Therefore, the plasma's motion uses more energy when the pressure is raised.

The average energy computed by Lee model code is the lowest, and the average energy computed by the finite element simulation is the highest. This can be explained by the assumption used for the finite element simulation that the energy lost is neglected where in real situation the energy can be lost though the spark gap, electrical lines and other loads in the discharge circuit.

From Lee model, the initial voltage is zero at the start of the axial phase. This is different for both experiment and the finite simulation as plasma only occur after breakdown voltage is reached. Therefore, it can be seen that the electric energy calculated by Lee model is the lowest.

In the finite element simulation, the plasma get full energy transfer to drive the plasma, therefore, the average plasma speed is expected to be the highest in comparison to the experiment and Lee model calculation.

However, the average plasma speed determined from Lee model is higher than the average plasma speed measured in the experiment as Lee model assume the plasma to be a thin circular sheath and no heat is transferred to the surrounding. In comparison to the experiment, the electrical energy is lost through resistance in the circuit, and the kinetic through collision. Therefore, the average plasma speed is found to be the lowest.

Since the electrical energy calculated from the finite element simulation is larger, it can be seen that the plasma reaches the end of the axial phase faster than the actual experiment as shown in Figure 4.17. The result is in agreement with issues discussed earlier in terms of the average plasma speed, voltage and current signal.

By comparing the results between Lee model and the finite element simulation, it can be seen that the finite element simulation can show how the plasma density and temperature change more realistically where Lee model will only give a discrete value at each positions. The results from the finite element simulation give more realistic profile of the plasma as it is evolving microscopically where Lee model make used of the assumption of plasma being as plasma slug which is a macroscopic assumption.

It can be seen that as plasma go through each observation points, the temperature of the plasma and the plasma density decreases. The results from the finite element simulation show that not all the mass of the gas is being swept by the plasma. These results confirm the significant of mass swept factor used in Lee model. The value of mass swept factor also depends on interaction of particles.

It has been shown that in the axial phase, the temperature of plasma can rise to 0.02 eV where species of argon ion can be generated up to Ar^{+8}. However, temperature of plasma is not high enough to generate Ar^{+18}. In the radial phase and pinch phase, the plasma temperature increases rapidly and the ions species up to Ar^{+18} can be generated. However, this is the limitation in the finite element simulation. For the plasma interaction done by COMSOL Multiphysics, the ions species of argon considered is only up to Ar^{+}. Thus the simulation only considers the movement of Ar^{+} species. The ionization process calculated in the simulation software will only be based on the cross section data of Ar and Ar^{+}. The result of species of argon's ions cannot be compared with the result from Lee model.

In this research, it has been demonstrated that the finite element simulation can be used to explain the plasma dynamics of breakdown phase and the axial phase where the plasma temperature has not yet been raised to high value. In the breakdown phase, majority of the ion species is Ar^{+}. The finite element simulation has given the result in the breakdown phase which Lee model does not consider.

5.2 Further Work

From the results of the experiment, Lee model code, and the finite simulation, the fundamental of the finite element simulation and the experiment can still be further improved in many aspects.

In the experiment, the high speed camera can be used to capture the picture of plasma dynamics. The gate repetition rate of this camera must be at least 0.3 μs in burst mode. The camera will also be able to show the dynamics of the plasma. Using of such high speed camera is necessary in order for the results generated by simulation can be verified and compared.

In the simulation, the dynamics of plasma should be extended to 3D as the real plasma dynamics is in 3D. Under this condition, the number of variables is more than the set that used in this research. In this research, the dynamics of plasma is simplified in 2D. The symmetry of plasma focus device is assumed in order to reduce the computational resource used. However, simulation in 3D needs computer with very high specification. Once the limitation of the resources mentioned is overcome then it will be possible to investigate further into the model that could represent more realistic dynamics of plasma for all phases in any PF devices.

REFERENCES

[1] L. Mahe, F. Xianping, V. S. Stuart, and S. Lee, "Soft X-ray yield measurement in a small plasma focus operated in neon," *IEEE transactions on plasma science,* vol. 26, pp. 135-140, 1998.

[2] D. Ngamrungroj, "Optimization of a modified plasma focus for ion beam generation," Doctoral, Department of Physics, Faculty of Science, Chulalongkorn University, 2007.

[3] P. Tangjitsomboon, D. Ngamrungroj, C. S. Wong, and R. Mongkolnavin, "Operating Parameters for Extreme Ultraviolet Radiation Generation based on the United Nations University/ International Centre for theoretical Physics (UNU/ICTP) Plasma Focus Device," *Journal of Science and Technology in the Tropics,* vol. 5, pp. 39-43, 2009.

[4] A. Lepone, H. Kelly, D. Lamas, and Marquez, "A Surface modification produced by a nitrogen operated plasma focus device: the role of the ion beam in the heating of a substrate," *Applied surface science,* vol. 143, pp. 124-134, 1999.

[5] B. Nayak, B. S. Acharya, S. R. Mohanty, T. K. Borthakur, and H. Bhuyan, "Surface nitriding of graphite substrate by plasma focus device towards synthesis of carbon nitride coating," *Surface and Coatings Technology,* vol. 145, pp. 8-15, 2001.

[6] R. Mongkolnavin, J. Srisawat, D. Ngamrungroj, and V. Pimpan, "Plasma Focus Application for Enhancing Polypropylene-polyester/Cotton Composites Lamination," *Jurnal Fizik Malaysia,* vol. 27, pp. 111-114, 2006.

[7] E. J. Lerner, "Prospects for p 11 B fusion with the Dense Plasma Focus: New Results," *Current Trends in International Fusion Research,* p. 25, 2008.

[8] J. Mather, "Dense Plasma Focus," *Methods in Experimental Physics,* vol. 9, pp. 187-249, 1971.

[9] N. Filippov, T. Filippova, and V. Vinogradov, "Dense high-temperature plasma in a non-cylindrical Z-pinch compression," *Nucl. Fusion, Suppl.,* 1962.

[10] S. Lee, "Radiative Dense Plasma Focus Model Computation Package RADPFV5.008," *NTU/NIE NSSE Plasma Radiation Source Laboratory,* 2005.

[11] Available: http://www.belljar.net/mini_f.htm

[12] H. Bruzzone and R. Vieytes, "The initial phase in plasma focus devices," *Plasma physics and controlled fusion,* vol. 35, p. 1745, 1993.

[13] C. S. Wong, *Plasma focus*: University of Malaya, 2000.

[14] S. Lee, S. P. Moo, C. S. Wong, and A. C. Chew, "Twelve years of UNU/ICTP PFF—a review," 1998.

[15] J. W. Mather, "Formation of a High-Density Deuterium Plasma Focus," *Physics of Fluids (1958-1988),* vol. 8, pp. 366-377, 1965.

[16] D. Potter, "Numerical studies of the plasma focus," *Physics of Fluids (1958-1988),* vol. 14, pp. 1911-1924, 1971.

[17] K. Behler and H. Bruhns, "Three-fluid magnetohydrodynamical simulation of plasma focus discharges," *Physics of Fluids (1958-1988),* vol. 30, pp. 3767-3776, 1987.

[18] S. Lee and T. Y. Tou, "Streak photography and focus pinch models," *Bull.Phys.M'sia,* p. 189, 1983.

[19] S. Lee, "Plasma focus model yield trajectory and structure," *World Scientific Publishing Co,* 1984.

[20] S. Mulyodrono, A. J. Smith, W. Suryadif', and M. U. Zakaullahf, "A simple facility for the teaching of plasma dynamics and plasma nuclear fusion," *American Journal of Physics,* vol. 56, p. 1, 1988.

[21] S. Lee and S. H. Saw, "Plasma focus ion beam fluence and flux—for various gases," vol. 20, p. 062702, 2013.

[22] M. Akel, S. A. Salo, S. H. Saw, and S. Lee, "Properties of ion beams generated by nitrogen plasma focus," *Journal of Fusion Energy,* vol. 33, pp. 189-197, 2014.

[23] M. Scholz and I. Ivanova-Stanik, "Initial phase in plasma focus device—model and computer simulation," *Vacuum,* vol. 58, pp. 287-293, 2000.

[24] W. Stepniewski, "MHD numerical modelling of the plasma focus phenomena," *Vacuum,* vol. 76, pp. 51-55, 2004.

[25] R. Amrollahi and M. Habibi, "Computational Simulation of Imploding Current Sheath Trajectory at the Radial Phase of Plasma Focus Performance," *World Academy of Science, Engineering and Technology, International Journal of Mathematical, Computational, Physical, Electrical and Computer Engineering,* vol. 2, pp. 376-379, 2008.

[26] S. Garanin and V. Mamyshev, "Two-dimensional MHD simulations of a plasma focus with allowance for the acceleration mechanism for neutron generation," *Plasma Physics Reports,* vol. 34, pp. 639-649, 2008.

[27] J. H. González, F. R. Brollo, and A. Clausse, "Modeling of the dynamic plasma pinch in plasma focus discharges based in Von Karman approximations," *IEEE Transactions on Plasma Science,* vol. 37, pp. 2178-2185, 2009.

[28] M. Zambra, D. Kalise, J. Fernandez, E. Hernandez, D. Pasten, and V. Munoz, "Current sheet thickness in the plasma focus snowplow model," *J. Plasma Fusion Res. SERIES,* vol. 8, pp. 879-882, 2009.

[29] C. Hollenstein and A. Howling, "Plasma Edge Simulations by Finite Elements using COMSOL," in *COMSOL Conference*, Hannover, 2008.

[30] I. Rafatov, E. Bogdanov, and A. Kudryavtsev, "On the accuracy and reliability of different fluid models of the direct current glow discharge," *Physics of Plasmas (1994-present),* vol. 19, p. 033502, 2012.

[31] S. Rebiaï, H. Bahouh, and S. Sahli, "2-D simulation of dual frequency capacitively coupled helium plasma, using COMSOL multiphysics," *IEEE Transactions on Dielectrics and Electrical Insulation,* vol. 20, pp. 1616-1624, 2013.

[32] C. Jia, J. Linhong, W. Kesheng, H. Chuankun, and S. Yixiang, "Two-dimensional simulation of inductively coupled plasma based on COMSOL and comparison with experimental data," *Journal of Semiconductors,* vol. 34, p. 066004, 2013.

[33] M. Valentinuzzi, E. Ceccolini, D. Mostacci, M. Sumini, and F. Rocchi, "COMSOL aided design of an extraction pipe for the electron beam from a plasma focus device," presented at the COMSOL Conference, 2012.

[34] S. Lee, "Laser and Plasma Technology," in *Proceedings of the First Tropical College on Applied Physics*, Physics Department, University of Malaya, Kuala Lumpur, 1985.

[35] C. S. Wong and M. Rattachat, "Elements of plasma technology," *Springer,* 2016.

[36] P. Tangjitsomboon, "Plasma focus device modification for generating of extreme ultraviolet radiation," Master, Department of Physics Faculty of Science, Chulalongkorn University, 2008.

[37] E. Gogolides and H. H. Sawin, "Continuum modeling of radio-frequency glow discharges. I. Theory and results for electropositive and electronegative gases," *Journal of applied physics,* vol. 72, pp. 3971-3987, 1992.

[38] G. Hagelaar and L. Pitchford, "Solving the Boltzmann equation to obtain electron transport coefficients and rate coefficients for fluid models," *Plasma Sources Science and Technology,* vol. 14, p. 722, 2005.

[39] G. J. M. Hagelaar, "Modeling of microdischarges for display technology," *Technische Universiteit Eindhoven,* 2000.

[40] COMSOL_Inc, "AC/DC Module User's Guide," USA Patent, 2013.

[41] (2009-2016). *The Plasma Data Exchange Project*. Available: http://www.lxcat.laplace.univ-tlse.fr

APPENDIX

Appendix I
Voltage signal and Current signal under operating pressure of 1.0 mbar to 2.0 mbar

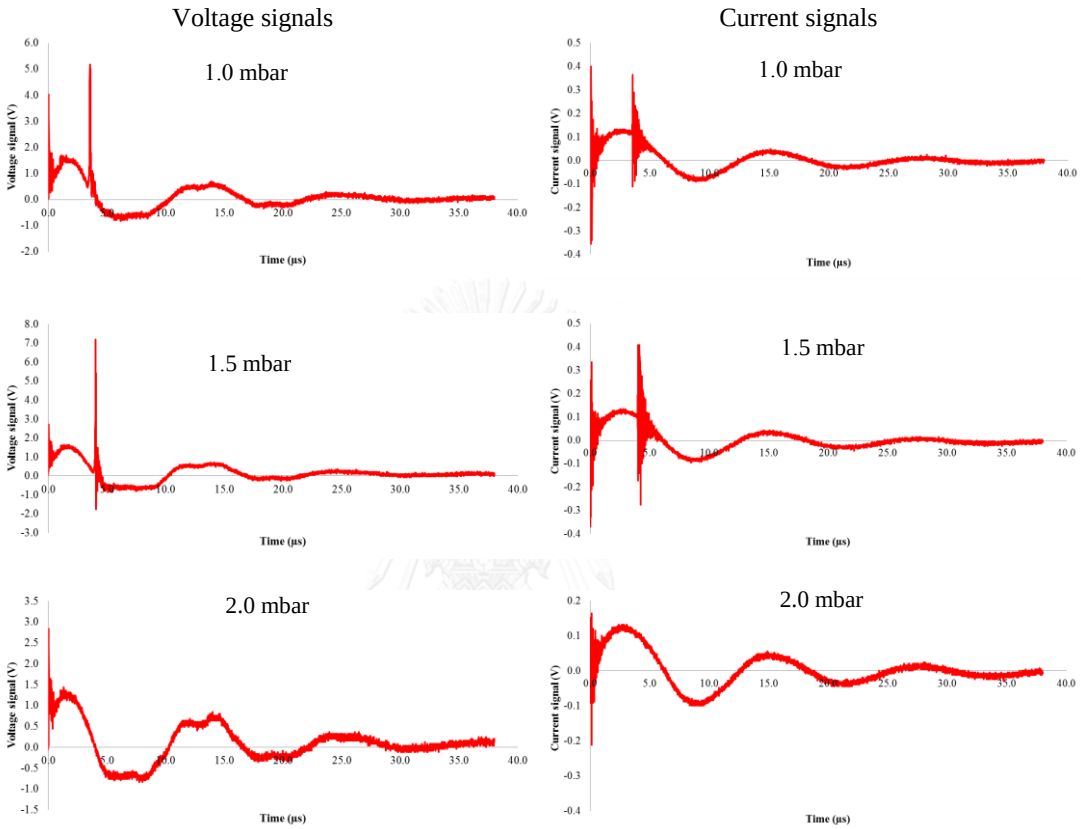

Appendix II
Signals from the magnetic probes

Positions of the magnetic Probes are 7cm, 9cm and 11 cm

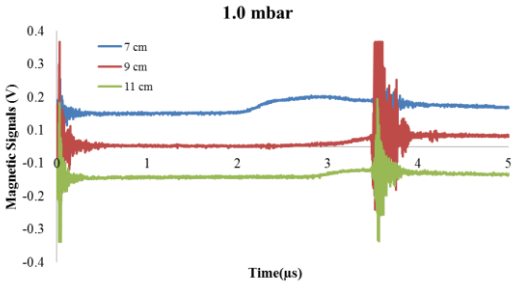

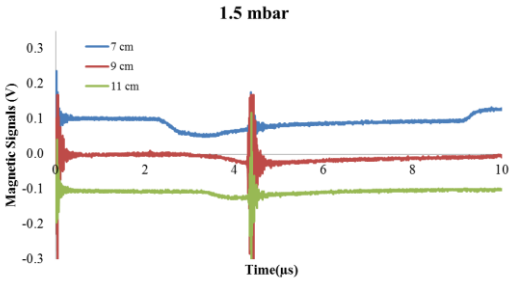

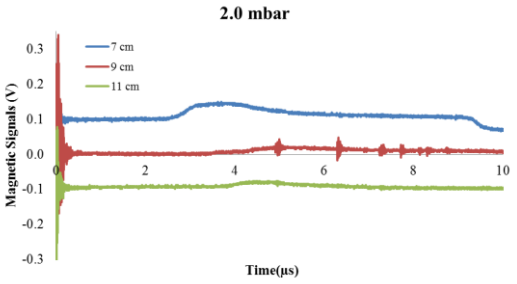

Positions of the magnetic Probes are 9 cm, 11cm and 13 cm

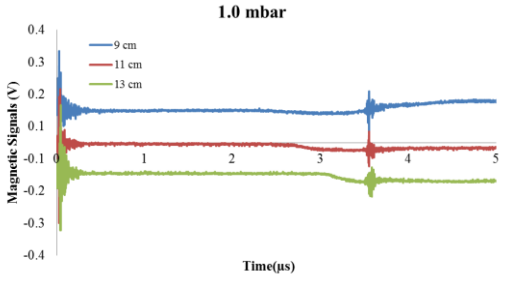

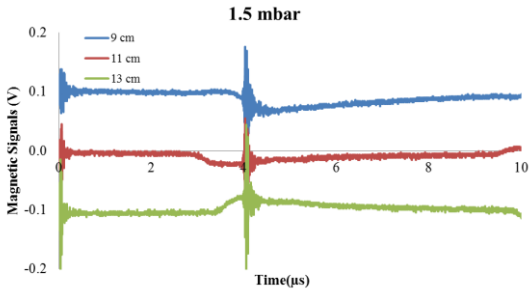

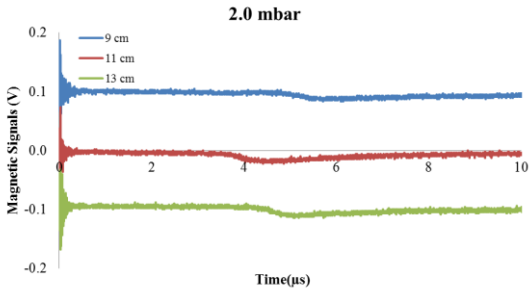

Appendix III
Comparison of voltage results measured in the experiment and generated by the finite element simulation

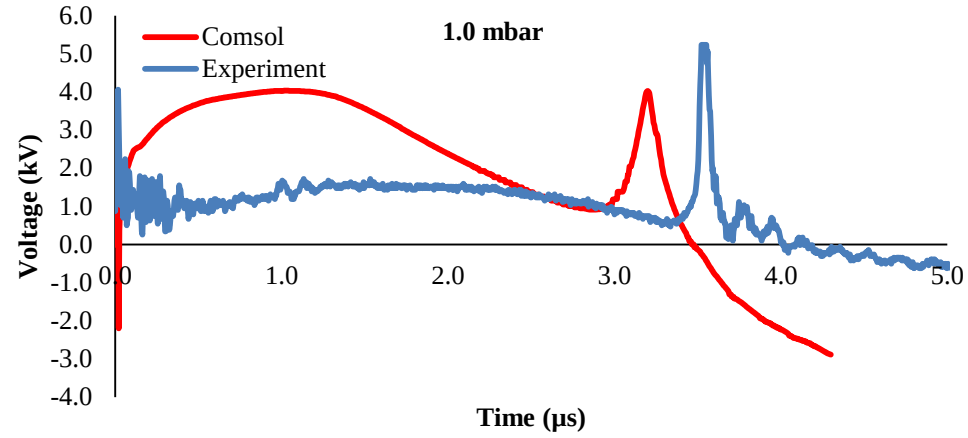

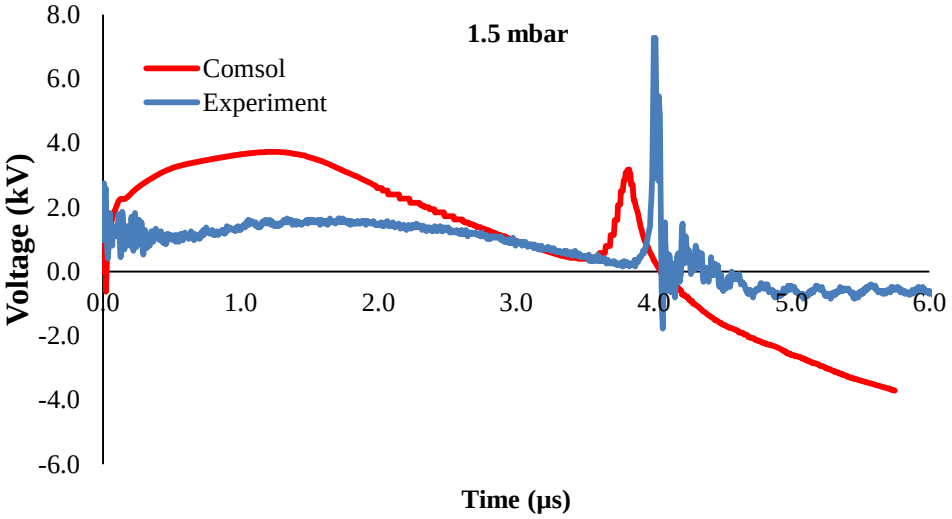

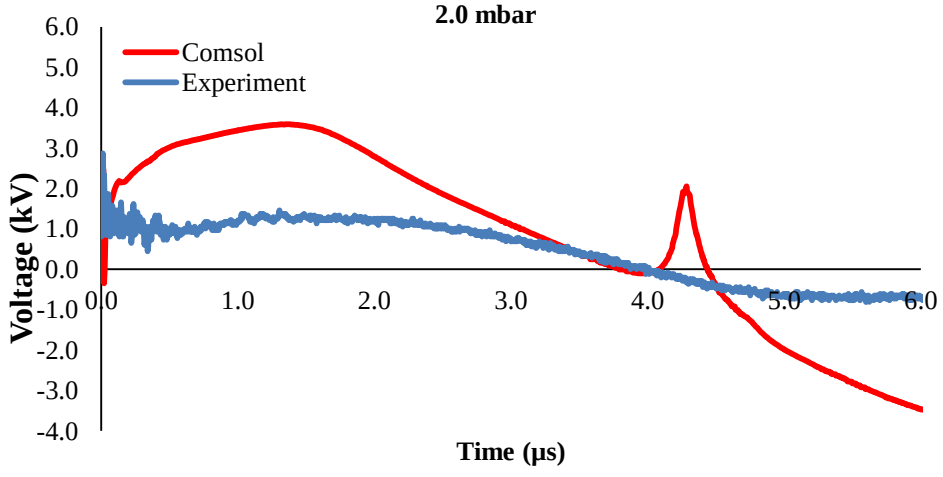

Appendix IV
Comparison of current measured in the experiment and generated by the finite element simulation

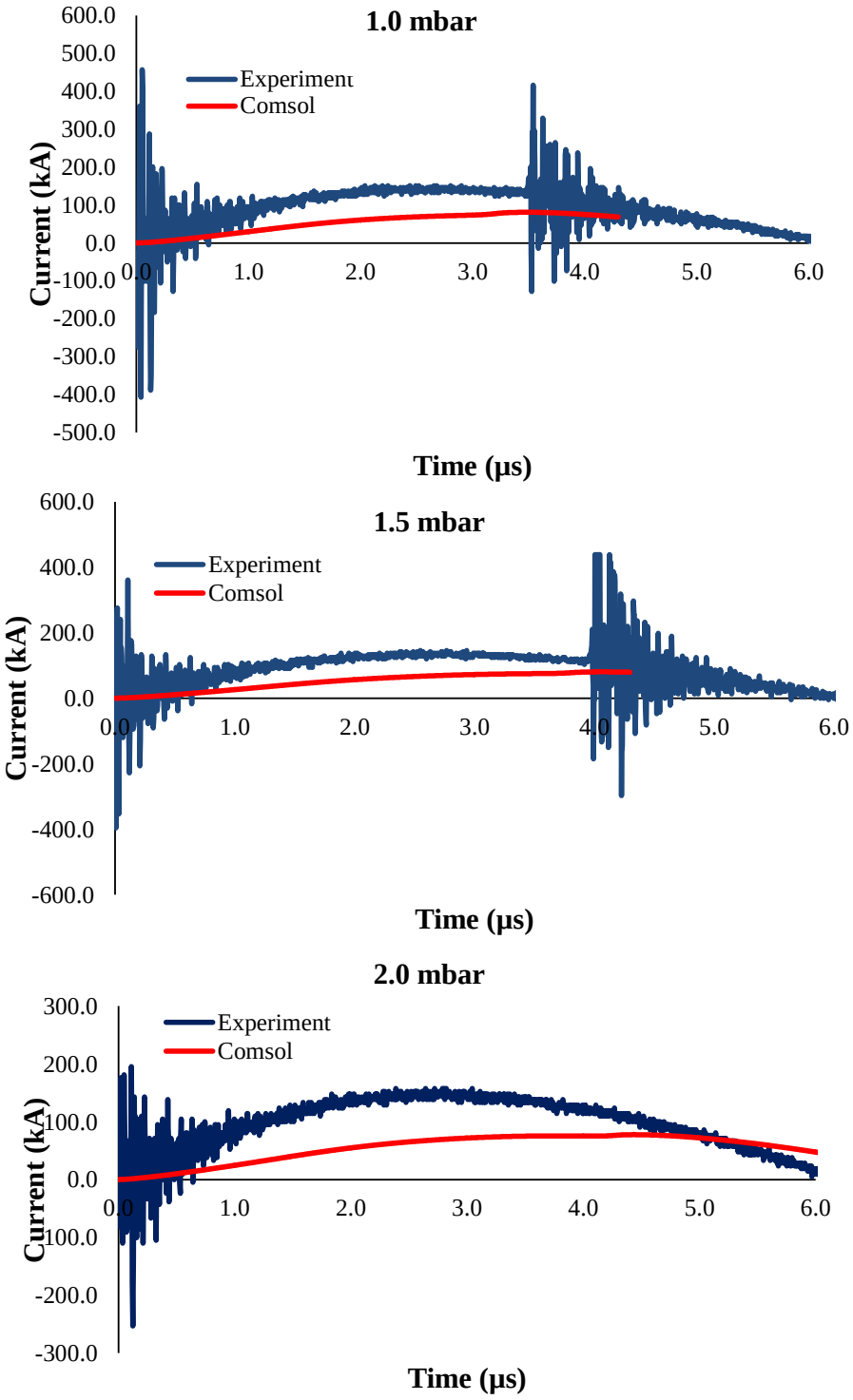

Appendix V
Graphs showing magnitude of magnetic field generated by the finite element simulation

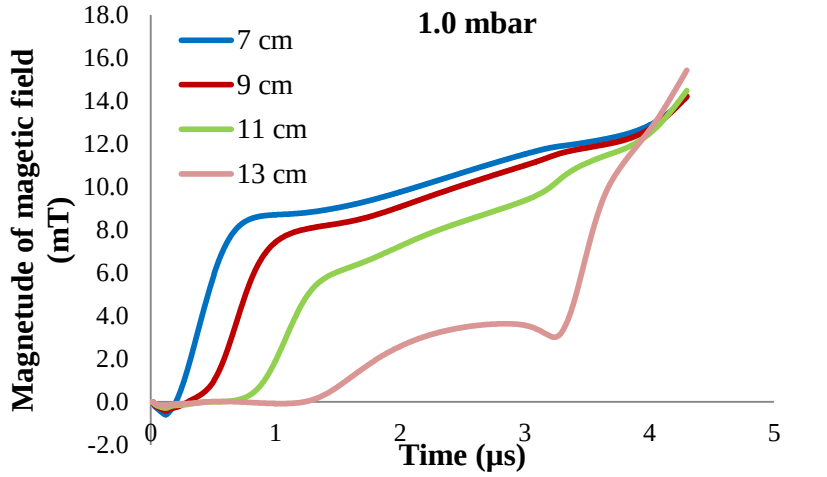

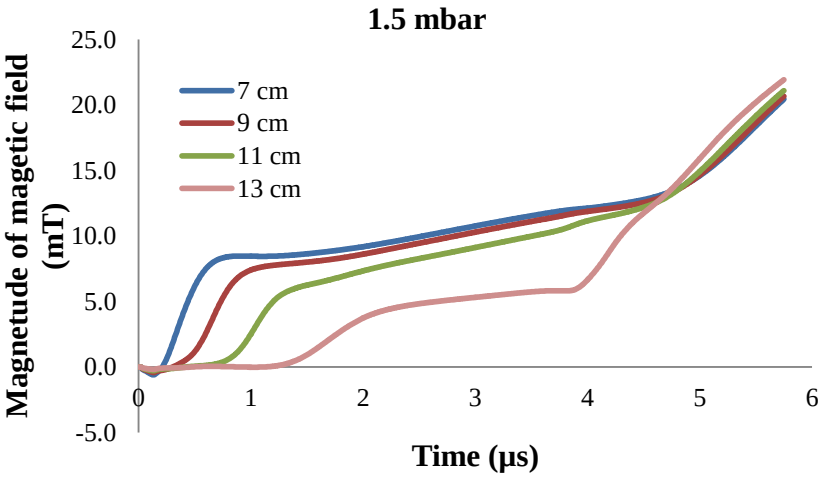

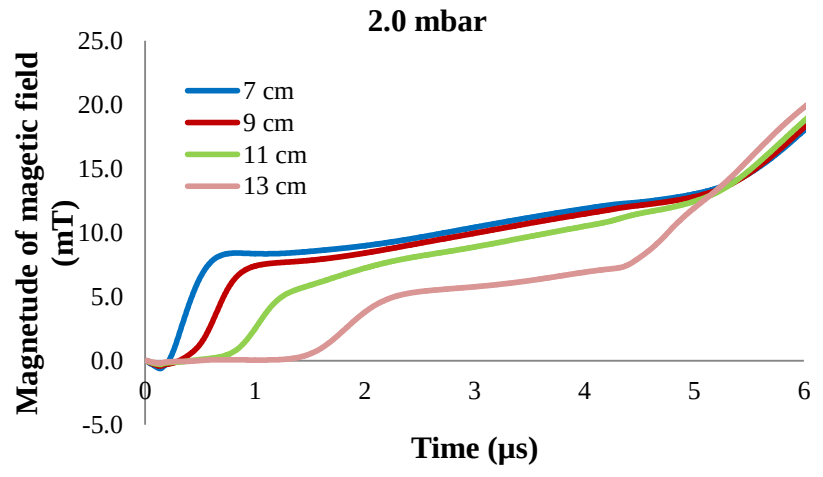

Appendix VI
Graph showing plasma temperature variation in time at each observing position calculated by Lee model and the finite element position

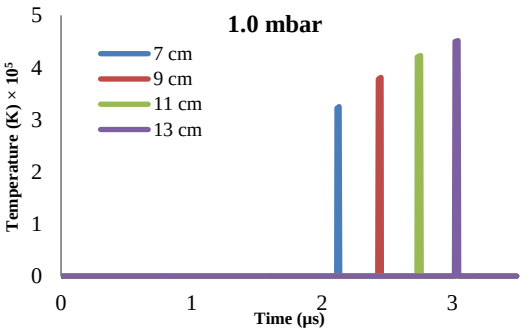

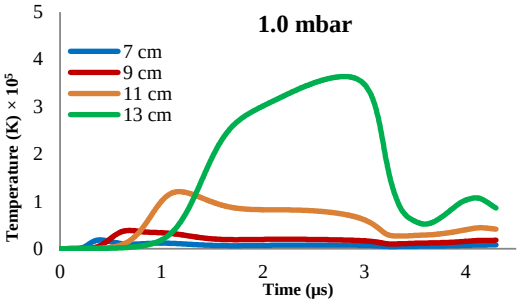

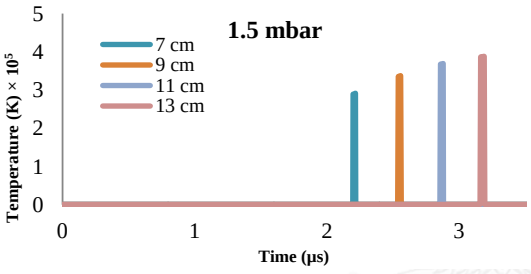

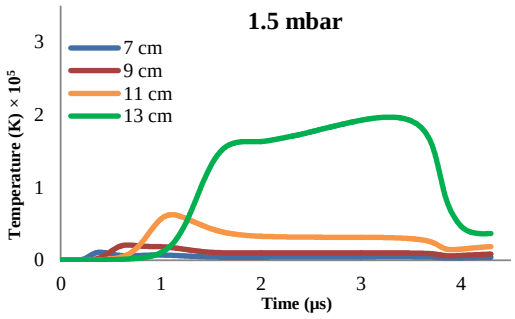

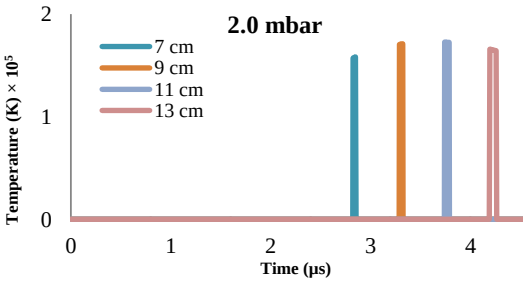

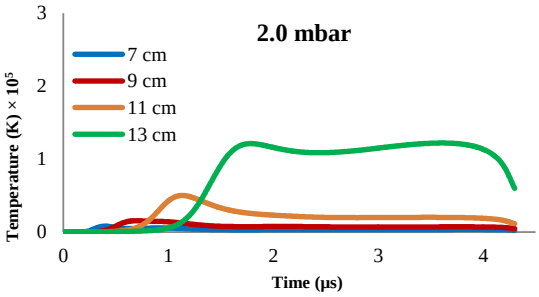

Appendix VII
Graph showing argon gas density variation in time at each observing position calculated by Lee model and the finite element position

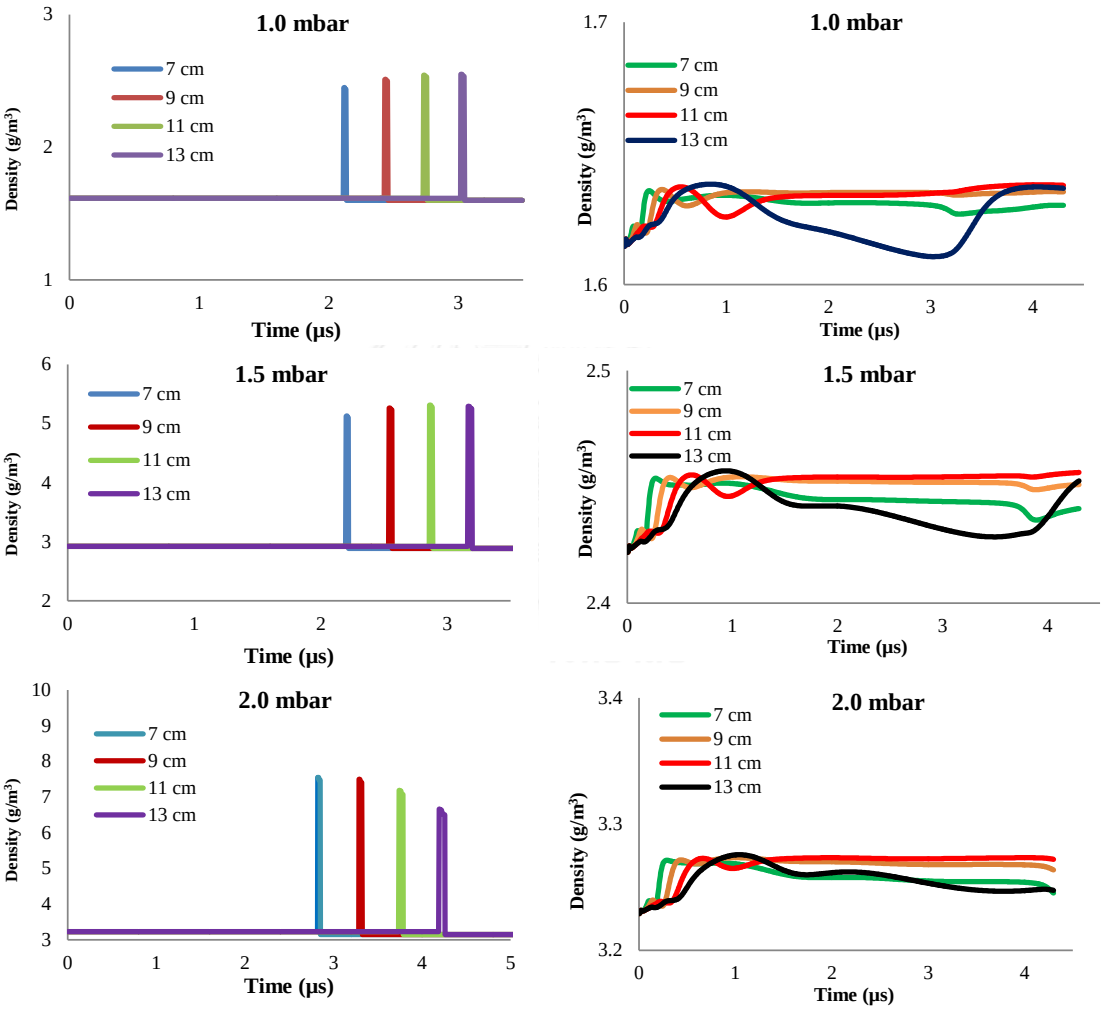

VITA

BIOGRAPHY

NAME Mr. Prajya Tangjitsomboon

BIRTH 22 October 1982

EDUCATION 2004-2008 M.Sc. Physics, Department of Physics, Faculty of Science, Chulalongkorn University

WORK EXPERIENCE

2009-present Researcher, Plasma Technology and Nuclear Fusion Research Unit, Chulalongkorn University

2010-present Academic Team, Ondemand Co-operation

PUBLICATION

-Tangjitsomboon P., Ngamrungroj D., Wong C. S. and Mongkolnavin R., Operating Parameters for Extreme Ultraviolet Radiation Generation based on the United Nations University/ International Centre for theoretical Physics (UNU/ICTP) Plasma Focus Device, Journal of Science and Technology in the Tropics, 2009 5, pp. 39-43.

-Chaisombat, S., Ngamrungroj, D., Tangjitsomboon, P., Mongkolnavin, R., Determination of Plasma Electron Temperature in a Pulsed Inductively Coupled Plasma (PICP) device. Procedia Engineering, 2012. 32: p. 929-935.

SUBMIT

-Tangjitsomboon P., Ngamrungroj, D., Chandrema, E., Wong, C.S., and Mongkolnavin R., Determination of Initial Ions Energy Produced by 3.3 kJ UNU/ICTP Plasma Focus using Computational Model, Vacuum (submit)